Numerical and Experimental Analyses of the Heat Transfer inside Infant Incubators using 3D Printed Thermal Manikin

Aziza Hannouch

DOCTORAT BRETAGNE LOIRE SCIENCES POUR L'INGENIEUR

université angers

THESE DE DOCTORAT DE

L'UNIVERSITE D'ANGERS

ECOLE DOCTORALE N° 602
Sciences pour l'Ingénieur
Spécialité : Thermique-Energétique

Par

Aziza HANNOUCH

Analyses Numériques et Expérimentales du Transfert Thermique dans un Incubateur Néonatal avec un Mannequin Imprimé en 3D

Numerical and Experimental Analyses of the Heat Transfer inside Infant Incubators using 3D Printed Thermal Manikin

Thèse présentée et soutenue à Angers, le 23/11/2021
Unité de recherche : LARIS EA 7315
Thèse N° : 211786

Composition du Jury :

Président :	
Prénom Nom	Fonction et établissement d'exercice
Rapporteurs :	
Pierre Tourneux	Professeur, PH, **CHU Amiens,** Réanimation Pédiatrique
Daniel Bougeard	Professeur, **IMT Lille Douai**, Département Energétique Industrielle
Examinateurs :	
Anne Heurtier	Professeur, **Polytech Angers**, LARIS EA 7315
Dominique Della Valle	Maitre de Conférences HDR, **ONIRIS Nantes**, GEPEA UMR CNRS 6144
Najib Metni	Associate Professor, **Notre Dame University-Louaizé**, Département de Génie Mécanique
Dir. de thèse :	
Thierry Lemenand	Maitre de Conférences HDR, **Polytech Angers**, LARIS EA 7315
Co-dir. de thèse :	
Khalil Khoury	Professeur, **Université Libanaise de Beyrouth**, Département de Génie Mécanique

La vie n'est facile pour aucun de nous. Mais quoi, il faut avoir de la persévérance, et surtout de la confiance en soi. Il faut croire que l'on est doué pour quelque chose, et que, cette chose, il faut l'atteindre coûte que coûte.

Marie Curie – Physicienne, Scientifique (1867 - 1934)

Acknowledgements

I would like to express my sincere gratitude to my PhD thesis director Thierry Lemenand for his priceless guidance and continuous assistance and help. I would like to also thank the PhD co-director Khalil Khoury for his motivation and support.

I would like to thank the thesis committee members: Pr. Pierre Tourneux, Pr. Daniel Bougeard, Pr. Anne Heurtier, Dr. Dominique Della Valle and Dr. Najib Metni for their insightful comments, recommendations and encouragement.

My sincere acknowledgment also goes to all research assistants from Notre Dame University-Louaize who participated to this project: Imad Alawiyeh, Karen El Asaad, Selim Khoury and Salim Tawk and to the mechanical engineering lab instructor Mrs. Sylvie Melki. I would like to thank my Dr. Charbel Habchi for his help and support in the CFD numerical simulations as well as in the analysis of the results. I also thank Dr. Najib Metni for his guidance and help in the PID control and instrumentation of the thermal manikin.

I owe my deep gratitude to: Notre Dame University-Louaize, LARIS Polytech Angers, MIR grant from Angers University, Lebanese CNRS, AUF, CEDRE Program for supporting and funding my research projects. We specially thank Drager and Prime Medical for donating the Caleo Drager infant incubator which was used in our numerical and experimental studies.

I am warmly thankful and fortunate for getting continuous encouragement from all my friends and parents especially my mother, Corgie, father, Georges, sister, Christine and brothers, Georges, Charbel and Tony.

Matheo, my wonderful son, I love you and thank you for the great moments we spend together. During the PhD I was also fortunate to have my little son Antonio during the COVID pandemic. You gave me motivation to continue this PhD thesis.

At the end, I want to sincerely thank my beloved husband Charbel for his constant motivation, support, patience, understanding, care, and love. I appreciate when you listen to me and when you give me brilliant ideas and thoughts about subjects and problems I am

facing in my work and personal life. It is thanks to you that I have prepared and defended my PhD thesis. I love you to the infinity and beyond!

Thank you God, and Saint Rita may you bless my work and my family.

Table of Contents

List of Figures

List of Tables

Chapter 1 Introduction Générale

À l'échelle mondiale en 2015, parmi les 5.9 millions de décès d'enfants de moins de 5 ans, **45.7% sont survenus pendant la période néonatale**. Les principales causes de décès d'enfants de moins de 5 ans sont les complications liées aux naissances prématurées avec un pourcentage de 17.9%, la pneumonie 15.6%, et les événements liés à l'accouchement 11.7% comme le montre la Figure 1.1 [1, 2]. Les **complications liées aux naissances prématurées** et la pneumonie sont toutes deux importantes dans les pays à **mortalité infantile** élevée comme l'Asie du Sud et l'Afrique subsaharienne [3]. D'après l'Organisation Mondiale de la Santé (OMS) [3], depuis 2010, **15 millions de naissances par an sont prématurées** parmi lesquelles plus de 80% se produisent entre 32-37 semaines de gestation dont la plupart peuvent survivre avec des soins néonataux essentiels. En fait, parmi les huit Objectifs du Millénaire pour le Développement (OMD) des Nations Unies, le 5ème OMD concerne l'amélioration de la santé maternelle en réduisant le taux de mortalité des nouveau nés [4, 5].

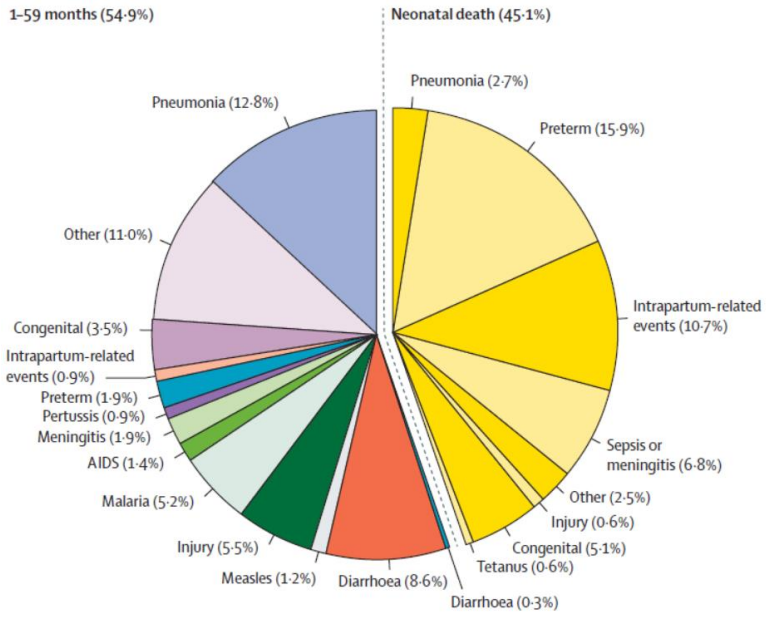

Figure 1.1: Causes globales pour les décès d'enfants de moins de 5 ans [2]

Les cartes de la Figure 1.2 illustrent les taux de naissances prématurées et le nombre absolu de naissances prématurées en 2010 par pays. Les taux estimés varient d'environ 5% dans plusieurs pays d'Europe du Nord à 18,1% au Malawi. Le taux estimé de naissances prématurées est inférieur à 10% dans 88 pays, tandis que 11 pays présentent des taux estimés de 15% ou plus (Figure 1.2 (a)). Les 10 pays où le nombre estimé de naissances prématurées est le plus élevé sont l'Inde, la Chine, le Nigeria, le Pakistan, l'Indonésie, les États-Unis, le Bangladesh, les Philippines, la République démocratique du Congo et le Brésil (Figure 1.2 (b)). Ces 10 pays représentent 60% de toutes les naissances prématurées dans le monde.

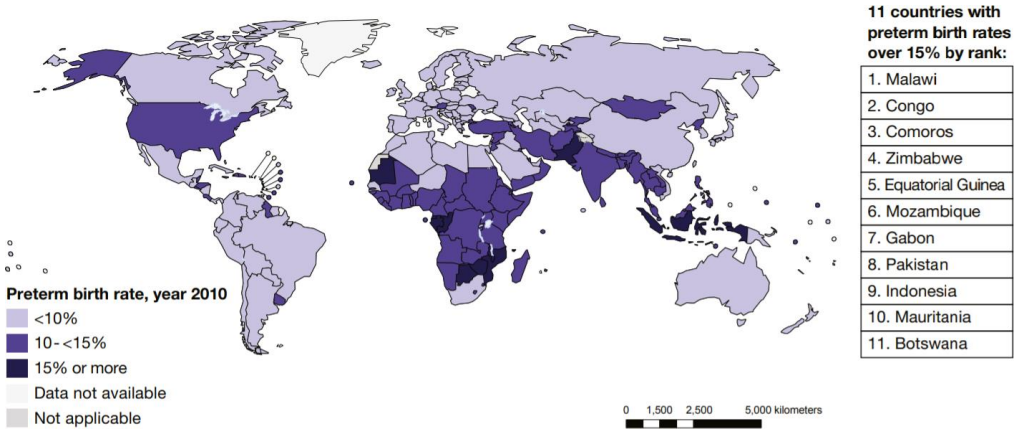

(a)

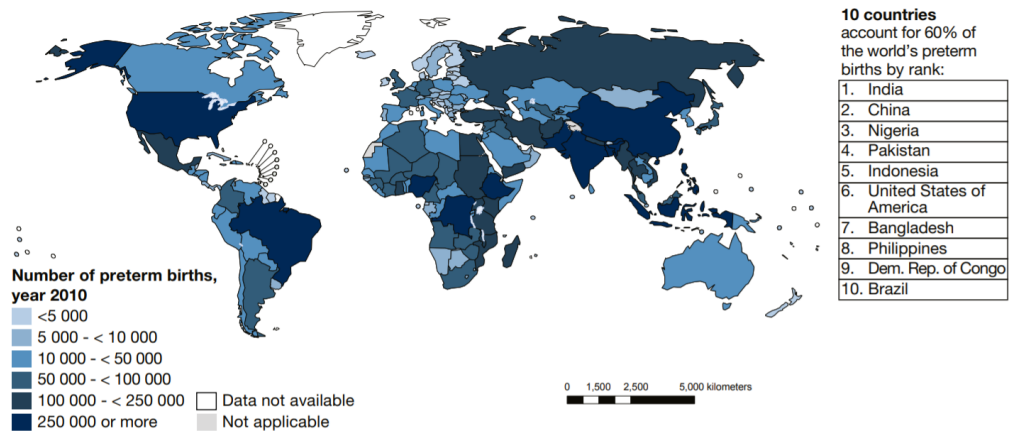

(b)

Figure 1.2: Distribution mondiale du (a) pourcentage de naissances prématurées par pays et (b) nombre total de naissances prématurées [1]

Dans ce contexte mondial, l'OMS a fixé une liste de recommandations sur les interventions visant à améliorer les résultats des naissances prématurées [6]. Une de ces recommandations concerne la **vigilance thermique pour les nouveau-nés prématurés** comme l'utilisation des couveuses.

En effet, l'adaptation du corps humain aux changements rapides des conditions hygrothermiques environnementales nécessite une grande dépense d'énergie métabolique. Chez les adultes et les nourrissons en bonne santé, cette adaptation est accomplie par plusieurs **réponses physiologiques** complexes et cohérentes telles que la génération de **chaleur métabolique**, la régulation du flux sanguin par la **vasodilatation** et la **vasoconstriction**, la **transpiration** et les **frissons**. Ce processus physiologique est appelé **thermorégulation** [7, 8, 9, 10]. Cependant, les nouveau-nés prématurés ont des capacités de thermorégulation peu développées et ils peuvent perdre de la chaleur beaucoup plus rapidement que les adultes, ajoutant à cela un rapport élevé de la surface de la peau au volume corporel [11, 12]. Par conséquent, ils rencontrent des dif**ficultés à ajuster leur température corporelle** dans un environnement non contrôlé, ce qui peut entraîner une hypothermie [13, 14]. Ainsi, dans les quelques jours ou semaines qui suivent l'accouchement, ces bébés doivent être placés dans des couveuses afin d'aider à **contrôler leur température** corporelle et de réduire les pertes de chaleur sensible et latente [15, 16, 17]. Les processus complexes de transfert de chaleur et de masse dans ces couveuses combinent la **convection, la conduction, le rayonnement thermique et l'évaporation** [18, 19]. Par conséquent, mieux interpréter et modéliser la biochaleur chez les nouveau-nés est déterminant pour leur survie et leur croissance.

En plus à ce chapitre d'introduction générale, ce rapport de thèse comprend cinq autres chapitres comme présenté ci-dessous.

Le **Chapitre 2** est consacré à l'état de l'art de la partie bibliographique. En fait, plusieurs méthodes sont utilisées afin de mieux comprendre les phénomènes physiques de pertes de chaleur des nouveau-nés et de l'interaction corps-environnement. Ces méthodes peuvent être classées en trois catégories principales comme le représente la Figure 1.3 : l'analyse analytique de la thermorégulation humaine, la dynamique des fluides numérique (Computational Fluid Dynamics, CFD) et les études expérimentales. L'objectif de ces

méthodes est d'analyser l'effet de différentes conditions ambiantes, telles que la température et l'humidité de l'air, sur les transferts de chaleur par convection, conduction et rayonnement ainsi que sur les pertes de chaleur latente dues à l'évaporation cutanée et la respiration. De plus, sur la base de ces méthodes, différentes techniques sont proposées pour améliorer les conditions hygrothermiques dans les incubateurs. Toutes ces questions sont examinées et discutées dans ce chapitre de littérature bibliographique.

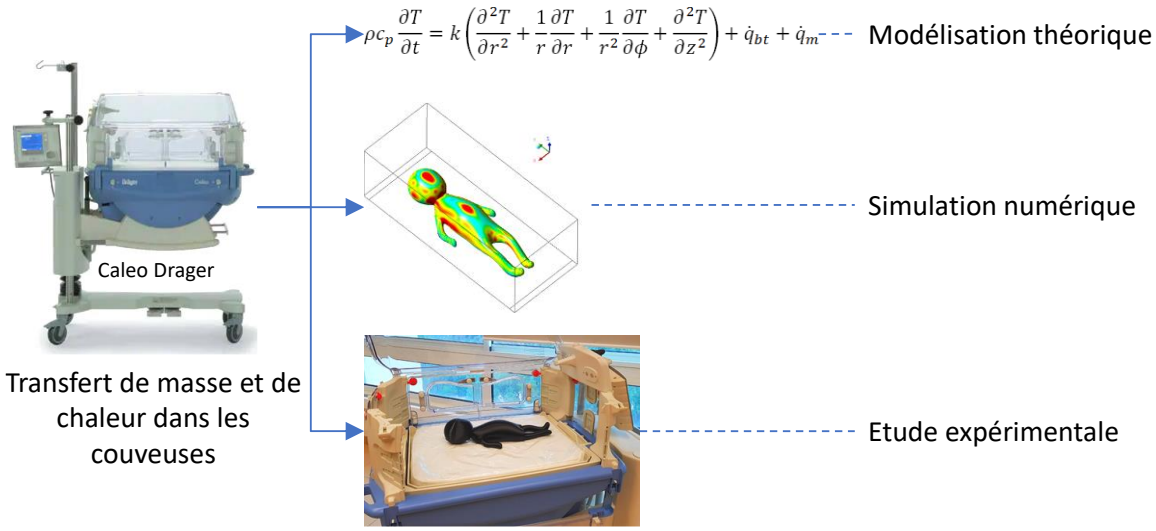

Figure 1.3: Schéma représentant les différentes méthodes utilisées pour l'analyse des transferts thermique dans les couveuses de nouveau-nés

Dans le **Chapitre 3** nous présentons le mannequin thermique et l'incubateur utilisés dans les études numérique et expérimentale. Un mannequin anthropomorphique représentant un nourrisson prématuré âgé de 35 semaines gestationnelles est fabriqué par la méthode de l'impression 3D et il est constitué de 5 segments corporels : tête, bras, torse, dos et jambes. Une géométrie virtuelle de ce mannequin est aussi utilisée dans les simulations numériques par la méthode de volumes finis. Le mannequin est placé à l'intérieur d'un incubateur Caleo Drager. Cette couveuse a été donnée par la compagnie Drager et est placée dans le laboratoire du Département de Génie Mécanique à l'Université Notre Dame-Louaizé au Liban. Le mode de fonctionnement de cet incubateur est présenté en détail dans ce chapitre. Un modèle virtuel de l'incubateur est préparé par un logiciel CAD (Computer Aided Design) afin que l'on puisse l'utiliser dans les simulations numériques.

Dans le **Chapitre 4**, des simulations numériques sont effectuées pour un nouveau-né prématuré composé de 5 segments (tête, bras, torse, dos et jambes) placé à l'intérieur d'un incubateur. Les études sont menées en faisant varier la température d'entrée de l'incubateur entre 29 et 35ºC et différents débits d'air entre 5 et 50 litres/min. On constate que le processus de transfert de chaleur dépend principalement de la température de l'air dans l'incubateur. On montre que le débit d'air de l'incubateur n'affecte pas de manière significative le transfert de chaleur convectif. Ainsi, il est conclu que le transfert de chaleur entre l'air de l'incubateur et le nourrisson est causé par la convection naturelle. L'effet de la structure de l'écoulement sur la distribution de la température est étudié et des corrélations pour les coefficients de transfert thermique radiatif et convectif sont obtenues pour chaque segment corporel. Le coefficient de transfert thermique radiatif varie entre 2,2 et 6,2 W/m^2K tandis que le coefficient de transfert thermique convectif varie entre 2,6 et 4,7 W/m^2K. Les résultats sont validés par des données expérimentales de la littérature. Finalement, un modèle de thermorégulation est développé en tenant compte des pertes de chaleur et de masse dues à l'évaporation cutanée et à la respiration. Ce modèle est utilisé pour quantifier le bilan thermique chez les nouveau-nés prématurés dans les incubateurs.

Le **Chapitre 5** est consacré à l'étude expérimentale menée sur le mannequin thermique placé à l'intérieur de l'incubateur. Nous discutons dans ce chapitre l'instrumentation du mannequin avec des fils chauffants fixés sur la surface intérieure et avec des thermocouples fixés sur la surface extérieure. Un régulateur PID (proportionnel, intégral, dérivé) est utilisé pour contrôler les températures des différents segments du mannequin. Nous adoptons la méthode de Ziegler-Nichols qui est une méthode heuristique pour le réglage du régulateur PID. Le logiciel LabVIEW est utilisé ensuite pour créer l'instrument virtuel avec une interface graphique. Trois campagnes de mesures ont été menées. La première consiste à fixer une température d'incubateur à 30ºC et dans la deuxième la température est augmentée à 35ºC tout en gardant les portes de l'incubateur fermées. Dans la troisième campagne de mesure, la température de l'incubateur est fixée à 35ºC avec les portes de l'incubateur ouvertes. Les résultats issus des trois études expérimentales sont discutés en termes de variation temporelle des températures des différents segments du mannequin ainsi en analysant les pertes de chaleur par convection et rayonnement thermique qui sont obtenues en couplant les données expérimentales aux coefficients d'échange de convection et de

rayonnement obtenues dans le Chapitre 3. Ces résultats sont aussi comparés avec des données numériques et expérimentales de la littérature. Nous constatons de cette comparaison que le mannequin conçu dans cette thèse ainsi que les méthodes expérimentales adoptées sont valides et donnent des résultats avec une bonne correspondance avec la littérature.

Finalement, le dernier **Chapitre 6** est consacrée à la conclusion générale et aux perspectives sur les idées futures.

Chapter 2 Literature Review

Les nouveau-nés, en particulier les prématurés et ceux qui sont malades, ont des difficultés à contrôler leur température corporelle. Ainsi, ils sont placés dans des incubateurs afin d'améliorer les conditions hygrothermiques et de surveiller leur température ainsi que d'autres signes vitaux. Les processus complexes de transfert de chaleur et de masse entre les nouveau-nés et l'air et les surfaces environnantes sont des facteurs essentiels à leur croissance et survie. Plusieurs méthodes sont utilisées afin de mieux comprendre les phénomènes physiques de pertes de chaleur des nouveau-nés et l'interaction corps-environnement. Ces méthodes peuvent être classées en trois catégories principales : l'analyse analytique de la thermorégulation humaine, la dynamique des fluides numérique (CFD) et les études expérimentales. L'objectif de ces méthodes est d'analyser l'effet de différentes conditions ambiantes, telles que la température et l'humidité de l'air, sur les transferts de chaleur par convection, conduction et rayonnement ainsi que sur les pertes de chaleur latente dues à l'évaporation cutanée et la respiration. De plus, sur la base de ces méthodes, différentes techniques sont proposées pour améliorer les conditions hygrothermiques dans les incubateurs. Toutes ces questions sont examinées et discutées dans ce chapitre de littérature bibliographique.

2.1 Introduction

Bioheat models were successfully developed in the open literature to study the whole body thermoregulation under different circumstances [18, 20, 21, 22, 23]. These models are valuable for contributing to a profound and better understanding of thermoregulation process. Moreover, experimental and computational methods are being extensively used to study and

analyze the heat and mass transfer in incubators [24, 25, 26] in order to design new devices or optimize existing ones.

Several studies were conducted in the open literature to evaluate the dry and latent heat losses from neonates nursed inside incubators. These studies are classified in three main categories:

- Bioheat modeling and thermoregulation: where multisegmental mathematical models are considered in order to analyze the bioheat transfer in the neonate body and to determine its thermal responses to ambient conditions [18, 21]. These models are based on the bioheat equation developed initially by Pennes [27] to compute the rate of heat transfer to the forearm. This model is widely adopted and extended to whole body in steady and transient processes. While most of the bioheat models in the open literature are dedicated for adults [18, 20, 28], less bioheat models were developed for preterm infant [21, 29, 30] due to several constraints such as lack in the knowledge of accurate thermophysical properties of the tissues and few data concerning the radiative, convective and evaporative heat transfer coefficients on the newborn skin.
- Numerical simulations of dry and heat losses from neonate using computational fluid dynamics (CFD) which is based on the finite volume method to discretize the Navier-Stokes and energy equations. Various studies have been conducted in the open literature aiming to better understand the effect of the flow structure inside the incubator on the rates of heat losses from preterm neonates [31]. The aim of this method is to enhance existing devices and to design new techniques aiming to enhance the hygrothermal conditions for neonates inside the incubators [31, 15, 16]. All these studies were focusing on dry heat losses while latent heat transfers were obtained using empirical correlations [15].
- Experimental study using cohort of human neonates or thermal manikins in order to evaluate convection, radiation and evaporation heat transfer coefficients and thermal balance in preterm neonates [13, 32, 33]. Studies performed on human neonates focus mainly on the evaluation of the metabolic heat generation, heat losses and core and skin temperatures with the hygrothermal conditions of incubators [34, 35, 36]. Moreover, preterm thermal manikins are used to evaluate the dry and heat losses for

different conditions such as naked and clothed newborn [37], incubator with or without heated mattress [38], double wall incubator [24], effects of clothing insulation and of occlusive polyethylene wrap to reduce skin evaporative heat loss and also to evaluate heat and mass transfer coefficients to be used in the theoretical bioheat models [39, 40, 41].

The aim of the present Chapter is to present a review of the different techniques used to study dry and latent heat losses and thermoregulation of neonates nursed in infant incubators. Moreover, we shed light on areas where more research and development are needed. In addition, some supplementary data analysis is performed from existing results in order to better understand the relation between metabolic heat generation, core and skin temperatures and mass and heat losses.

Before reading through the Chapter, we need to distinguish between skin and core temperature. In neonates, skin temperature is usually often recorded at one or two points of the skin surface area. While core or body core temperature is the internal temperature measured at the level of the rectum and more generally at the level of the skin surface of the abdomen by a probe attached in the midline between the umbilicus and the xiphoïd region.

This Chapter is organized as follows: in section 2.2 we discuss the thermoregulation models applied to neonates; section 2.3 is devoted to a review on recent advancements in CFD numerical simulations of heat transfer for neonates in intensive care units; the experimental studies on cohort of human neonates and anthropomorphic manikins are presented in section 2.4; a summary of the different methods discussed in this Chapter are presented in section 2.5 and finally concluding remarks are given in section 2.6.

2.2 Thermoregulation modeling

2.2.1 Pennes bioheat model

Most bioheat models are based on the blood perfusion model proposed by Pennes [27] which could be adopted to different body segments. Thus, this model is briefly presented in this section before moving to the models dedicated for preterm neonates. In fact, this model

was initially developed to evaluate the temperature radial distribution in the human forearm tissues and brachial arterial blood.

Fick's principle could be used to compute the volumetric rate of heat transfer from blood to tissue resulting in the following equation [27]:

$$\dot{q}_{bl} = \dot{V}\rho_{bl}c_{bl}(T_{bl} - T) \tag{1.1}$$

where $\dot{q}_{bl}$ is the volumetric rate of heat transfer from the blood to tissues, $\dot{V} = \dot{m}/V_t$ is the blood perfusion rate $(\dot{m})$ per unit volume of tissue (V_t), ρ_{bl} and c_{bl} are the density and thermal capacity of blood respectively, T_{bl} is the arterial blood temperature and T the tissue temperature.

For steady-state process and constant thermophysical properties and assuming one-dimensional conduction in cylindrical coordinate system with uniform metabolic rate, the diffusion equation simplifies to the below Bessel's equation:

$$k\left(\frac{d^2T}{dr^2} + \frac{1}{r}\frac{dT}{dr}\right) - \dot{V}\rho_{bl}c_{bl}T = -\dot{q}_m - \dot{V}\rho_{bl}c_{bl}T_{bl} \tag{1.2}$$

where $\dot{q}_m$ is the metabolic heat generation and k the thermal conductivity of the tissue.

Solving this partial differential equation in terms of Bessel's functions, the following expression is obtained for the tissue temperature [27]:

$$T = \left(T_s - T_{bl} - \frac{\dot{q}_m}{\dot{V}\rho_{bl}c_{bl}}\right)\frac{\mathbf{J_0}\left(i\sqrt{\frac{\dot{V}\rho_{bl}c_{bl}}{k}}r\right)}{\mathbf{J_0}\left(i\sqrt{\frac{\dot{V}\rho_{bl}c_{bl}}{k}}R\right)} + \left(T_{bl} + \frac{\dot{q}_m}{\dot{V}\rho_{bl}c_{bl}}\right) \tag{1.3}$$

where $\mathbf{J_0}$ is the zero order and first kind Bessel's function of an imaginary variable, R is the outer radius of the forearm and T_s the skin temperature obtained using Newton's cooling law and Stephan-Boltzmann model and it reads:

$$T_s = \frac{\left(\frac{\dot{V}\rho_{bl}c_{bl}T_a + \dot{q}_m}{k\sqrt{\dot{V}\rho_{bl}c_{bl}k}}\right)\left[-i\mathbf{J_1}\left(i\sqrt{\frac{\dot{V}\rho_{bl}c_{bl}}{k}}R\right)\right] + 1.21(h_c + h_r)T_\infty\left[\mathbf{J_0}\left(i\sqrt{\frac{\dot{V}\rho_{bl}c_{bl}}{k}}R\right)\right]}{\sqrt{\dot{V}\rho_{bl}c_{bl}k}\left[-i\mathbf{J_1}\left(i\sqrt{\frac{\dot{V}\rho_{bl}c_{bl}}{k}}R\right)\right] + 1.21(h_c + h_r)\left[\mathbf{J_0}\left(i\sqrt{\frac{\dot{V}\rho_{bl}c_{bl}}{k}}R\right)\right]} \tag{1.4}$$

where $\mathbf{J_1}$ is the first order and first kind Bessel's function, $(h_c + h_r)$ is the overall heat transfer coefficient for convection and radiation respectively and T_∞ is the ambient air temperature in the room.

The main disadvantage of this model is the absence of evaporation heat loss modeling. This is a great concern in preterm neonates owing very thin skin layer causing transepidermal water losses [42, 43].

In 1998, Wissler [44] revisited Pennes paper [27] and he showed that the analysis of experimental data used by Pennes was inappropriate and led to a variance with the results obtained from its model. Therefore, Wissler [44] suggested to use normalized temperature and radius to better represent the experimental and theoretical data.

Several studies in the open literature modified the Pennes bioheat model to suite their applications such as analyzing the transient temperature response to unsteady heat fluxes and to include thermophysical properties dependence on tissue temperature [45, 46, 47]. Despite all controversies and criticism about Pennes bioheat model; most mathematical analyses in bioheat transfers are based on this model. The reasons behind the hunger to use Pennes model are its mathematical simplicity and its ability to predict the temperature field reasonably well in several applications.

Meanwhile, the challenge in using such theoretical model is the estimation of the thermophysical properties of the different tissues such as bone, muscle, fat and skin. These properties have a great impact on the temperature variation through the different layers. Moreover, additional experimental and computational studies need to be performed in order to obtain the heat and mass transfer coefficients for different body segments for preterm neonates.

2.2.2 Thermoregulation modeling in neonates

A multi-node mathematical model of the thermoregulatory system of newborn infant was carried out by Pereira *et al.* [21] who used seven compartments to model the infant as depicted schematically in Figure 2.1.

Similarly, to the bioheat model developed by Fiala *et al.* [48, 20] in adults, this bioheat model consists of two main systems: the passive controlled system and the active controller

system. The passive system consists of modeling the neonate body and bioheat transfer in tissues and surface. Moreover, the model includes a central blood compartment to take into consideration the convective heat transfer between blood and other body compartments. The blood exchanges heat by convection with each tissue while the tissues exchange heat by conduction. Then the skin exchanges heat by conduction with the mattress and by convection and radiation with the environment, *i.e.* air and surrounding surfaces as shown in Figure 2.1. Meanwhile, the active system predicts and simulates the regulatory responses to thermal stress in neonate such as nonshivering thermogenesis and peripheral vasomotion.

The bioheat transport equation (Eq. (1.5)) adapted from Pennes [27]) within the tissues was modeled along with the interactions with the environment.

$$\rho_i c_i \frac{\partial T_i}{\partial t} = k\left(\frac{\partial^2 T_i}{\partial r^2} + \frac{\alpha}{r}\frac{\partial T_i}{\partial r}\right) + \dot{q}_{m,i} + K_i \rho_{bl} c_{bl} w_{bl,0_x}\left(T_{bl,a} - T_i\right) \tag{1.5}$$

In this equation the index *i* represents the tissue type and *bl* represents the blood. The coefficient α is a geometry factor ($\alpha = 1$ for cylindrical coordinates, $\alpha = 0$ for spherical coordinates). $w_{bl,0_x}$ is the blood perfusion (1/s), $T_{bl,a}$ the temperature of the arterial blood, *K* is a countercurrent factor. The left-hand side corresponds to the heat storage in the tissue. The first term to the right-hand side corresponds to the conduction inside the layers, the second term $\dot{q}_{m,i}$ is the volumetric heat generation by metabolism and the last term is for the convection with the blood circulating through the arteries. Heat and mass transfer with the environment were considered as boundary conditions.

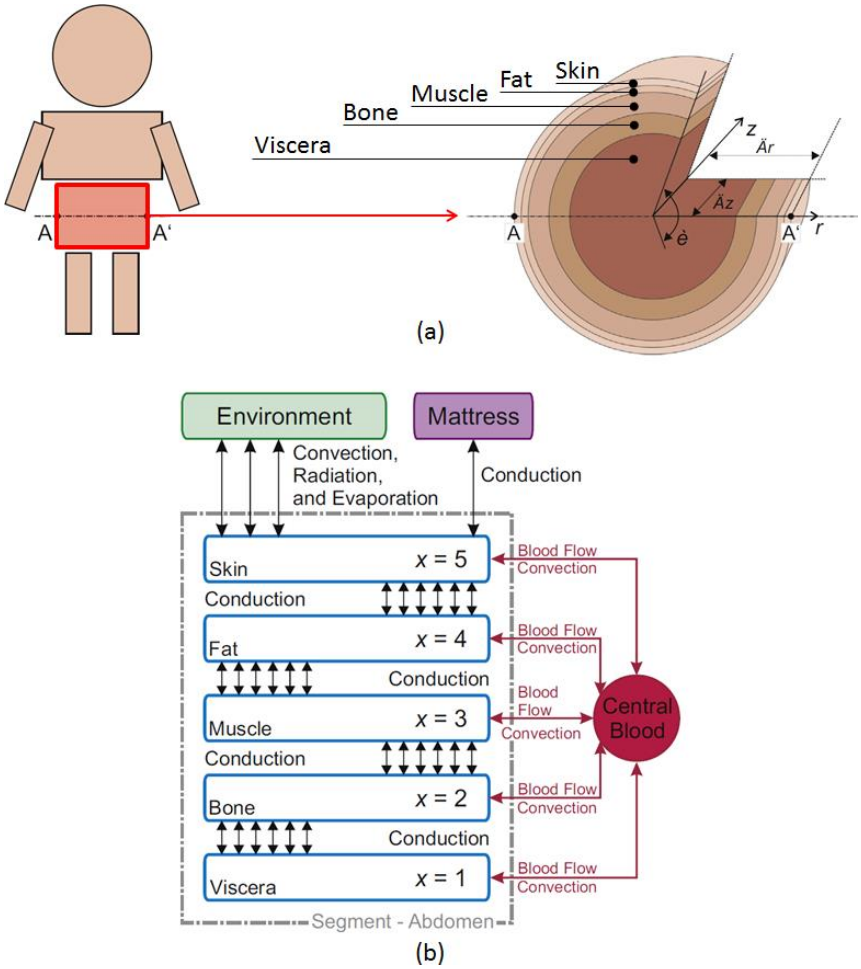

Figure 2.1: (a) Schematic representing the seven body segments: head, thorax, abdomen, upper and lower limbs along with a transverse section of the abdomen (section A-A') showing the different layers. (b) Diagram depicting the one-dimensional radial conduction model in the abdomen, convective heat transfer with central blood system and the dry and latent heat losses with the environment (Modified from Pereira *et al.* [21]).

The results obtained by Pereira *et al.* [21] were first successfully validated against experimental data obtained by Hammarlund *et al.* [43] in thermal neutrality conditions for 19 newborns of 39 weeks gestational age. Fair agreement was also observed when comparing results obtained from this model to those obtained experimentally in case of transient thermal conditions on two healthy preterm babies [21]. The experimental protocol for the transient thermal conditions consists of measuring the core and skin temperature during transition from incubator to kangarooing care and vise-versa.

Thermoregulation models are also used for the evaluation of the incubator set point temperature, which is the incubator air temperature set by the nursing staff. The accuracy to which the climate inside incubators should be controlled is defined in two ways: the static and the dynamic [49]. The static is the difference between the incubator temperature set point and the actual measured mean temperature. The dynamic is based on the standard deviation of the temperature variation relative to the mean level. Dane [49] proposed a method to investigate the required dynamic accuracy of the temperature control inside incubators using a simplified thermoregulation model. It was found that a standard deviation around 3℃ inside the incubator results in 0.5℃ standard deviation in the infant skin temperature which leads to only 0.25-Watt increase of metabolic heat generation. Meanwhile, the simplified bioheat model proposed by Dane [49] consists of only two compartments: a core compartment surrounded by skin with different temperature. Thus, further developments are needed in order to enhance the accuracy and reliability of this model.

Fraguela *et al.* [29] proposed a bioheat model to describe the variation of the peripheral and blood temperature of newborn infant and a functional for minimizing the time core temperature remains outside the thermal stability range. An algorithm was proposed in order to control the incubator air temperature by considering the continuously measured core temperature of premature newborn. In this study the infant body was simplified to a single compartment with three components: core, blood and skin.

2.2.3 Finite element simulation of neonatal thermoregulation

Instead of modeling the body as simplified two-dimensional multisegments, Silva *et al.* [50, 51] considered complex three-dimensional multisegmental neonate body obtained from MRI scan medial images. Pennes equation [27] and Fiala blood pool model [52] were adopted in this study and computed using the finite element method (FEM). The aim was to study the hypothermia procedure for the treatment of encephalopathy hypoxic ischemia (EHI) in neonate infants. EHI occurs when the flow of oxygenated blood to the brain is interrupted due to any injury or complications [53]. Two hypothermia methods were analyzed. The first consisted of selective brain cooling by using a cooling helmet. The second consisted of whole-body cooling where the neonate is lying down on a cooling mattress.

Figure 2.2 (a-b) and (c-d) show the temperature distribution on the skin and in the core of a neonate after 24 hours of using a cooling helmet or using a cooling mattress, respectively. Using a cooling mattress, the feet are at very low temperature which could lead to a bad thermal condition. Meanwhile, in the cooling helmet case, the process is localized where it is needed, *i.e.*, brain cooling where the temperature drops to 34℃ half an hour faster than using a cooling mattress. In the rewarming phase, the whole-body method leads to a higher rate of temperature increase and the normal body temperature of 37°C is reestablished after 4 hours. In the selective brain method, the temperature needs 5.5 hours to reach its normal value. Using a similar numerical model and computational domain, Bandoła *et al.* [54] and Laszczyk *et al.* [55, 56] performed experimental and numerical analysis of neonate's brain cooling using a cooling helmet. The results were in good agreement with those found by Silva *et al.* [50, 51] except that the maximum temperature did not exceed 34℃ (on the limbs) while it reaches around 36℃ at the extremities in the study done by Silva *et al.* [50, 51].

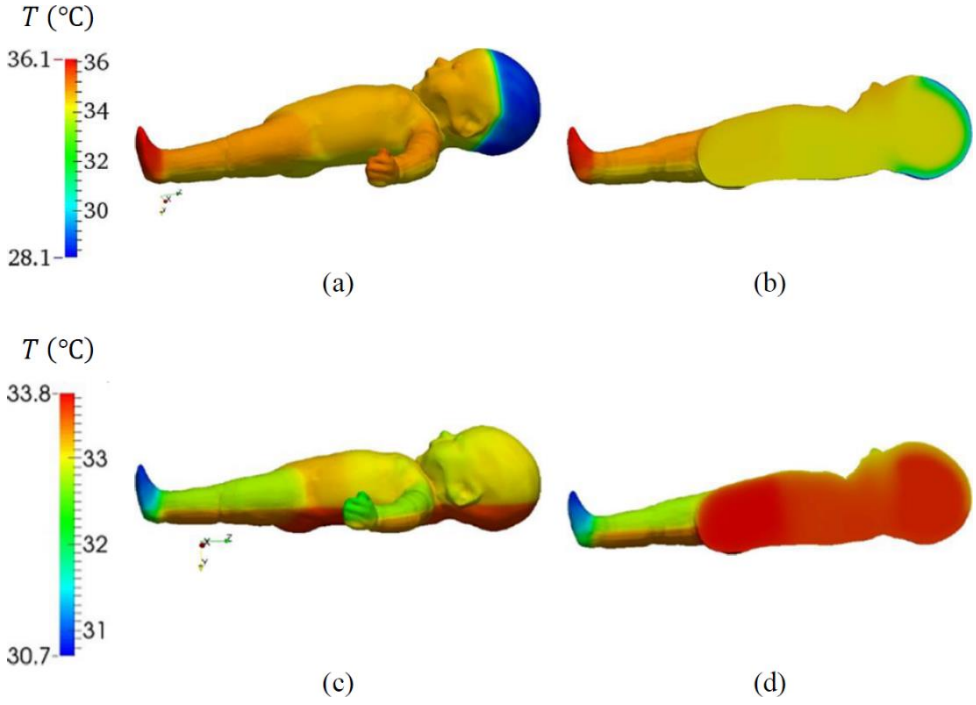

Figure 2.2: (a) Skin and (b) interior temperature after 24 hours of using a cooling helmet and (c) skin and (d) interior temperature after 24 hours of using a cooling mattress [50, 51]

2.2.4 Summary on Thermoregulation Modeling

Very few multisegmental models for neonatal thermoregulation are found in the open literature. These models are mainly based on the Pennes bioheat model [27] to compute the core and skin temperature under different conditions. However, the environmental conditions, *i.e.*, convection, radiation and air speed, were assumed almost uniform on the outer surface of the body. Meanwhile, these parameters can vary spatially on the skin since they depend on the location of the ventilation system and the radiation source. This has a great impact on the neonate, and it necessitates performing numerical simulations using the computational fluid dynamics (CFD) technique to model the convection and radiation heat transfer modes inside neonate incubators. Moreover, the evaluation of heat and mass transfer coefficients is fundamental for thermoregulation models since they are required in the boundary conditions of the mathematical models. Another important issue is the lack in accurate and universal data on the thermophysical properties of preterm body segments such as thermophysical properties of skin, muscles and bones. These are crucial since they have a direct impact on the uncertainty of the results obtained theoretically.

In the next section we will discuss the different CFD studies performed in the literature inside neonate incubators aiming to better understand the effect of the ventilation system in the thermoregulation of newborn infants.

2.3 CFD Simulations of Neonates in Intensive Care Units

This section is devoted to the recent progress in CFD studies for heat and mass losses from preterm neonates nursed inside incubators. The section is divided into four subsections. The first and second subsections concern the studies on dry and latent heat losses, respectively. Then some method on the enhancement of hygrothermal conditions inside incubators is presented followed by a summary on CFD studies.

2.3.1 Dry heat loss

To our knowledge, the earliest CFD analysis of dry heat inside infant incubators was performed by Kim *et al.* [57] in 2002. In this study both experimental and numerical methods were used to study the airflow inside infant incubator in presence of a baby manikin. A constant heat flux of 0.54 W/m^2 at the neonate's body surface was assumed. Meanwhile, radiation heat losses were neglected. It was observed experimentally and numerically [57] that a large-scale vortex is produced inside the incubator with a number of small stationary vortices which can interfere with the thermoneutrality of the infant.

Amezzane *et al.* [58] used CFD simulations to study the airflow, heat transfer and CO_2 transport in neonate incubator. A simplified model was used, where the infant is represented by a phantom model consisting of a half-cylinder. The phantom model has an opening to simulate the respiratory airway, which has a prescribed constant mean flow velocity corresponding to pulmonary ventilation of 1 L/min at a frequency of 40 breaths/min. Steady state simulations are carried out using the RNG $k-\epsilon$ turbulence model. Boussinesq approximation was used to account for buoyancy. All other thermophysical properties are assumed constant. Radiation heat transfer and conduction are neglected, and the CO_2 fraction introduced during the exhalation process is assumed 4%. Amezzane *et al.* [58] found that the near skin temperature reaches values around 33°C, which are relatively lower than acceptable threshold which is around 37°C especially that neonates are nude inside incubators. However, Amezzane *et al.* [58] suggested raising the clothing isolation coefficient in order to enhance the thermoneutrality. From the CO_2 distribution over the baby skin, Amezzane *et al.* [58] found that the average concentration inside the incubator did not exceed 700 ppm, which is acceptable according to ASHRAE-62.1 standard [59].

Ginalski *et al.* [60] performed more elaborated numerical simulations for dry heat loss from two different baby manikins nursed inside Caleo Drager Incubator [61]. The first is small manikin with a mass of 900 g and the second is large with a mass of 1800 g. Conduction heat losses are considered negligible in this study. The results obtained numerically by Ginalski *et al.* [60] are compared to those obtained experimentally by Elabbassi *et al.* [62] as shown in Figure 2.3. The numerical results are almost 20% lower than

those obtained experimentally. This discrepancy in the results could be caused by the different types of incubators used in experimental and numerical studies which could affect the boundary conditions. However, the same trends could be observed where the dry heat loss decreases with increasing ambient air temperature since the neonate will lose less heat in warm environment. Moreover, the heat losses from the larger manikin are greater than those from the smaller one as depicted in Figure 2.3.

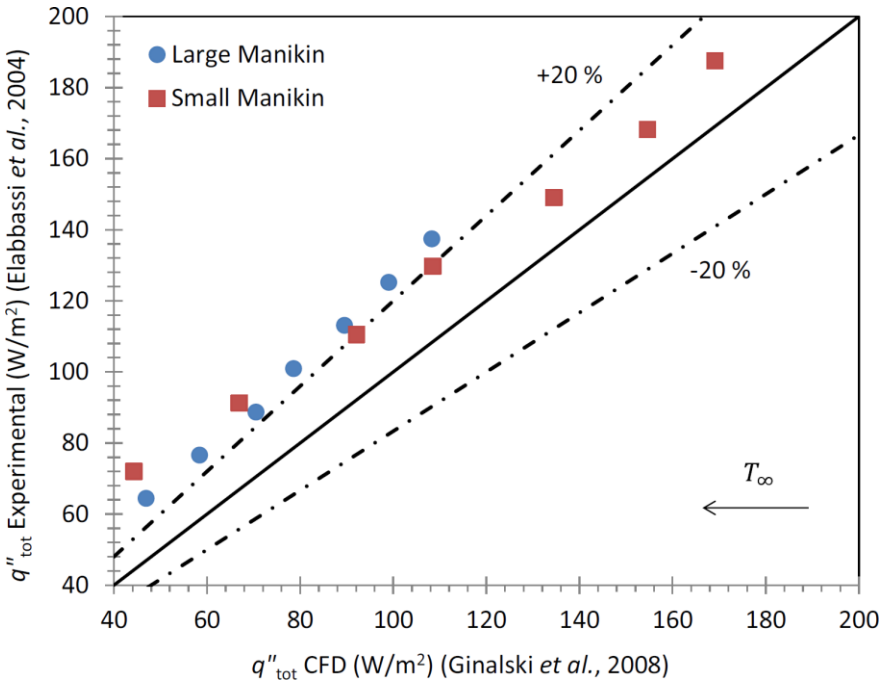

Figure 2.3: Comparison of experimental [62] and CFD [60] results for total dry heat losses $\boldsymbol{q}''$ (the curve is based on data from references [60] and [62])

2.3.2 Latent heat loss

The metabolic heat generated inside human body is dissipated through the skin to the environment as sensible, or dry, heat and as latent heat. Latent heat loss represents the evaporation of water in the respiratory system and from the skin. Thus, latent heat depends on the moistness of the skin and relative humidity of surrounding air [60].

The energy balance for human body is written as follows [63]:

$$\Delta q = \dot{q}_m \pm \dot{q}_{Cond} \pm \dot{q}_{Conv} \pm \dot{q}_{Rad} \pm \dot{q}_{Resp} - \dot{q}_E \tag{1.6}$$

where $\dot{q}_m$ is the rate at which metabolic heat is generated inside the body, $\dot{q}_{Cond}$ the conductive heat transfer, $\dot{q}_{Conv}$ the convective heat transfer, $\dot{q}_{Rad}$ the radiative heat transfer, $\dot{q}_E$ the evaporative heat loss from the skin and $\dot{q}_{Resp}$ is the rate of sensible heat transfer from respiratory system due to convection during respiration and the latent heat loss by evaporation while respiration. The $\pm$ sign refers to the fact that some rates of heat transfer could be gained or lost from the neonate depending on the incubator air temperature relative to the neonate temperature.

In Eq. (1.6), Δq could be negative or positive. If Δq is negative, this means that the body is losing heat faster than it could generate, and thus additional metabolic heat generation should be produced to maintain constant body temperature and thus to avoid hypothermia. In the opposite, when the neonate's body heat storage Δq is positive, the metabolic heat production cannot be reduced significantly since it supplies the requirements for the vital physiological functions. In this situation the thermoregulatory responses are increased in peripheral vasodilation, water evaporation and change in body posture. Thus, the goal is to increase the skin's surface area to enhance the heat exchanges with the environment. Meanwhile, this so-called sunbathing posture is of limited effectiveness in neonate.

Metabolic heat generation is usually obtained from empirical correlations while the remaining dry and latent heat losses in equation (1.6) are directly computed from the CFD simulations. Meanwhile, very few studies in the open literature have modeled the evaporation heat losses with CFD in adults [64, 65, 66] and almost none did it for neonate infants. Instead, empirical relations obtained from experimental studies were used to account for transepidermal water losses from the skin and losses due to respiration [60]. Thus, modeling the moisture transport by adding an extra scalar field equation for instance is of great importance to better analyze the relation between the humidity of air inside the incubator and the rate of water loss from neonates, especially preterm.

Ginalski *et al.* [60] developed an Infant Heat Balance Module (IHBM) coupled to ANSYS Fluent CFD solver to study and simulate latent heat losses from neonates. In this study, the sensible heat losses, i.e., convection and radiation, were obtained from the CFD solution while the other heat and mass losses are evaluated from empirical correlations.

According to the IHBM model, the conduction heat transfer $\dot{q}_{Cond}$ in equation (1.6) was neglected assuming that the mattress and infant skin are at same temperature. The metabolic heat generation $\dot{q}_m$ is obtained from the empirical equation taken by curve fitting of experimental data obtained experimentally by Bruck [67] which depends on the infant mass m_{inf}, body volume V_{inf} and postnatal age in days t_{inf}:

$$\dot{q}_m = \frac{m_{inf}}{V_{inf}}\left(0.0522 t_{inf} + 1.64\right) \tag{1.7}$$

The volumetric heat lost due to evaporation $\dot{q}_E$ from the skin is the combination of sweat and water diffusion through the skin as expressed in equation (1.8) assuming that the skin is fully wetted [63]. However, it should be noted that the sweat glands of neonates are not always fully mature, and thus evaporation is mainly due to transepidermal water loss due to the diffusion of water through the pores of the skin barrier:

$$\dot{q}_E = \frac{\dot{m}_{H_2O} i_{fg}}{V_{skin}} \tag{1.8}$$

where $\dot{m}_{H_2O}$ is the mass flow rate of evaporating water, i_{fg} is the latent heat of evaporation of water which is around 2430 kJ/kg at 30°C [63] and V_{skin} is the skin volume.

During respiration, air enters the respiratory system at ambient conditions and leaves nearly saturated at a temperature very close to the core body temperature. The heat loss accompanying air during respiration is a combination of sensible heat loss by convection and latent heat loss by evaporation and could be expressed as [63]:

$$\dot{q}_{Resp} = \frac{\dot{m}_{air}}{V_{inf}}\left[c_p(T_{ex} - T_\infty) + i_{fg}(\omega_{ex} - \omega_\infty)\right] \tag{1.9}$$

where T_{ex} and ω_{ex} are the temperature and absolute humidity of exhaled air respectively, and T_∞ and ω_∞ are the temperature and absolute humidity of ambient air, respectively. $\dot{m}_{air}$ is the mass flow rate of exhaled air by the lungs and c_p the specific heat of air.

The mass flow rate of air during respiration varies in time according to a sinusoidal function expressed as [68]:

$$\dot{m}_{air} = \eta(V_{tid} - V_{ded}) \sin(2\pi t) \tag{1.10}$$

where V_{tid} is the lungs tidal volume ranging between 22 and 23 ml, V_{ded} is the tidal dead volume which is around 8 ml and η the respiration rate which is around 52 breath/min [60, 69].

The model presented here can be readily adjusted to include clothing resistances to compute for instance the effect of wearing head cap, pajamas and diapers on the heat transfer processes. In fact, in neonatal care units, the neonates always wear a diaper associated sometimes to a head cap and even to a transparent plastic bag to reduce transepidermal water loss. Using the above thermoregulation model, Ginalski *et al.* [60] performed CFD study for different ambient conditions by varying the relative humidity between 20 and 60% and compared their data to those obtained experimentally by Hammarlund *et al.* [43] as shown in Figure 2.4. It is observed that the evaporative heat loss obtained from both methods decreases with the same slope of -0.008 with increasing relative humidity. The maximum relative difference between the experimental and numerical results reaches around 18%, mainly caused by the difference between the incubators used in both methods.

To verify the respiration modeling, Ginalski *et al.* [60] compared their results obtained from numerical simulations to those obtained experimentally by Sulyok *et al.* [70] for 4 different infants with different respiration characteristics (*i.e.* different respiration rate and flow rate, different tidal and dead lung volumes). The results for mean skin and core body temperatures are presented in Figure 2.5. The maximum relative error is around 2% which confirms the accuracy of the CFD simulations. The mean skin temperature ranges between 35.4 and 36°C while the core body temperature ranges between 36.6 and 36.9°C.

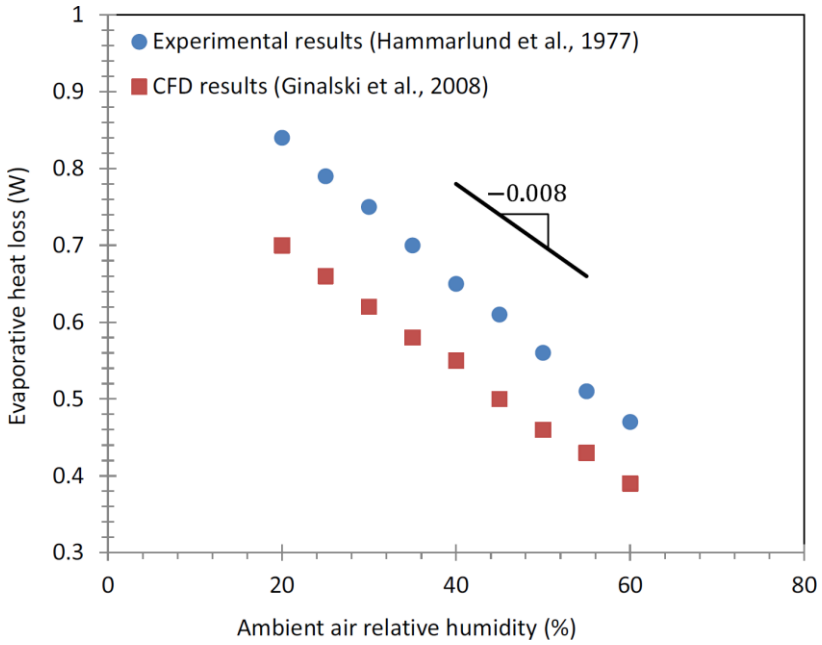

Figure 2.4: Comparison of experimental [43] and CFD [60] results for evaporative heat loss (curve is based on data from references [60] and [43])

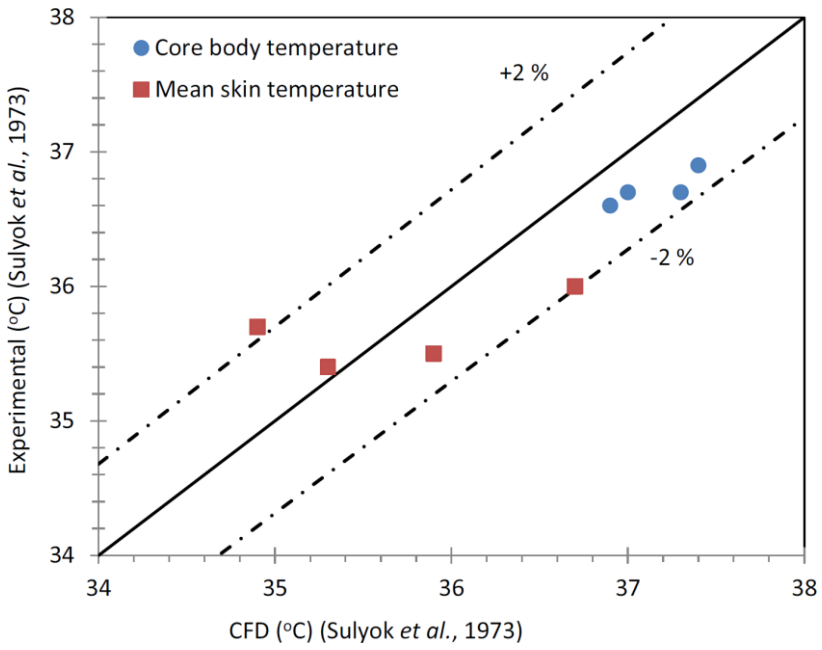

Figure 2.5: Comparison of experimental [70] and CFD [60] results for mean skin and core body temperature for 4 different infants with different respiration characteristics (curve is based on data from references [60] and [70])

2.3.3 Hygrothermal enhancement in incubators

CFD studies are also used to enhance the hygrothermal conditions in incubators. Many methods are proposed in the open literature [31]. In this section, three methods are presented namely, heated mattress [16], oxygen hood [60] and overhead screen [15].

Hannouch *et al.* [16] used a simplified geometry of an incubator with a phantom model for neonate body consisting of combination of primitive geometries. The baby skin temperature was assumed uniform and constant at 36°C. Two cases were studied: adiabatic mattress and heated mattress having a uniform heat flux equal to 5 W/m^2. The energy balance on the neonate body can be written as follows:

$$\Delta q = \dot{q}_{Metabolic} - \dot{q}_{Evaporation} - \dot{q}_{Convection} - \dot{q}_{Radiation} \tag{1.11}$$

If Δq is negative this means that the baby needs additional heating, and vice versa. It is found that without using a heated mattress Δq was around -5 W, which means that the neonate is losing heat. Meanwhile, this value was decreased to -0.13 W which means that the heat added by the mattress was beneficial to avoid cold stress.

Ginalski *et al.* [60] analyzed numerically the respiration process of a newborn infant with oxygen hood. The simulations are performed for 25 minutes respiration process. It is concluded that the CO_2 dissipated quickly which confirms that the oxygen hood is efficiently ventilated and provides the required amount of oxygen to the neonate. This type of studies helps to determine the optimum location of oxygen sensor for example in order to monitor the respiration rate of neonates.

In another study Ginalski *et al.* [15] suggest modifying the incubator by adding an overhead screen to provide additional heating by radiation. The temperature distributions on the neonate skin and inside the incubator for both cases with and without overhead screen are shown in Figure 2.6.

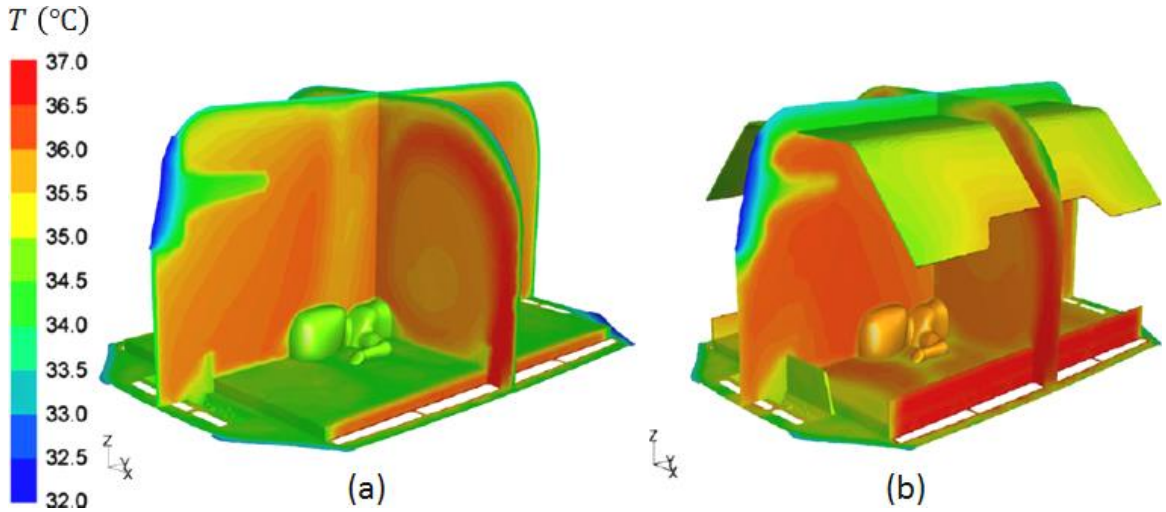

Figure 2.6: Temperature distribution for the case (a) without overhead screen and (b) with radiating overhead screen [15]

It is well observed in Figure 2.6 that by adding the overhead screen, the neonate mean skin temperature raises from around 34°C to 36°C which reduces the risk of cold stress. Moreover, Ginalski *et al.* [15] show that this modification can decrease the heat losses by radiation to the half which lead to decrease the imbalance in infant energy by almost 20%. Similar analysis was performed by Hannouch *et al.* [26] were the addition of radiant heaters increased the skin temperature by 2°C avoiding thus hypothermia.

2.3.4 Summary on CFD studies

A literature review on CFD studies for neonates in infant incubators is presented in this section and classified as dry and latent heat transfers. Some studies used primitive geometries to model the neonates while others used more robust methods by considering complex 3D geometries. Table 2.1 summarizes the different CFD studies performed in the literature with their characteristics, assumptions, and numerical models.

The main lack in CFD studies is in unsteady simulations which are essential to examine the thermal response of neonates to transient modification in ambient conditions such as air temperature and humidity. This requires coupling between CFD simulations, such as those performed in references [26, 60], and mathematical thermoregulation models, like those developed in references [21, 29]. Moreover, the modeling of transepidermal water loss

by evaporation needs more attention in future studies by computing the moisture transport equations using additional scalar equation in the CFD simulation or for instance by using the volume of fluid (VoF) approach.

Additional efforts should be done in CFD simulations to develop empirical correlations for local heat and mass transfer coefficients for different body segments. These will be of great interest for thermoregulation models which are currently assuming uniform heat and mass transfer coefficients for the whole neonate body.

Author	**Computational Domain**	**Numerical Models**	**Objectives**
Fic *et al.* [71]	• Radiant warmer • Neonate consists of half cylinder • Constant neonatal skin temperature	• Dry heat • RNG $k-\epsilon$ • Buoyancy with ideal deal gas model • Discrete Ordinates (OD) model for radiation • Neglected conduction	Convection and radiation heat losses in radiant warmers
Fic *et al.* [72]	• Radiant warmer • Neonate consists of half cylinder • Neonate as volumetric heat source simulating metabolic heat generation	• Dry heat • RNG $k-\epsilon$ • Buoyancy with ideal deal gas model • Discrete Ordinates (OD) model for radiation • Neglected conduction	Enhance the skin temperature homogeneity by placing: • a highly conductive blanket over the neonate • additional reflective screens on the mattress sides to recover the escaped radiation
Rojczyk and Szczygiel [73]	• Radiant warmer • Neonate consists of a combination of primitive geometries • Constant heat flux on neonate skin simulating metabolic heat generation	• Dry heat • RNG $k-\epsilon$ • Buoyancy with ideal deal gas model • Discrete Ordinates (OD) model for radiation • Neglected conduction • 2D and 3D models	• Convection and radiation heat losses in radiant warmers • Compare 2D and 3D results to experimental visualization
Kim *et al.* [57]	• Incubator • Neonate geometry based on 3D scanning • Constant heat flux on neonate skin simulating metabolic heat generation	• Dry heat • Standard $k-\epsilon$ • Constant thermophysical properties • Neglected conduction and radiation	• Study the vortices around the neonate • Temperature distribution at the skin

Amezzane *et al.* [58]	• Incubator • Neonate consist of a parallelepiped • Constant heat flux on neonate skin simulating metabolic heat generation	• Dry heat • RNG $k-\epsilon$ • Buoyancy with Boussinesq approximation • Neglected conduction and radiation	• Airflow, heat transfer and CO_2 transport
Hannouch *et al.* [16]	• Incubator • Neonate consists of a combination of primitive geometries • Constant neonatal skin temperature	• Dry heat • $k-\omega$ SST • Buoyancy with Boussinesq approximation • Discrete Ordinates (OD) model for radiation • Neglected conduction	• Convection and radiation heat losses with and without heated mattress
Ginalski *et al.* [60]	• Incubator • Neonate geometry based on 3D scanning • Metabolic, latent, respiratory and blood rates of heat transfer using empirical correlations	• Dry and latent heat • $k-\omega$ SST • Buoyancy with Boussinesq approximation • Discrete Ordinates (OD) model for radiation • Neglected conduction	• Effects of varying incubator air conditions (temperature and humidity) on heat losses and skin and core temperatures • Using an oxygen hood to enhance the respiratory process
Ginalski *et al.* [15]	• Incubator • Neonate geometry based on 3D scanning • Metabolic, latent, respiratory and blood rates of heat transfer using empirical correlations	• Dry and latent heat • $k-\omega$ SST • Buoyancy with Boussinesq approximation • Discrete Ordinates (OD) model for radiation • Neglected conduction	• The temperature distributions on the neonate skin and inside the incubator with and without overhead screen
Wahyuono *et al.* [74]	• Incubator • Neonate consists of a combination of primitive geometries • Constant heat flux on neonate skin simulating metabolic heat generation	• Dry heat • $k-\omega$ SST • Buoyancy with Boussinesq approximation • Radiative transfer equation (RTE) for an absorbing, emitting, and scattering medium • Conduction modeled using 1D Fourier's law	• Enhance neonate thermal comfort using an overhead screen
Wahyuono *et al.* [75]	• Incubator • Neonate consists of a combination of primitive geometries • Constant heat flux on neonate skin simulating metabolic heat generation	• Dry heat • $k-\omega$ SST • Buoyancy with Boussinesq approximation • Radiative transfer equation (RTE) for an absorbing, emitting, and scattering medium • Conduction modeled using 1D Fourier's law	• Enhance neonate thermal comfort using double wall with overhead screen

Table 2.1: Summary of different CFD studies on radiant warmers and incubators

2.4 Experimental Studies

Experimental studies on neonates nursed inside incubator can be classified into two main categories: clinical studies on newborn infants and experimental studies on thermal manikins. Mainly, manikins are used to determine the heat transfer coefficients for convection, radiation, conduction, and evaporation. These parameters are then used to determine the metabolic rate for instance.

2.4.1 Cohort of human neonates

Wheldon and Rutter [35] performed experimental studies on 12 preterm infants (mean gestation 32 weeks) to analyze the metabolic heat produced by the infant's body and the energy stored or dissipated to the ambient air and surrounding surfaces by radiation, convection, evaporation of water from the skin and respiratory track. The study was performed first in an incubator then in a radiant warmer.

The metabolic heat production was calculated by the indirect method from the rate of oxygen consumption where 1 ml of O_2 produces 20.3 Joules of heat. Radiation and convection were estimated from Stephan-Boltzmann and Newton's cooling law, respectively. Skin evaporative water loss was measured in g/m^2.h at 11 sites using an evaporimeter while respiratory water loss and oxygen consumption were measured directly using an open circuit system. Radiation, convection and skin evaporation heat losses were multiplied by 85% to account for surface area covered by the nappy. It should be noted that in their study, Wheldon and Rutter [35], disabled the incubator humidifier. Hence, they were not controlling the relative humidity inside the incubator.

Figure 2.7 shows the mean value of metabolic heat production and heat losses in incubator and radiant warmer. In this figure, the x axis correspond to heat fluxes due to metabolic generation (M), radiation (R), convection (C), skin evaporation (E_s), respiration evaporation (E_r), energy stored (S) and X is the total heat loss. When the heat flux is negative it means it is a heat gain by the infant body and vice-versa.

Three major observations can be deduced from Figure 2.7. In the incubator there is a significant heat loss by radiation, while in radiant warmer radiation is being gained by the infant body due to the presence of a radiant element. Meanwhile, the convection heat loss under incubator is much lower than that under radiant warmer because the air temperature inside incubator is controlled while under radiant warmer the infant body is exposed to ambient air inside the room. When nursed under radiant warmers, the neonate is exposed to low air humidity and, thus, the large increase in transcutaneous water loss is mainly related to the low water partial pressure of the air of the nursery room. In this case, special surveillance is required to avoid the risk of body dehydration. Moreover, the total heat loss (X) is slightly different than the metabolic heat generation, denoted M in this figure, while in concept these two terms should be equal. However, since all heat fluxes are affected by their individual measurement error, furthermore the conductive heat transfer was neglected, then the measured metabolic heat generation is not equal to the total heat loss. Thus the relative difference between X and M could be used as a measure of the percent error. We can conclude that the percent error in incubator is around 12% and around 6% in radiant warmer.

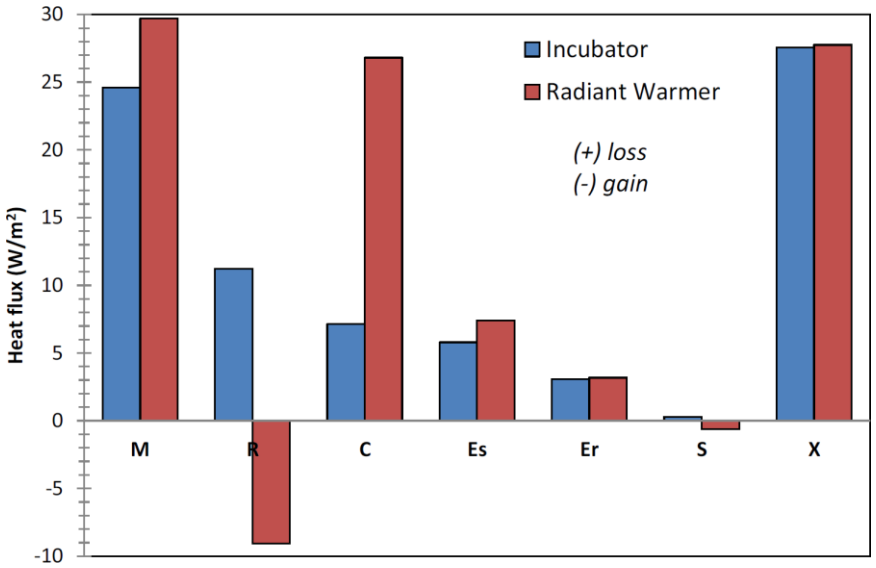

Figure 2.7: Metabolic heat production and heat losses in incubator and radiant warmer (modified from Wheldon and Rutter [35]).

Sauer *et al.* [34] performed experiments on 27 infants which postnatal age ranges between 1 and 28 days with gestational ages ranging from 29 to 34 weeks at two different levels of humidity. The incubator temperature ranges between 35°C, for babies aged less than

one week, and 33°C for babies aged more than one week. Thus, the relative humidity for babies within first week after birth ranges from 38% to 59% while after one week from birth the relative humidity ranges between 42% and 66%. The amount of evaporative losses was measured as the difference in humidity between air leaving and entering the incubator using a dewpoint hygrometer. Results show that there is no correlation between water loss and postnatal age. Moreover, the metabolic heat generation and neutral temperature did not show any significant variation with humidity, thus suggesting no need for humidification for infants born after 30-34 weeks [34]. Indeed, this could reduce additional potential risks of humidifiers in causing bacterial infections and unneeded costs [34].

In another study, Sauer *et al.* [76] defined new guidelines for the neutral temperature for healthy neonates of 29 to 34 weeks gestational age and suggested a new standard for neutral temperature as the ambient air temperature at which the core infant temperature at rest is between 36.7 and 37.3°C, and the rate of change of the core and skin temperature is less than 0.2 and 0.3°C/hour, respectively. Based on this definition, and after performing several experiments, it was shown that the neutral temperature during the first week of life is correlated to the gestational and postnatal age, according to Eq. (1.12), while after the first week of life it is correlated to the postnatal age and body weight, according to Eq. (1.13).

$$T_a = 36.6 - 0.34(GA - 30) - 0.28t_{inf} \tag{1.12}$$

$$T_a = 36 - 1.4m_{inf} - 0.03t_{inf} \tag{1.13}$$

where T_a is the neutral temperature (in °C), GA the gestational age (in weeks), t_{inf} the postnatal age (in days) and m_{inf} the body weight (in kg).

Dane and Sauer [30] designed a research double-walled incubator in order to study the dynamics of core and skin temperature of newborn babies. The experiments were performed inside the research incubator by fixing the dew point temperature at 18°C and by varying the incubator wall temperature periodically with a fundamental period length of about 1 hour. Thus, Dane and Sauer [30] correlated the thermal capacities to the body weight using linear regression. The combined thermal capacity per body weight is found to be around 3.5 kJ/kg.K which is very close to that obtained from previous studies [77]. Besides,

the combined heat transfer coefficient per unit skin surface area was around 7.5 W/m^2.K which is very close to the values obtained from experiments on neonate manikin by Wheldon [40].

A sample of heat rates and temperatures variation with time is shown in Figure 2.8 as adopted from Dane and Sauer [30]. As it can be observed the neonate response to variation in incubator temperature is highlighted by a period around 1 hour which corresponds to that of the input variation. It is also noticed that the metabolic rate is almost 4 times greater than the evaporative heat loss and that the core temperature varies very slightly around 37.35°C. Meanwhile, the skin temperature varies in the range of 35 to 37°C. However, since the dew point temperature is fixed and the air temperature varies, it would be useful to compute the variation of the relative humidity inside the incubator which has not been done by Dane and Sauer [30]. Thus, using the Magnus approximation [25], the relative humidity could be obtained from the dew point temperature and air temperature.

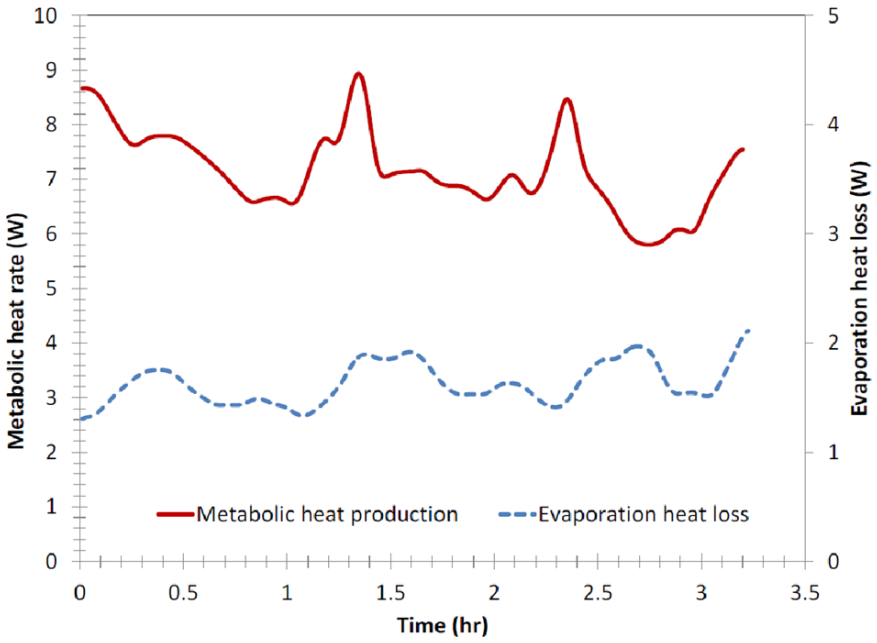

(a)

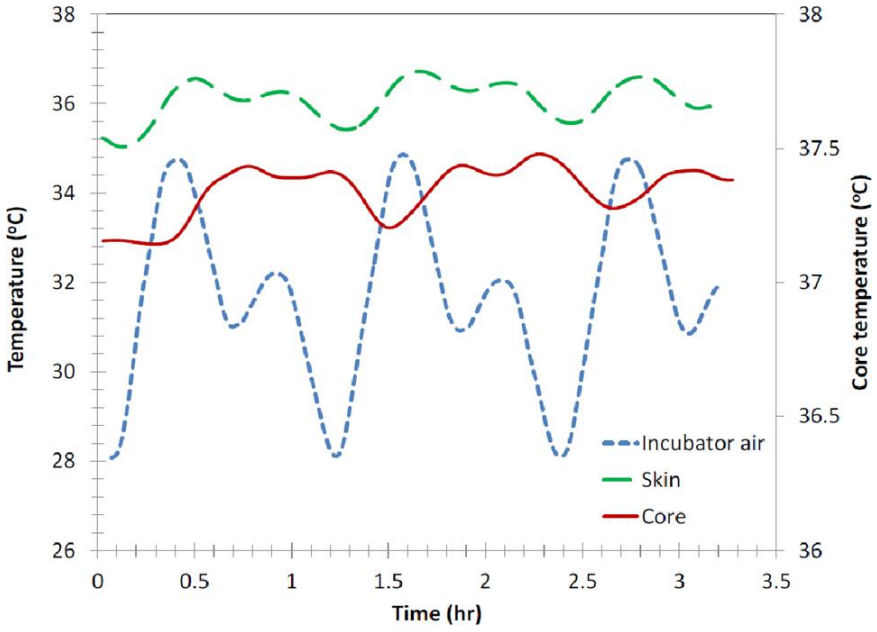

(b)

Figure 2.8: (a) Metabolic and evaporative heat rates and (b) incubator and baby temperature variation in time (modified from Dane and Sauer [30])

The variation of the relative humidity versus time is shown in Figure 2.9. The period is also close to one hour and the relative humidity is varying periodically between 37 and 54%. Calculating the Pearson's correlation coefficient ρ_{cor} between the different parameters shown in Figure 2.8 and Figure 2.9, we found that the highest correlation exist between the evaporation heat losses and the incubator temperature and relative humidity with coefficients equal to 0.8 and -0.8, respectively. The Pearson's correlation coefficient is a measure of the linear correlation between two variables. The negative correlation coefficient means that the evaporative heat losses decrease with increasing relative humidity. Meanwhile, moderate correlation existed between the metabolic rate and skin temperature with a coefficient of -0.64 which means that the skin temperature decreases with increasing metabolic rate. This is logical since once the skin temperature tends to decrease, the metabolic heat generation will increase to avoid hypothermia. Moreover, moderate correlation exists between the incubator temperature and humidity and the core temperature with respective values of -0.56 and 0.53. The other parameters have relatively low correlation with values less than ± 0.36.

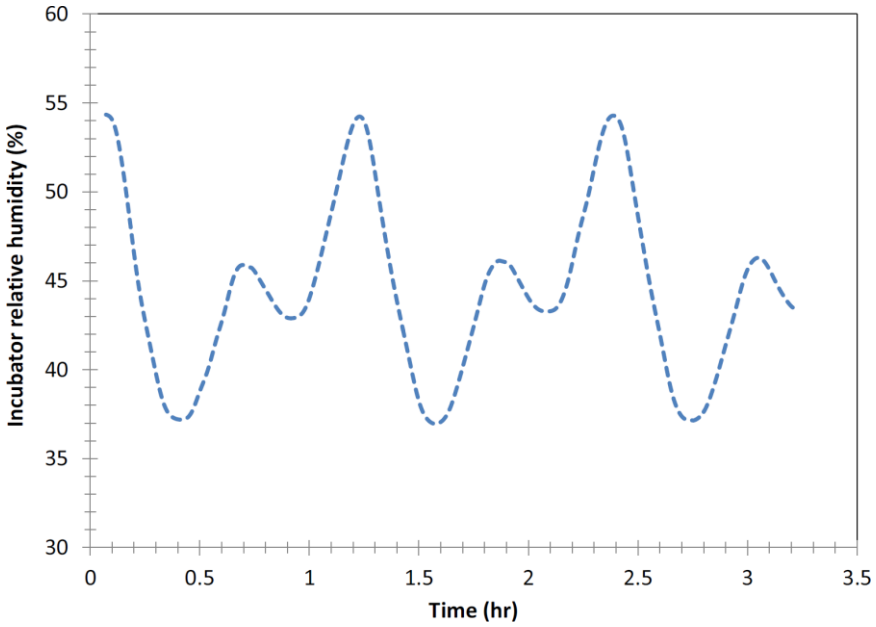

Figure 2.9: Variation of relative humidity in time based on data from Dane and Sauer [30]

Delanaud *et al.* [17] developed a mathematical model (PRETHERM®) to determine the optimal or neutral incubator temperature in terms of the air relative humidity. Their model was validated against clinical study performed on low-birth-weight infants (LBW). The clinical study is performed on 23 infant weighting about 1200 g and with 30 weeks gestational age. The Stephan-Boltzmann model for radiation and Newton's cooling law for convection are modified to take into consideration the reduction due to clothing. Delanaud *et al.* [17] defined thermal neutrality by minimizing the difference between the metabolic heat production M required to maintain homeothermia and the neonate minimal metabolic heat rate M_r obtained from definition by Chessex *et al.* [78] in terms of the postanatal age t_{inf}. Using the mathematical model and performing the experimental analysis, the neutral temperature T_a is correlated to the relative humidity ϕ, postnatal age t_{inf} and body mass m_{inf}:

$$T_a = a + b\phi + ct_{inf} + dm_{inf} \tag{1.14}$$

where a, b, c and d are coefficients depending on t_{inf} and are given in Delanaud *et al.* [17].

Compared to the correlation for T_a obtained by Sauer *et al.* [76] in Eq. (1.12) and (1.13), this study includes the effect of relative humidity on the neonatal heat losses which is

essential mainly during the first days of life for which the evaporative heat loss is very significant. By contrast, maintaining high values of ϕ is not essential after the 1st week of life because the infant skin becomes quickly mature. Hence, for instance it is found that the effect of a $\pm 20\%$ variation in ϕ could change the optimal incubator air temperature by 1°C for LBW infants. ϕ should be high enough to reduce the evaporative heat losses and reduce the neutral temperature during 1st day of newborn life.

Using similar procedure, Museux *et al.* [79] calculated the metabolic heat generation from cohort of 20 neonates with two different approaches, namely the partitioned calorimetry (PC) and indirect respiratory calorimetry (IRC). An infrared camera was used to measure the neonate surface skin temperature so that to take into consideration the heterogeneity of the skin temperature distribution. In the PC method, the metabolic heat generation M_{pc} is obtained from the energy rate balance equation while the following expression is used for the MIRC metabolic rate M_{IRC} [80]:

$$M_{IRC} = \frac{4.185(3.815 + 1.232R_{er})\dot{V}_{O_2}}{m_{inf}} \tag{1.15}$$

where $\dot{V}_{O_2}$ is the oxygen volumetric consumption (L/h), $R_{er} = \dot{V}_{CO_2}/\dot{V}_{O_2}$ is the respiratory exchange ratio and m_{inf} is the body mass. $\dot{V}_{CO_2}$ and $\dot{V}_{O_2}$ are obtained from measurement of the concentration of CO_2 and O_2 [79].

Figure 2.10 compares the metabolic heat generation obtained from IRC and PC method by Museux *et al.* [79]. It is noted that the metabolic heat generation increases by about 20% in the cool incubator relative to the case of thermoneutrality. Moreover, the data obtained from both methods agree within a relative error of about $\pm 20\%$.

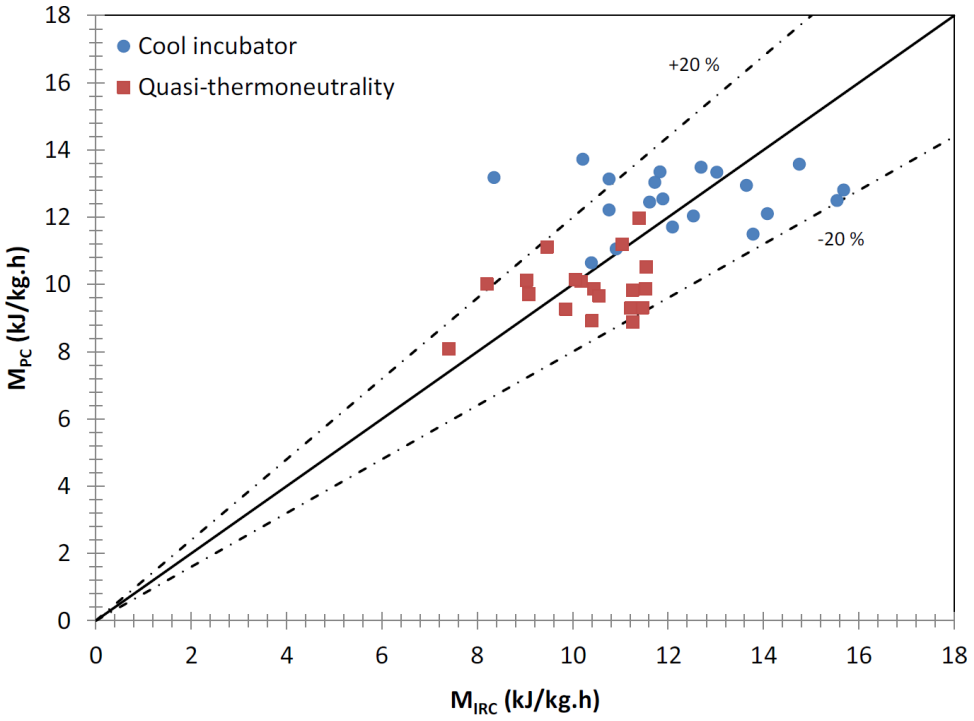

Figure 2.10: Comparison of the metabolic heat generation obtained from IRC and PC method (modified from Museux *et al.* [79])

2.4.2 Anthropomorphic thermal manikins

2.4.2.1 Dry heat loss

The main objective of experimental studies on dry heat losses from anthropomorphic thermal manikins is to provide suitable correlations and expressions for the convective (h_c) and radiative (h_r) heat transfer coefficients and for the mean radiant temperature. Moreover, using thermal manikins is beneficial to compare different systems used for neonatal nursing. In this section we discuss the different methods used to obtain these parameters. Wheldon [40] used three postures heated manikin that correspond in weight (3.3 kg) and body surface area (0.23 m^2) to that of a newborn baby, in order to study the convective and radiant heat loss from a baby inside the incubator. Conduction heat losses are neglected in this study. The surface temperature was measured using 137 thermocouples. Incident radiation was measured at ten positions over the surface using a miniature thermopile radiometer. Air temperature was measured using nine thermocouples connected in parallel and suspended uniformly

around the manikin. The mean values of convective h_c and radiative h_r heat transfer coefficients obtained by Wheldon [40] are summarized in Table 2.2. As shown in this table, both h_c and h_r increase from foetal to relaxed to spread-eagle posture except that same h_c is obtained in relaxed and spread-eagle postures. These heat transfer coefficients are within the range of those obtained for adults human bodies in the open literature [81, 82, 83].

	h_c $(\mathbf{W/m^2.K})$	$h_r(\mathbf{W/m^2.K})$
Foetal	4	3.1
Relaxed	5.4	3.7
Spread-eagle	5.4	4.9

Table 2.2: Fraction of radiant surface area A_f, convective (h_c) and radiative (h_r) heat transfer coefficients [40]

Sarman *et al.* [38] modeled a thermal manikin of size corresponding to a preterm baby weighting 1 kg with a surface area of around 0.096 m^2. The objective was to measure the dry heat losses for two different cases: incubator with adiabatic mattress and infant in bed with heated water-filled mattress (HWM). The manikin consists of eight segments in which the temperature is fixed to around 36.5°C. For the incubator case, several scenarios were studied by varying the incubator air temperature, opening one or two portholes, etc... For the HWM case, two different quilts were compared with different thermal conductivities, and it is shown that the heat losses are reduced by about 25 to 40% when doubling the thermal conductivity of quilt covering the mattress. Moreover, it is shown that the HWM case reduces the heat loss from all segments except for the anterior head relative to the manikin inside incubator.

Dry heat loss from anthropomorphic newborn manikin was also studied by Elabbassi *et al.* [62] where they compare two body sizes representing a small preterm infant of 900 g and a larger preterm infant of 1800 g with respective surface area of 0.086 m^2 and 0.15 m^2. The temperature in each segment is controlled separately by using a simple model of Proportional Integral and Derivative (PID) regulator. The values obtained by Elabbassi *et al.* [62] for the two manikins are shown in Figure 2.11 (a), and are compared to those obtained by Sarman *et al.* [38] plotted in Figure 2.11 (b). Linear regression is used to fit the experimental data for both cases. It is shown that the smaller manikin exhibits higher heat

losses than the larger one especially at low incubator air temperature by more than 20% for the cases studied by Elabbassi *et al.* [62] and between 14 and 22% for the cases studied by Sarman *et al.* [38]. However, this difference vanishes when the incubator air temperature reaches around 35 to 36°C. In fact, these results are in good agreement with the fact that the heat losses increase with increasing surface area to mass ratio (S/m) [84]. The difference in the results between Sarman *et al.* [38] and Elabbassi *et al.* [62] could be related to the difference in the manikin geometries and the heating methods as well as to the experimental techniques used in the studies. In a previous study by Elabbassi *et al.* [37], the same large manikin [62] was used to study the effect of clothing and head covering on the total dry heat losses under different incubator air temperatures. For all cases, the heat loss decreases linearly with increasing air temperature and with increasing clothing thermal insulation. Comparing the total heat lost from the whole body, it is shown that there is no significant difference between bonneted and bonnetless scenarios for all cases except for nude infant for which the addition of a bonnet can decrease heat losses by 10%. Meanwhile, adding a bonnet can decrease the local heat losses from the head up to 26% when the manikin is nude and at the lowest air temperature. Thus, it could be concluded that adding a bonnet will not decrease significantly the total heat losses from the body, but it could cause overheating of the brain as stated by Elabbassi *et al.* [37].

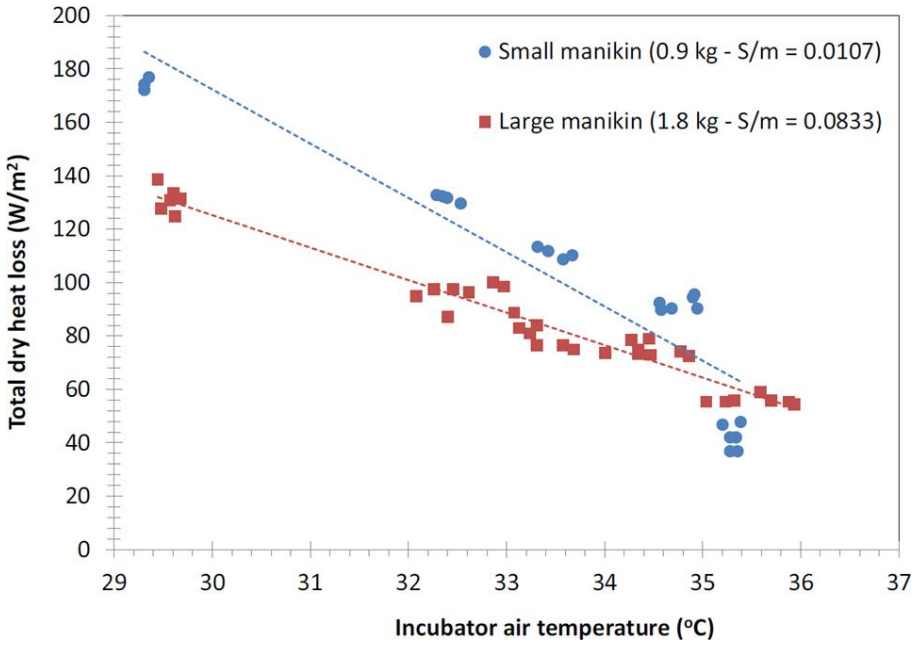

(a)

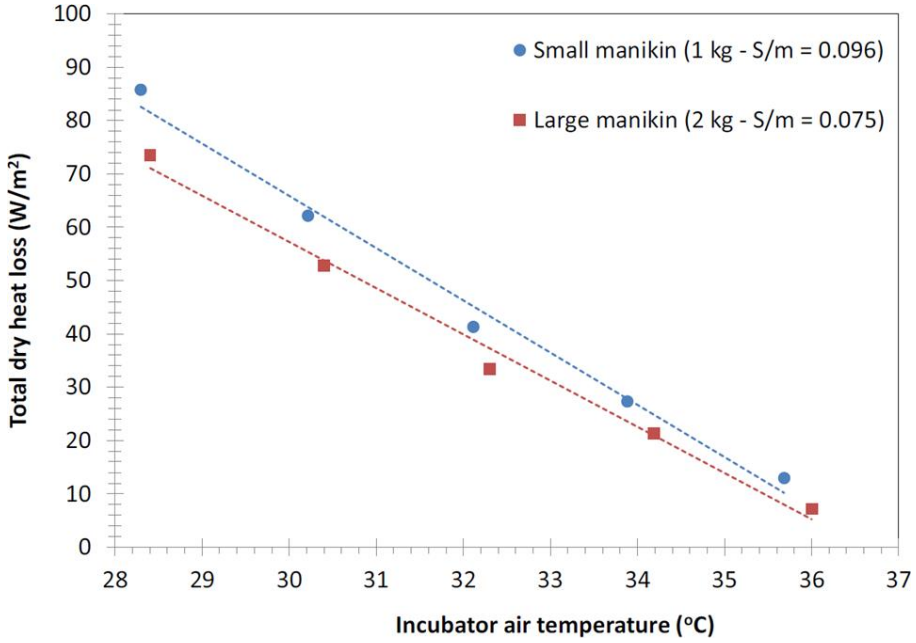

(b)

Figure 2.11: Total dry heat loss on small and large manikins obtained by (a) Elabbassi *et al.* [62] and (b) Sarman *et al.* [38]

Most of radiation heat losses occur from the roof of the incubator where there is the largest projected skin surface area [24]. Therefore, Delanaud *et al.* [24] suggested using a double roof panel. In their study, they used an anthropomorphic six segments thermal manikin simulating a low-birth-weight neonate with a body surface area of 0.086 m^2 and a weight of 900 g. The manikin was cast in copper and two cases are considered: case 1) the manikin is painted in black with a thermal emissivity $\epsilon_b = 0.97$ and case 2) covering the manikin surface by aluminum foil with emissivity $\epsilon_{al} = 0.05$. Then the mean radiant temperature T_r was evaluated from the difference in required electric power for the two cases considered. From their study, it is shown that the use of a double roof wall can reduce the mean radiant temperature by only less than 2% relative to a single roof wall.

Ostrowski *et al.* [85, 86] performed a study on dry heat losses from an anthropomorphic thermal manikin in radiant warmer fitted inside a controlled climate chamber. This experimental setup is used to represent newborn baby under free convection regime which usually occurs in radiant warmers. The objective was to obtain a correlation for the convective heat transfer coefficient [86]. It is shown that the convection heat transfer rates

based on empirical correlations for primitive geometries are overestimated by around 35% relative to those obtained experimentally using the anthropomorphic thermal manikin. Thus, a new correlation for Nusselt number Nu_D in natural convection from newborn baby is proposed in terms of Rayleigh number Ra_D and it reads:

$$Nu_D = 9.179 + 1.043 \times 10^{14} Ra_D^{-2.452} \tag{1.16}$$

In this correlation, the thermophysical properties of air are evaluated at film temperature $\left(T_f = (T_s + T_a)/2\right)$ and the trunk diameter was chosen as characteristic dimension.

Décima *et al.* [39] reviewed the different methods used to evaluate the mean radiant temperature T_r and compared the resulting metabolic rate with that obtained from IRC method which is considered as reference value. The four methods used to calculate T_r are as follows:

- Globe thermometer (GT): a method using a black globe thermometer where T_r is obtained from the globe temperature and air incubator temperature.
- View factor (VF): the view factor method where T_r is obtained by weighting the incubator surface temperatures with view or shape factors.
- Wheldon's equation (WH): the method defined by Wheldon [40] as discussed in the beginning of this section where the evaluation of T_r is based on the measurement of the incident radiation with thermopile radiometers for a simplified manikin.
- Anthropomorphic manikin (MAN): this method is proposed by Décima *et al.* [39] using a six segment manikin (similar to that used in References [62, 79]) and using the calculation procedure adopted by Delanaud *et al.* [24].

The mean radiant temperatures T_r obtained from the different methods are correlated to T_a using linear fitting as follows:

$$T_{r,GT} = 0.881(T_a - 31.93) + 31.44 \tag{1.17}$$

$$T_{r,VF} = 0.833(T_a - 31.93) + 30.39 \tag{1.18}$$

$$T_{r,WH} = 0.760(T_a - 31.93) + 29.88 \tag{1.19}$$

$$T_{r,MAN} = 0.724(T_a - 31.93) + 29.00 \quad (1.20)$$

The values for T_r are used to obtain corresponding metabolic rates using PC method introduced by Museux *et al.* [79]. The reference metabolic rate is obtained using the IRC method. To access the accuracy of each method, the resulting metabolic rate is compared to that obtained from M_{IRC} method, which is considered as reference value in Figure 2.12 for two cases: manikin in spread-eagle position and in relaxed position. As shown the lowest accuracy occurs for the GT method followed by the VF and WH methods. The MAN method based on anthropomorphic manikin represents the lowest error relative to M_{ref} where the error dropped to less than 1% for spread-eagle position and less than 5% for the relaxed position.

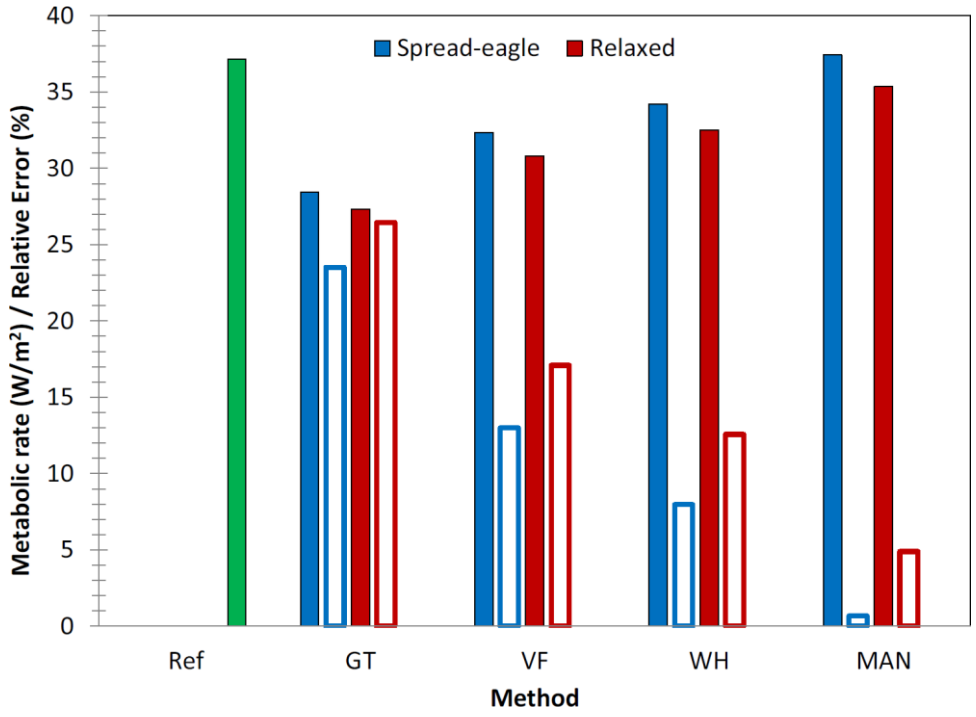

Figure 2.12: Metabolic rates obtained from the different methods for neonate in spread-eagle and relaxed positions compared to the reference value obtained from IRC which is the same for both positions. Empty bars correspond to the relative error in %. (Data taken from Decima *et al.* [39])

2.4.2.2 Latent heat loss

Most of the studies on thermal manikins are dedicated for dry heat losses, i.e., convection and radiation. However, preterm thermal manikins with sweating capabilities are very rare in the open literature as discussed in this section.

Belghazi *et al.* [41] performed experimental study to evaluate the evaporative heat loss coefficient h_e from an anthropomorphic, sweating, thermal mannequin nursed in an incubator and representing very small premature neonate with body mass 900 g. The manikin is similar to that used by Elabbassi *et al.* [62] but with some modifications to account for evaporation. The manikin's surface was shielded with a black cotton stocking to simulate sweating and water evaporation. From their study, it is observed that the evaporation heat losses increase with increasing air velocity and decreasing relative humidity but did not show significant effect with varying air temperature at fixed relative humidity. Moreover, the evaporative heat transfer coefficient was evaluated for each segment and for the whole body. For natural convection case, the whole body h_e was $7\ \mathrm{W/m^2.K}$ while its value increased from 11.7 to 14.1 $\mathrm{W/m^2.K}$ when the air speed increases from 2 to 7 cm/s. Here, and based on the data in Belghazi *et al.* [41], we developed the following correlation for h_e in terms of the air speed in the forced convection regime ($R^2 = 0.9854$):

$$h_e = 4.868V_a + 10.624 \tag{1.21}$$

Using the same manikin, Belghazi *et al.* [87] evaluated the effect of posture on the thermal efficiency of a plastic bag wrapping in neonate. It is shown that the posture has no significant effect on the evaporative heat loss for nude and covered manikin. However, the whole-body evaporative heat losses were decreased by about 3 times when using a plastic bag wrapping in neonate.

2.5 Summary on experimental studies

In this report, we review the dry and latent heat losses obtained from experimental studies on both cohort of human neonates and anthropomorphic thermal manikins. It is shown that the use of thermal manikin is promising to obtain data on heat and mass losses from

preterm neonates. Meanwhile, studies on latent heat losses are very rare and not fully developed. This type of studies is crucial to access the effect of transepidermal water losses and respiration on the thermoregulation process of neonates. More efforts should be done on the promotion of remote sensing methods, such as infrared thermography, to reduce the use of invasive methods and wires inside neonatal incubators. Experimental studies are also of great importance to validate results obtained from CFD simulations and from thermoregulation models. The different types of thermal manikins with some key features are summarized in Table 2.3.

Author	**Weight - BSA**	**Manikin**	**Dry/Latent**	**Objectives**
Wheldon [40]	3.3kg - 0.23m^2	• Manikin based on combination of primitive geometries • 3 segments • 3 different postures: foetal, relaxed and spread-eagle • Head made of thin copper ballock • Trunk and limbs are made of aluminum • Connections are made of polystyrene • Surface painted matt black with $\epsilon = 0.98$ • Electrical heating using resistance wires	Dry	Convection and radiation heat transfer coefficients
Sarman *et al.* [38]	1kg - 0.09m^2	• Cast in plastic foam • 8 segments • Electrical heating using resistance wires	Dry	Dry heat losses for two different cases: incubator with adiabatic mattress and infant in bed with heated water-filled mattress
Elabbassi *et al.* [62]	Two models: 0.9 kg - 0.086 m^2 1.8 kg - 0.15 m^2	• Cast in copper • 6 segments • Surface painted matt black with $\epsilon = 0.95$ • Electrical heating using resistance wires	Dry	• Compare the dry heat loss from two manikin with different sizes representing a small preterm infant and a larger preterm infant • The large manikin was used to study the effect of clothing and head covering on the total dry heat losses under different incubator air temperatures [56]

Delanaud *et al.* [24]	0.9 kg - 0.086 m^2	• Elabbassi *et al.* [62] manikin • 2 cases are considered: 1) the manikin is painted in black with a thermal emissivity $\epsilon_b = 0.97$ 2) covering the manikin surface by aluminum foil with emissivity $\epsilon_{al} = 0.05$. • Electrical heating using resistance wires	Dry	Measure the mean radiant temperature (T_r).
Museux *et al.* [79]	0.9 kg - 0.086 m^2	• Elabbassi *et al.* [33] manikin	Dry	Evaluate T_r, h_r, h_c and $h_{conduction}$
Ostrowski *et al.* [86]	0.13278 m^2	• Cast in copper • 1 segment • Surface painted matt black with $\epsilon = 0.99$ • Water heating system	Dry	Obtain a correlation for the convective heat transfer coefficient in natural convection
Bandola *et al.* [54] and Laszczyk *et al.* [55, 56]		• Ostrowski *et al.* [57]	Dry	Neonate brain cooling using a cooling helmet
Kang *et al.* [88]	2 years old baby 0.47 m^2	• Fiberglass shell reinforced with plastic • 16 segments • 32 sweating pores drilled through its surface • The manikin was dressed in cotton knitted suit simulating the human skin • Manganese wires with platinum resistance thermometers	Latent	Evaluate the sweat rates from the manikin and compare the values against those obtained for a two-year-old Japanese infant
Belghazi *et al.* [41]	0.9 kg - 0.086 m^2	• Elabbassi *et al.* [33] manikin • Black wet cotton to simulate sweating	Latent	Evaluate the evaporative heat loss coefficient h_e

Table 2.3: Summary of the different types of neonate thermal manikins

2.6 Conclusions

This Chapter presented a review of the different methods used to model and analyze bioheat transfer and thermoregulation in neonatal intensive care units especially incubators. Bioheat transfer models range from multi-node mathematical one-dimensional modeling to finite element simulations of complex neonate body obtained from 3D scanning method. The aim is to provide an insight into the heat losses from neonates and body-environment interaction under different ambient conditions, namely air temperature and humidity. These

models can predict the skin and core temperature during both thermal neutrality and transient clinical processes. The heat and mass transfer coefficients needed by these mathematical models are obtained from numerical or experimental studies performed mainly on thermal anthropomorphic manikins.

CFD methods have been widely used to analyze the dry heat losses from neonates in both radiant warmers and incubators. The modeling ranges from using phantom models consisting on primitive geometries to realistic numerical manikins obtain from 3D scanning methods. Fewer studies are performed for latent heat losses in which respiratory and skin evaporation processes should be included. Moreover, CFD analyses are used to enhance hygrothermal conditions by using for instance double wall incubator, overhead screens, heated mattress, and cooling helmet. The objective is always to avoid hypothermia and injuries for preterm neonates.

Finally, experimental methods were classified into studies on cohort of human neonates and thermal manikins. The latter is more preferred by scientists since it does not require involving human neonates in experimental studies and the use of thermal manikins can avoid errors caused by motion and disturbance from neonates. Meanwhile, more progress should be done on latent heat losses from anthropomorphic manikins from point of view of the evaporation system used and on the measurement devices.

In this Chapter we focus on the continuing challenges of achieving and maintaining optimal thermal environment in infant incubators to avoid the risk of hypothermia. However, the same theoretical, numerical, and experimental methods, discussed in this Chapter, can be applied to manage, and analyze heat stress and hyperthermia. There is no doubt that neonates are particularly at risk of body cooling, however, hyperthermia induced by impaired heat losses can be implicated in pathophysiological problems such as hemorrhagic shock, apneic attacks, and encephalopathy.

Chapter 3 Preterm Manikin and Incubator Geometries

Dans ce chapitre nous présentons le mannequin thermique et l'incubateur utilisés dans les études numérique et expérimentale. Un mannequin anthropomorphique représentant un nourrisson prématuré âgé de 35 semaines gestationnelles est fabriqué par la méthode de l'impression 3D et il est constitué de 5 segments corporels : tête, bras, torse, dos et jambes. Une géométrie virtuelle de ce mannequin est aussi utilisée dans les simulations numériques par la méthode de volumes finis. Le mannequin est placé à l'intérieur d'un incubateur Caleo Drager. Le mode de fonctionnement de cet incubateur est présenté en détail dans ce chapitre. Un modèle virtuel de l'incubateur est préparé par un logiciel CAD afin que l'on puisse l'utiliser dans les simulations numériques.

3.1 Introduction

In the present thesis, the experimental setup as well as the computation domain consist mainly of two systems. The first system is the infant incubator in which the temperature of the air and its humidity could be controlled. Another control method would be by monitoring the infant skin and core temperatures and controlling the air temperature accordingly. The second system is the thermal manikin which is designed to mimic realistic preterm neonates' geometry and dimensions as well as a thermal control system simulating the metabolic heat generation. In this Chapter we present the infant incubator adopted in our studies in section 3.2 and in section 3.3 we present the geometry and dimensions of an anthropomorphic thermal manikin and its manufacturing method.

3.2 Infant Incubator

The infant incubator used in our studies consists of a Drager Caleo incubator [38] and it is shown in Figure 3.1. This incubator was donated to us by Drager[1] (Germany) and Prime Medical[2] (Lebanon) and it is located in the Thermo-Fluids laboratory at Notre Dame University-Louaize[3].

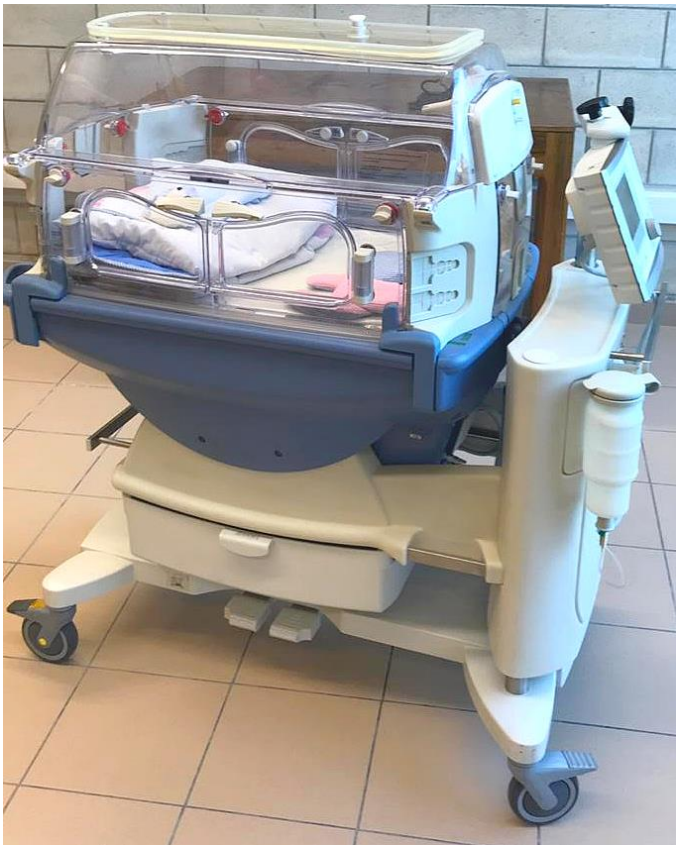

Figure 3.1: Caleo Drager infant incubator in the Thermo-Fluids laboratory at Notre Dame Univresity-Louaize.

The heating occurs below the mattress where an electric heater is used and a fan below the mattress circulates the heated air to the hood from, both sides as shown schematically in Figure 3.2. The air is then directed down back to the heater from the transverse sides by suction. A fan impeller is used to circulate the air in the incubator, and it

[1] Dräger, Lübeck, Germany: https://www.draeger.com/
[2] Prime Medical S.A.L., Beirut, Lebanon: http://www.saturntrust.com/primeMedical.html
[3] https://www.ndu.edu.lb/

is located below the mattress along with an electrically powered heater and humidifier. It insured that low air speeds are maintained in the hood so that the nursed neonate lies in a calm environment. The maximum electric power of the air and water heaters is around 700 W.

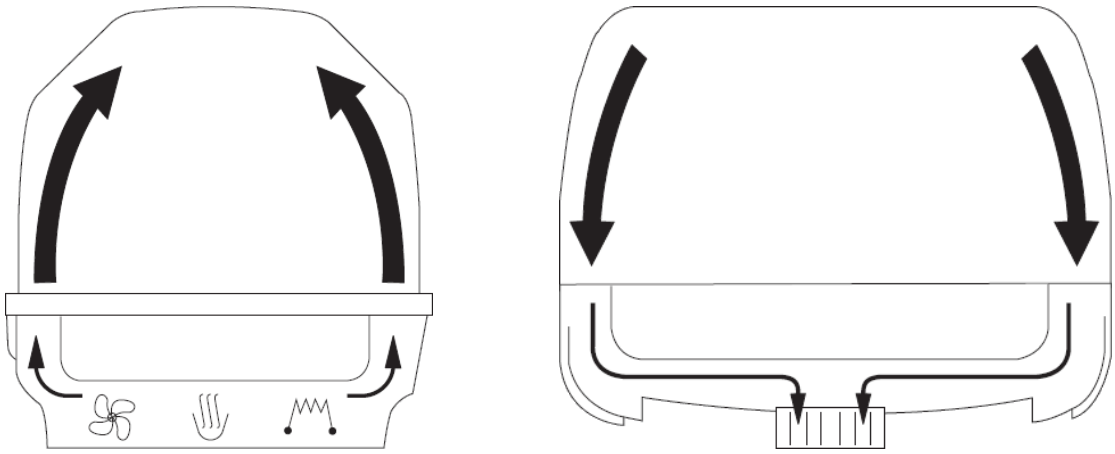

(a) (b)

Figure 3.2: Schematic showing the airflow routing in the Caleo Drager incubator [38].

This incubator has advanced thermoregulation capability by delivering the appropriate temperature, humidity, and oxygen levels. Moreover, the infant temperature inside this incubator could be monitored continuously measuring both central (core) and peripheral (skin) temperatures (Figure 3.3) which is important to predict hypo or hyperthermia. In fact, when the difference between the central temperature and the peripheral temperature is less than a set value there will be a risk of hyperthermia and the alarm will be triggered. When this temperature difference becomes larger than a set value, there will be a risk of hypothermia and the alarm would be also triggered as depicted graphically in Figure 3.3.

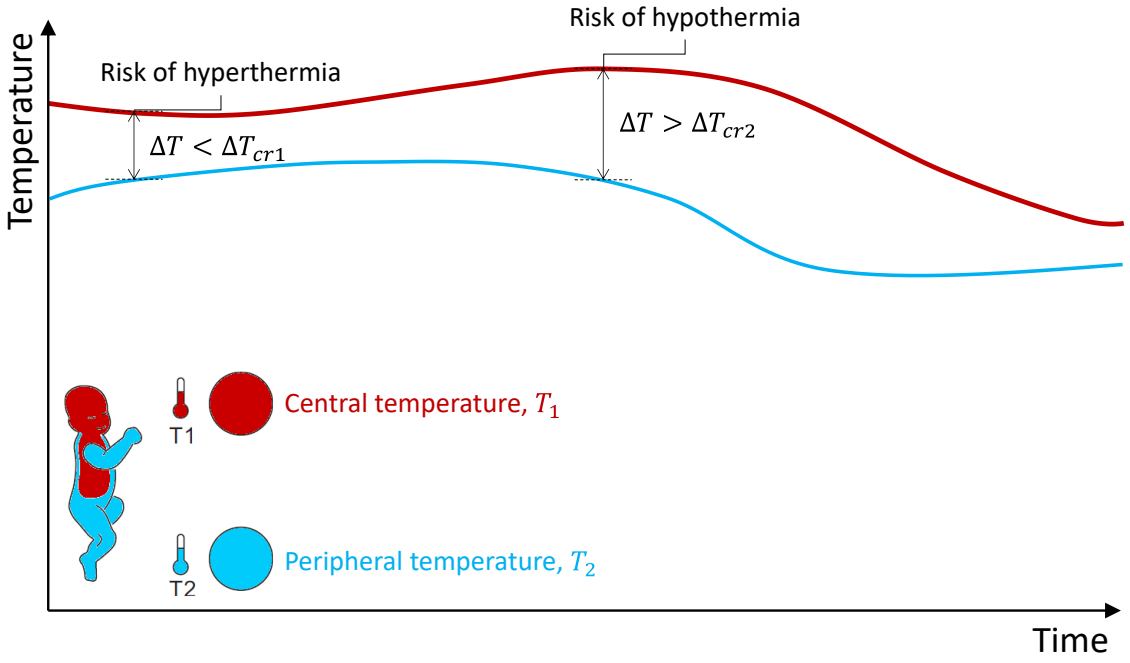

Figure 3.3: Sketch showing graphically when the alarm would be activated in case a risk of hyperthermia or hypothermia are detected.

In addition to controlling the air temperature, the humidity could be also set to a fixed value or auto controlled as a function of the air temperature according to the graph shown in Figure 3.4. This relation is based on the observation that immature neonates require higher air temperature and humidity than full term neonates.

Oxygen concentration could be also controlled in this incubator where the additional oxygen supply is metered by a microprocessor-controlled valve. The oxygen is thereby channeled into the air routing system, so that it is heated and humidified with the air.

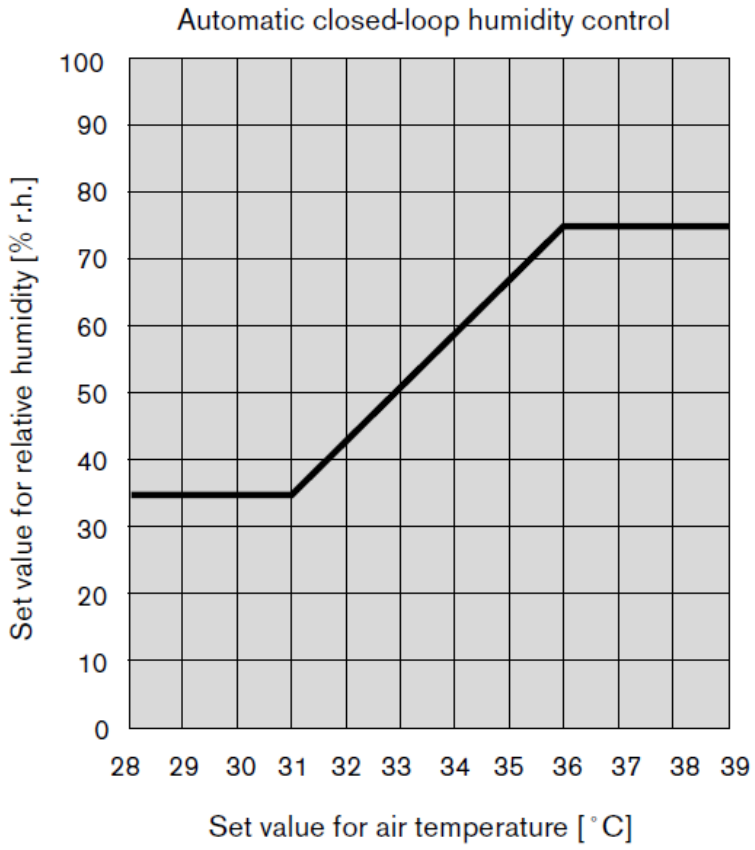

Figure 3.4: The graph used to calculate and auto control the relative humidity as function of the air temperature [38].

The incubator has double air curtain offering a stable climate even when access windows are open by health care providers as shown in Figure 3.5. This feature is possible since the air inlets are located just in front of the access windows from both sides of the incubator. Moreover, the incubator operates according to two different modes. In the air mode, the nurse can set the incubator air temperature and humidity to a fixed value. In the skin mode, the nurse will fix the skin set temperature and the incubator will regulates the air temperature automatically.

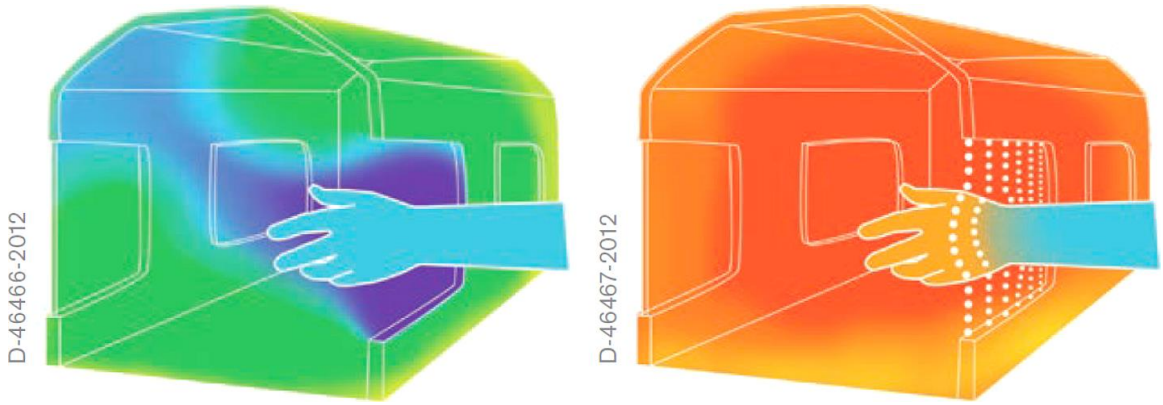

Figure 3.5: Temperature distribution on a random RGB scale: blue for cold and red for hot. (left) Incubator without air curtain and (right) incubator with air curtain during healthcare provider intervention with open access windows [61].

Since a 3D numerical model did not exist and since it is needed for the CFD simulations, we used SolidWorks CAD software to draw the incubator based on actual dimensions of the real incubator. Figure 3.6 shows a rendered image obtained from SolidWorks where the similarity between the real incubator and the numerical one is clear (compare with Figure 3.1). The warm air inlets are located on the windows side and they can act as air curtains when the windows are open by the care giving staff. A centrifugal fan below the mattress is used to recirculate the heated air in the incubator. Even though a specific infant incubator has been used in the present study, however, the results obtained in this paper could be still valid for other incubators in the market which are somehow similar from their dimensions and location of air inlets.

Figure 3.6: Rendered figure showing the Caleo Drager neonatal incubator drawn using SolidWorks with the preterm neonate manikin laying on its mattress.

3.3 Preterm thermal manikin

An anthropomorphic manikin is designed to represent a moderate preterm infant of 35 week of gestational age in the 50^{th} percentile [36]. Thus the manikin mimics a neonate weighting 2.5 kg with a length of 46 cm based on the revised growth chart by Fenton *et al.* [36] as shown in Figure 3.7. The total surface area of the manikin is $0.133\ m^2$ as suggested by Ostrowski and Rojczyk [33].

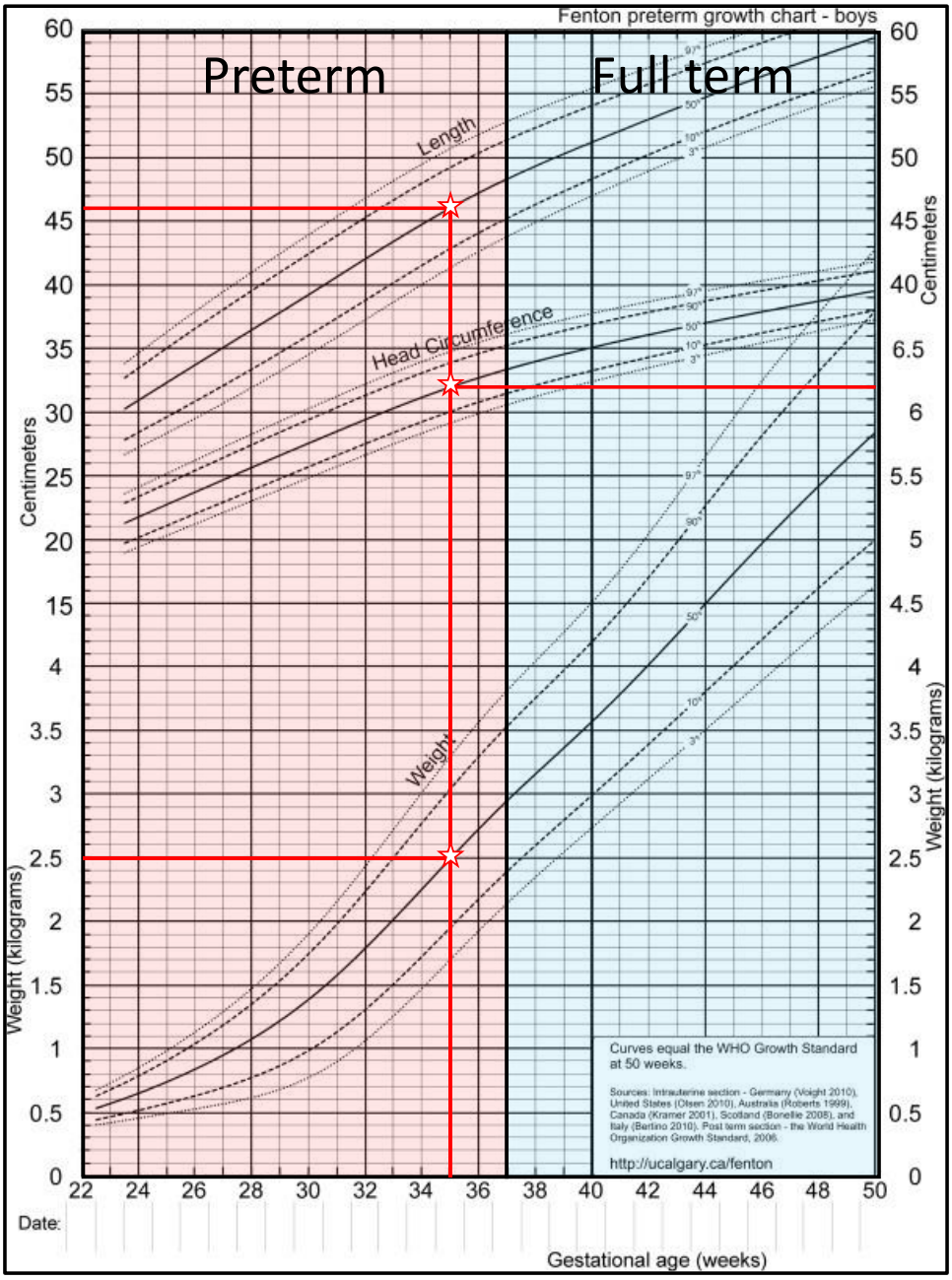

Figure 3.7: Revised growth chart for boys suggested by Fenton and Kim [36] showing the region for preterm neonates (gestational age less than 37 weeks) and full term neonates (above 37 gestational weeks) [89]. In the present study, a preterm neonate 35 week of gestational age in the 50th percentile is considered. The corresponding weight, length and head circumference are depicted on this figure.

The manikin is designed using Autodesk 3DS Max software which is a powerful computer graphics for complex 3D geometries [90]. Figure 3.8 shows different isometric views of the thermal manikin which dimensions are presented in the previous paragraph.

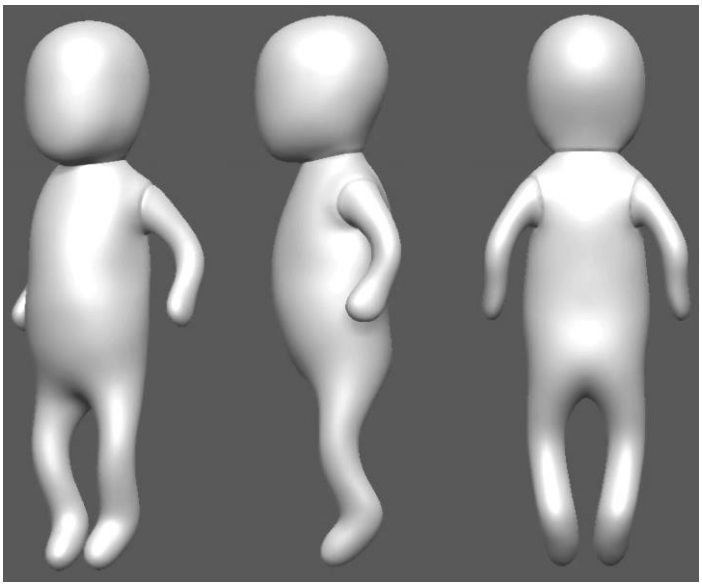

Figure 3.8: Three images showing different views of the thermal manikin designed using Autodesk 3DS Max software.

In the present study we aim to investigate the segmental heat losses from the preterm thermal manikin, i.e., local heat transfer from different body segments. Therefore, the manikin is divided into five body segments, as shown in Figure 3.9, consisting of the head, arms, legs, back and trunk. The percentage of total body surface area or surface fractions are represented in Table 3.1.

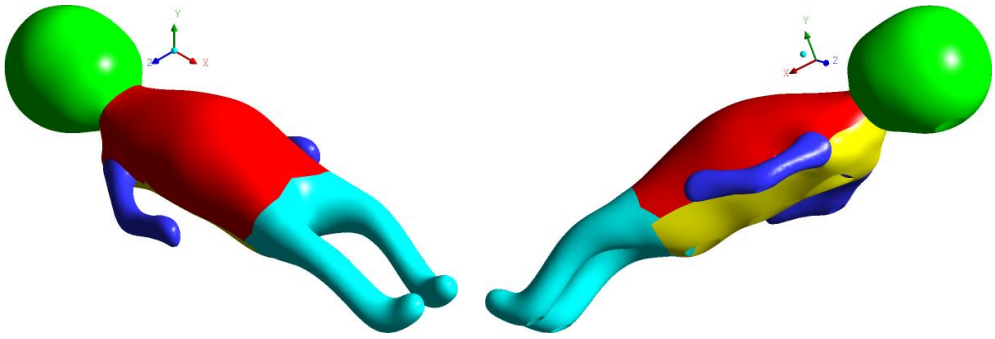

Figure 3.9: Isometric views showing the thermal manikin with the different body segments: head (green), arms (blue), legs (cyan), back (yellow) and trunk (red)

On each body segment, different skin surface set temperatures are imposed as given in Table 3.1. These values are commonly observed for healthy preterm neonates as reported by Elabbassi *et al.* [37] and Belghazi *et al.* [35]. The method adopted to maintain constant segmental average surface temperature for the manikin during the experimental studies will be discussed in detail in Chapter 1.

Segment	**Arms**	**Back**	**Head**	**Legs**	**Trunk**
Surface fraction (%)	10.8	13.4	25.7	24.6	25.5
Skin temperature (°C)	33.53	36.60	36.40	35.54	35.54

Table 3.1: Characteristics of the thermal manikin showing the surface relative size of different body segments with corresponding surface temperatures.

Different manufacturing methods and materials are used in developing multisegment thermal manikins in the open literature, such as copper, aluminum, plastic and various types of fabrics [91, 92]. For preterm thermal manikin, the most widely used manufacturing method is by cast in copper and painting the surface in matt (graphite) black so that the emissivity is around 0.95; similar to that of human skin. Preterm thermal manikins used in the open literature are presented in Figure 3.10.

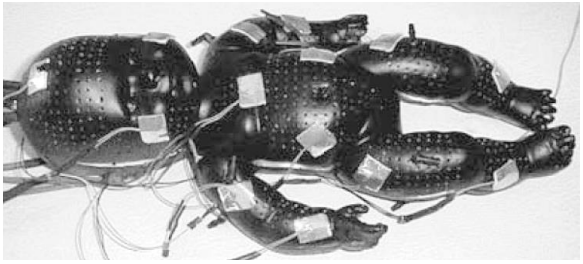

Elabbassi and Belghazi [62]

(b) Ostrowski and Rojczyk [86]

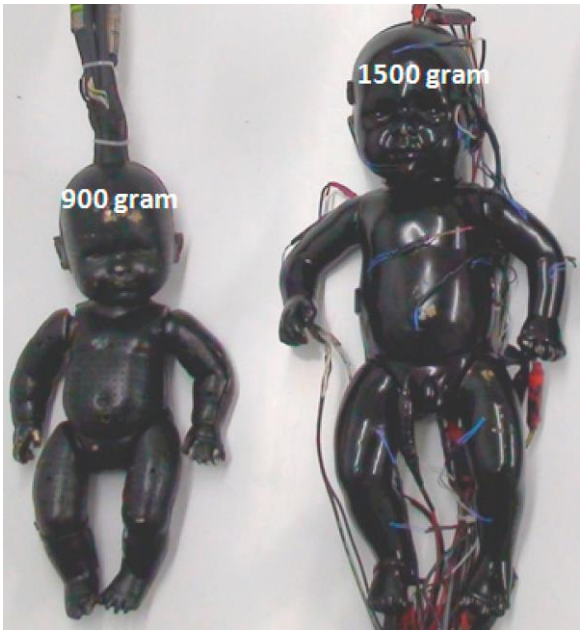

(c) Delanaud et al. [93]

Figure 3.10: Preterm thermal manikins used in the literature.

While copper cast anthropomorphic thermal manikins are practical to use due to the high thermal conductivity of copper, however, their manufacturing is relatively complex and expensive. Thus, in our study we decided to use 3D printing technique in order to construct the manikin. The 3D printing technique is called Fused Deposition Modeling (FDM) 3D printing where the objects are constructed by selectively depositing the melted material in a pre-defined path layer by layer [94] as depicted in Figure 3.11 (a). The 3D printer we used is the Flashforge Guider II [95], as shown in Figure 3.11 (b), and the material consists of PETG filaments.

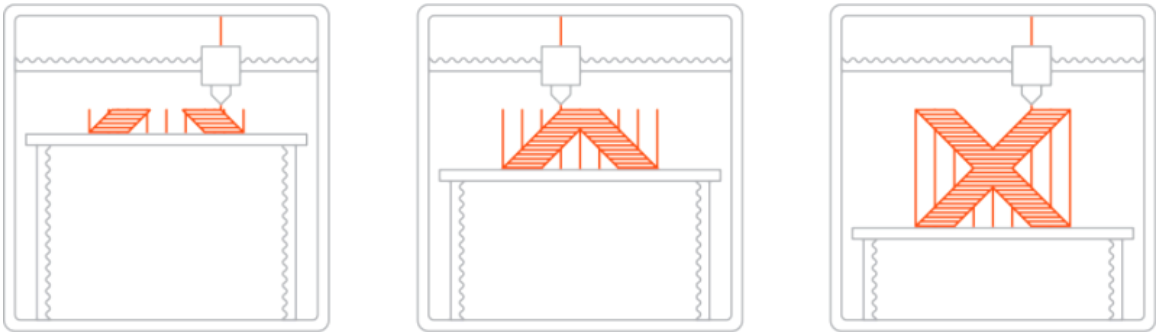

(a)

(b)

Figure 3.11: (b) A schematic showing the FDM printing process where the are constructed by selectively depositing the melted material in a pre-defined path layer by layer [96] and (b) the Flashforge Guider II 3D printer we used [95].

Since the size of the manikin exceeds the dimensions of the 3D printer, it was divided into smaller parts which were later welded together. 3D printing PETG wires were used to connect the parts together and fill the gaps. The wires are melted on the joints to fix them to each other, making the surface homogeneous. The color of the manikin surface is matt black so that its emissivity is set very close to 0.95 to mimic real emissivity of human skin [37, 60]. The instrumentation of the thermal manikin with heating wires and thermocouples and the control method will be presented in Chapter 1 devoted to the experimental analysis.

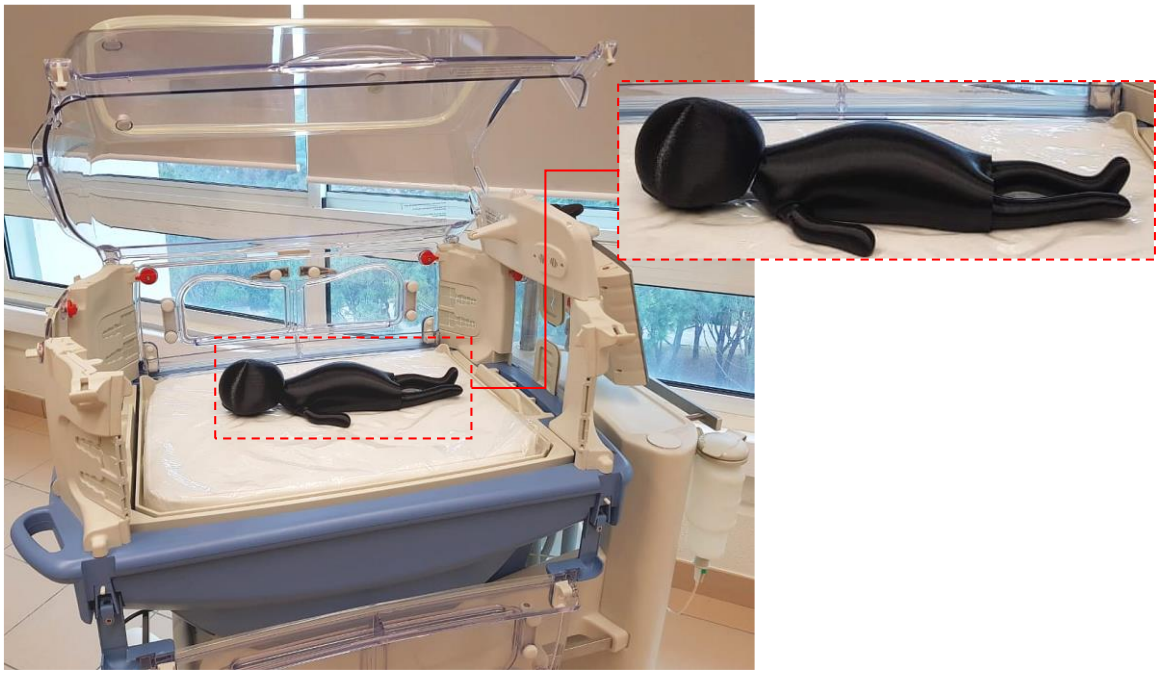

Figure 3.12: The preterm thermal manikin called “Calor” laying inside the Caleo Drager incubator.

The neonate thermal manikin numerical model prepared with 3DS Max is imported to Solidworks and implemented inside the infant incubator presented in the previous section. Figure 3.13 shows a rendered image of the preterm thermal manikin nursed inside the Caleo infant incubator. The manikin color is black but was modified in this figure for esthetic purposes.

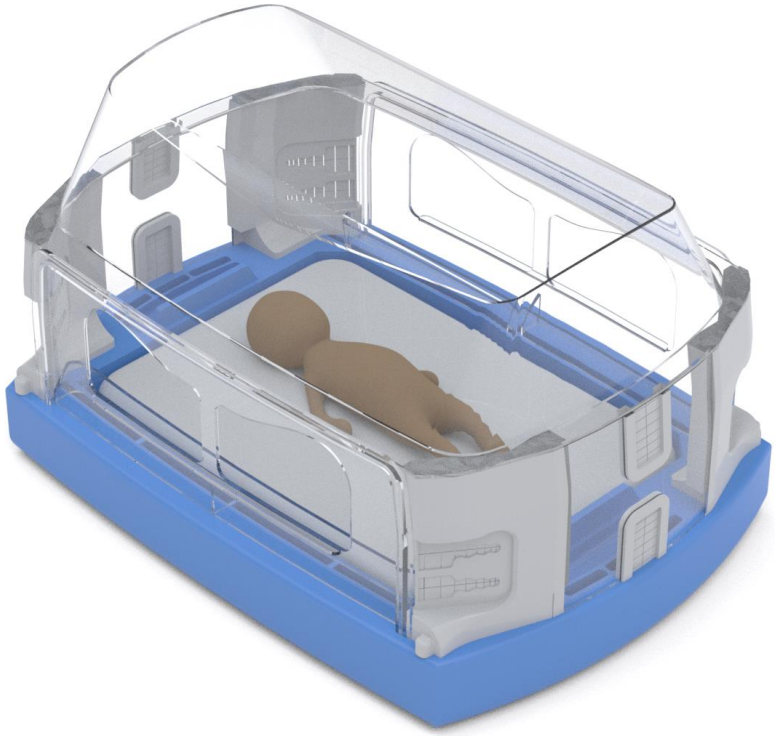

Figure 3.13: Numerical model of the preterm infant manikin nursed inside the Caleo incubator.

3.4 Conclusions

In this chapter we presented the geometries and dimensions of the infant incubator and preterm thermal manikin used for both experimental and numerical analyses. A Caleo Drager infant incubator was donated to our research group by Drager (Germany) and Prime Medic (Lebanon) and it is located at Notre Dame University-Louaize. This incubator was later drawn, and a numerical model was generated using SolidWorks CAD software so that it could be implemented in the CFD simulations.

The 3D printing technique was used to build an anthropomorphic thermal manikin representing a preterm neonate of 35 weeks gestational age. This manikin was divided into 5 segments to allow us to determine local segmental heat transfer coefficients and processes. The thermal manikin was then inserted inside the numerical model of the infant incubator to form the computational domain used in the CFD simulations.

Chapter 4 Numerical Analysis

Plusieurs modèles de thermorégulation et de transfert de chaleur pour les nouveau-nés prématurés sont utilisés pour étudier le transfert de chaleur à l'intérieur des incubateurs. Ces modèles nécessitent de connaitre les coefficients de transfert de chaleur de rayonnement et de convection distinctifs pour différents segments du corps. Dans ce chapitre, des simulations numériques sont effectuées pour un nouveau-né prématuré composé de 5 segments (tête, bras, torse, dos et jambes) placé à l'intérieur d'un incubateur. Les études sont menées en faisant varier la température d'entrée de l'incubateur entre 29 et 35°C et différents débits d'air entre 5 et 50 litres/min. On constate que le processus de transfert de chaleur dépend principalement de la température de l'air dans l'incubateur. On montre que le débit d'air de l'incubateur n'affecte pas de manière significative le transfert de chaleur convectif. Ainsi, il est conclu que le transfert de chaleur entre l'air de l'incubateur et le nourrisson est causé par la convection naturelle. L'effet de la structure de l'écoulement sur la distribution de la température est étudié et des corrélations pour les coefficients de transfert thermique radiatif et convectif sont obtenues pour chaque segment corporel. Le coefficient de transfert thermique radiatif varie entre 2,2 et 6,2 W/m^2K tandis que le coefficient de transfert thermique convectif varie entre 2,6 et 4,7 W/m^2K. Les résultats sont validés par des données expérimentales de la littérature. Finalement, un modèle de thermorégulation est développé en tenant compte des pertes de chaleur et de masse dues à l'évaporation cutanée et à la respiration. Ce modèle est utilisé pour quantifier le bilan thermique chez les nouveau-nés prématurés dans les incubateurs.

4.1 Introduction

Defining the optimal hygrothermal conditions inside an incubator requires understanding and quantifying heat and mass transfers between the neonate and its surrounding environment which is done using experimental, numerical, and theoretical studies [62, 31, 50, 56]. In the meantime, theoretical modeling of bioheat transfer requires the knowledge of radiative and convective heat transfer coefficients on the skin surface which could be obtained using experimental or numerical thermal manikins.

With regards to thermoregulation in adults, numerous studies are performed to derive correlations for the heat transfer coefficients under various environmental conditions [83, 97, 98]. Ishigaki *et al.* [99] obtained experimental correlations for the convective heat transfer coefficient in natural, mixed and forced convection and deduced thermally equivalent sphere and cylinder diameter for adult human body. De Dear *et al.* [82] used experimental thermal manikin to determine both convective and radiative heat transfer coefficients in natural and forced convection for individual body segments in standing and sitting postures. Similar correlations were also obtained by Kurazumi *et al.* [100] only for natural convection but for five various body postures. Gao *et al.* [101] and Oh *et al.* [81] extended this study by using both experimental and computational fluid dynamics (CFD) allowing analysis of the airflow around the manikin to better understand its effect on heat transfer processes. In addition, Oh *et al.* [81] computed the equivalent temperature to evaluate the effects of airspeed and wind direction on the thermal comfort of human body. Li *et al.* [102] examined heat losses and convective heat transfer coefficient in strong convective flow mimicking windy situations using both experimental and CFD methods. Several turbulence models were used, and they found that the $k-\omega$ SST turbulence model agrees better with experimental findings for front facing wind for velocities lower than 6 m/s. This was later confirmed in another study in which the $k-\omega$ SST results were better than those obtained using the $k-\epsilon$ turbulence models [103].

With regards to neonates, and especially preterm babies, most of the studies focus on the evaluation of sensible and latent heat losses using different methods such as theoretical bioheat modeling [29, 21], experimental studies on cohort of human neonates [24] or on

anthropomorphic thermal manikins [38, 37] and using numerical simulations [60, 26]. For instance, Sauer *et al.* [34] performed experiments on cohort of newborn infants aged between 1 and 28 days with gestational ages ranging from 29 to 34 weeks at two different levels of humidity. It is found that the metabolic heat generation and neutral temperature did not show any significant variation with humidity, suggesting thus no need for extra humidification for these infants. Adams *et al.* [13] developed novel method to determine the energy expenditure from neonates by using infrared thermographic calorimetry inside an incubator. A good agreement was found when comparing their infrared methodology to classical experimental methods to evaluate both dry and latent heat losses. Coupling computational fluid dynamics to an infant theoretical heat balance module, Ginalski *et al.* [60] analyzed the radiative and convective heat losses from preterm neonates inside incubators and validated their results against data from the literature. They hence proposed new methods to enhance the thermal balance and decrease dry and latent heat losses by using for instance a radiant overhead screen [15].

While most of the studies on neonates focus on quantifying heat and mass losses, very few were developed to determine suitable correlations for heat transfer coefficients [40, 86]. We cite for instance the experimental study performed by Museux *et al.* [79] who evaluated the whole body mean radiant temperature and heat transfer coefficients for convection and radiation using a anthropomorphic thermal manikin inside an incubator with natural convection. Belghazi *et al.* [41] used a multi-segment thermal manikin inside an incubator to determine evaporation heat transfer coefficient in natural and forced convection from individual body segments. They found that increasing the airspeed led to an increase in the heterogeneity of skin cooling as well as raising the evaporation losses. Finally, Ostrowski and Rojczyk [73] determined whole body correlations for convective heat transfer coefficient using a thermal manikin in a radiant warmer. In all these studies, there are no correlations for the heat transfer coefficients for individual preterm body segments inside an incubator. These correlations are fundamental for theoretical bioheat models so that they could be used as boundary conditions. Thus, the main objective of the present paper is to develop segmental correlations for the convective and radiative heat transfer coefficients for a preterm neonate nursed inside an incubator. Moreover, a heat balance model for the preterm neonates is developed to access their thermal comfort inside incubators.

In the present Chapter, CFD simulations are carried out using an anthropomorphic thermal manikin representing a preterm baby nursed inside a Caleo Drager incubator as described in section 4.2. The numerical methods are discussed in section 4.4 followed by a mesh sensitivity analysis in section 4.5. This study focusses on both analyzing the flow structure and heat losses from the neonate as well as determining individual body segment correlations for convection and radiation as presented in section 4.7. In addition, an assessment of the thermal balance is performed by coupling the numerical results to a simplified theoretical model. Finally, section 4.8 is devoted for the concluding remarks.

4.2 Computational Domain and Boundary Conditions

The computational domain consists of the Caleo Drager incubator presented in section 3.2 in which the preterm neonate manikin presented in section 3.3 is inserted. The manikin consists of five segments as shown in Figure 3.9. The assembly of the incubator and thermal manikin forming the computational domain for the CFD analysis is shown in Figure 4.1. In this figure, the heated air inlets are colored in green while the heated air outlets are colored in red. The boundary and operating conditions are presented in the next section of this chapter.

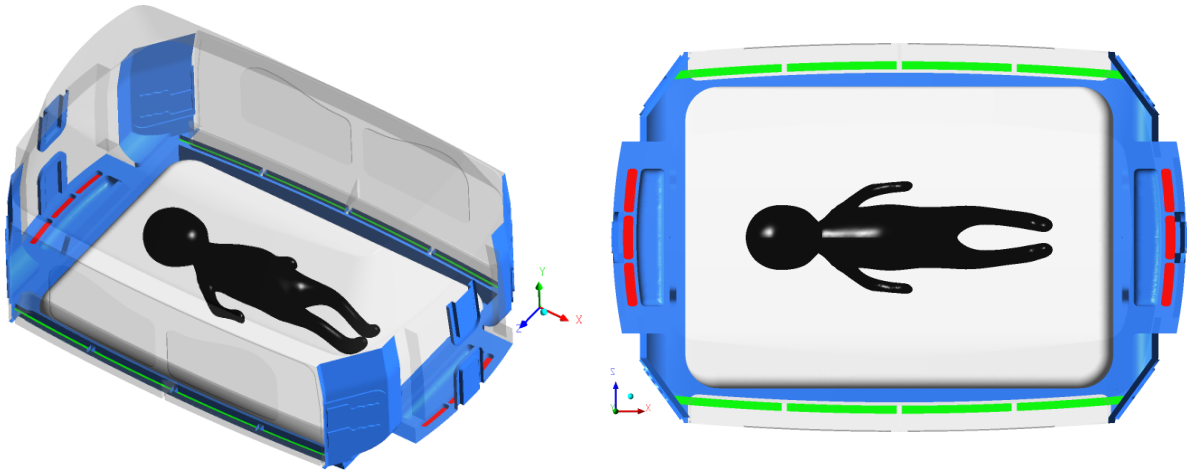

(a) (b)

Figure 4.1: (a) Isometric view showing the thermal manikin inside the incubator. (b) Top view of the incubator showing the airflow inlets in green and outlets in red.

The numerical simulations are carried out with varying air temperature and flowrate at the inlets. The different entering air temperatures T_{in} are $29, 30, 33$ and $35℃$ corresponding to common values used for incubators for both experimental [62, 39] and CFD simulations [15, 60]. The entering air flowrate is varied from around 5 to 50 Liters/min corresponding to 2 and 20 air change per hour (ACH), respectively. These flowrates correspond to typical values inside Caleo Drager incubator [104] insuring smooth air flow at very low velocity to avoid disturbing the neonate. Hence, the air velocity at the inlets did not exceed 0.05 m/s.

Dirichlet thermal boundary conditions are set at the manikin surfaces as explained in section 3.2 and presented in Table 3.1.

The radiant temperature T_r (℃) of the incubator walls is obtained from a correlation suggested and validated by Decima *et al.* [39]:

$$T_r = 0.724(T_{in} - 31.93) + 29 \tag{4.1}$$

In fact, the radiant temperature T_r is one of the most challenging parameters and it is very hard to evaluate experimentally so that it could be used later as boundary condition for CFD simulations. T_r depends on several parameters, mainly the incubator air temperature, the radiation properties of the incubator wall and the room temperature. Decima *et al.* [39] performed extensive study to determine this radiant temperature using different experimental methods. Equation (4.1) was obtained by Decima *et al.* [39] on an anthropomorphic thermal manikin nursed inside an incubator and it is valid for room temperature ranging between 23 and 25°C. This equation gives us the inner incubator wall temperature which means, there is no need any more to account for what is happening between the outer surface of the incubator and the room or to the conduction thermal resistance in the incubator wall. Hence, using Equation (4.1) for each air temperature at the inlet, a radiant temperature is calculated and the values for T_r range from $26.88℃$ to $31.22℃$. The emissivity of these opaque surfaces is set to 0.8. The incubator mattress is made from memory foam material whose thermal conductivity is very low [38]. Thus, we assume that the heat transfer through the mattress is negligible. Therefore, the mattress is assumed adiabatic so that conduction heat transfer between the manikin back and mattress is neglected. Similar assumption has been made in other CFD studies in the open literature [16, 51].

4.3 Flow nature

In infant incubators, the inlet air velocity should be relatively low so that the heated flowing air does not perturb the infant. However, natural convection will occur due to temperature gradients between the infant skin and surrounding air. This natural convection creates upward motion of the hot air particles from the infant skin surface. The nature of the natural convection, whether laminar or turbulent, depends thus on the temperature difference between the infant skin and incubator air with respect to viscous forces. This could be evaluated by calculating the Reynolds and Rayleigh numbers for the inlet jet and for the incubator flow as presented in Table 4.1.

The Reynolds number for the inlet jet and incubator flow are given as follows, respectively:

$$Re_{in} = \frac{4\dot{m}_{in}}{\pi \mu D_h} \tag{4.2}$$

$$Re_b = \frac{U_{up} L}{\nu} \tag{4.3}$$

where Re_{in} is the inlet jet Reynolds number, Re_b the incubator flow Reynolds number, $\dot{m}_{in}$ (kg/s) is the inlet incubator air flow rate, D_h (m) the inlet jet hydraulic diameter, and U_{up} (m/s) the thermal plume upward velocity inside the incubator.

These Reynolds numbers vary with the inlet air flow rate as well as with its temperature. For instance, the inlet Reynolds number varies between 37 and 370 with increasing flow rate from 2 to 20 ACH, and the incubator Reynolds numbers vary between 4000 and 6000 accordingly.

The Rayleigh number is obtained as follows:

$$Ra = \frac{g \beta \Delta T L_c^3}{\nu \alpha} \tag{4.4}$$

with β (K^{-1}) the air thermal expansion coefficient, ν (m^2/s) the kinematic viscosity of air and α (m^2/s) the air thermal diffusivity. In this equation, L_c is a characteristic length. The

characteristic length equals the hydraulic diameter for the calculation of the inlet jet Rayleigh number, and it is equal to the incubator characteristic length $L = V_{inc}^{1/3}$, where V_{inc} is the incubator volume, for the calculation of the incubator Rayleigh number. The term ΔT in this equation, stands for the temperature difference between the inlet air temperature and the incubator air temperature, when calculating the inlet jet Rayleigh number, and it is equal to the difference between the infant skin temperature and the incubator air temperature, when calculating the incubator Rayleigh number.

In Table 4.1, we also compute the ratio Ra/Re^2 to verify if the convection is forced or natural. For the inlet jet flow, this ratio is much less than 1 which means that the convection heat transfer from these jets is forced. Moreover, the maximum inlet jet Reynolds number did not exceed 370 which means that the heated air jets from the inlets could be assumed as laminar flow. Meanwhile, the ratio Ra/Re^2 for the incubator air flow is always greater than 1 which means that natural convection occurs inside the incubator. Moreover, the Rayleigh number for the air flow inside the incubator ranges from 3.52×10^7 to 6.56×10^7. These high Rayleigh numbers correspond to turbulent natural convection inside enclosures. Therefore, a turbulence model must be adopted to account for turbulent natural convection as explained in the following text. It is worthy to note that turbulent flow was also assumed in previous studies in the open literature for flows inside incubators [16, 26, 72].

Inlet air temperature (℃)	29	30	33	35
Incubator air bulk temperature (℃)	28.3	28.4	30.5	31.7
Infant average skin temperature (℃)	35.7			
Inlet jet Rayleigh number ($\times \mathbf{10^{-3}}$)	0.99	2.11	3.40	4.41
$\boldsymbol{Ra_{in}/Re_{in}^2}$	0.10	0.21	0.34	0.44
Incubator flow Rayleigh number ($\times \mathbf{10^{-7}}$)	6.56	6.41	4.62	3.52
$\boldsymbol{Ra_b/Re_b^2}$	1.70	2.02	2.01	1.97

Table 4.1: Rayleigh numbers for the inlet air jet flow and the incubator air flow due to natural convection.

4.4 Numerical Procedure

The flow is governed by Reynolds Averaged Navier-Stokes equations. The heat transfer process is computed by solving the energy equation. Two different turbulence models are used in the open literature when analyzing thermoregulation of neonates. These are the RNG $k-\epsilon$ model [72, 73] and the SST $k-\omega$ model [15, 16, 60, 26]. In the present study the SST $k-\omega$ turbulence model is adopted since it predicts the flow structure much better than other models and it is more suitable for turbulent flows with relatively low Reynolds numbers [102, 103]. Using this turbulence model, two additional equations need to be solved for the turbulence kinetic energy k and its specific rate of dissipation ω. For more details about the SST $k-\omega$ model, the readers can refer to Menter [105].

Since the convective heat transfer process inside the incubator is mainly due to natural convection, the Boussinesq approximation is used for the buoyancy term in the governing equations. Thus, the density varies locally with the air temperature inside the computational domain.

Moreover, radiation is a major concern in this type of problems. Thermal radiation can be emitted from a surface in all possible directions, creating thus a directional distribution. These directional effects are described by the radiation intensity which could be computed from the radiative heat transfer equation (RTE). Due to its nature, mathematical treatment of thermal radiation requires using the spherical coordinate system. The discrete ordinates (DO) radiation model transforms the RTE into a transport equation for the radiation intensity in the global Cartesian coordinate system. The angular space is then discretized into a finite number of discrete solid angles each associated with a vector direction fixed in the global Cartesian system. The DO model computes the radiation intensity transport equation for each vector direction by using iterative numerical solution like that used for the Navier-Stokes and energy equation [106, 107]. This model has been extensively used in the open literature when studying heat exchange with preterm neonates [29, 30, 41] [60, 26, 72].

The solver used for the present study is the CFD code ANSYS Fluent 2019 R1 [108]. This solver is based on the cell-centered finite volume method. The flow equations are computed sequentially with double precision and second order upwind scheme for spatial

discretization of the convective terms [109]. The diffusion terms are second order accurate with central difference scheme. The COUPLED algorithm is adopted for pressure-velocity coupling which has superior performance over the staggered algorithms. The low Reynolds correction model is used with the SST $k-\omega$ turbulence model to better capture the near wall region and handle adverse pressure gradients which may occur. This approach requires a wall distance y^+ value lower than 4 to ensure that the viscous sublayer is fully modeled. The pseudo transient model is enabled to enhance and accelerate the convergence of the governing equations. The residuals for the flow and energy solutions are set to 10^{-5}. Beyond this value no significant changes were observed in the velocity, temperature fields and turbulence quantities.

4.5 Mesh sensitivity analysis

An initial tetrahedral unstructured non-uniform three-dimensional mesh is generated inside the incubator with local refinement near solid surfaces such as infant skin, incubator walls and mattress. These tetrahedral cells are then converted into polyhedral elements as shown in Figure 4.2. Polyhedral elements allow lower mesh density relative to the tetrahedral mesh with enhanced accuracy and faster convergence especially in complicated geometries [60, 110].

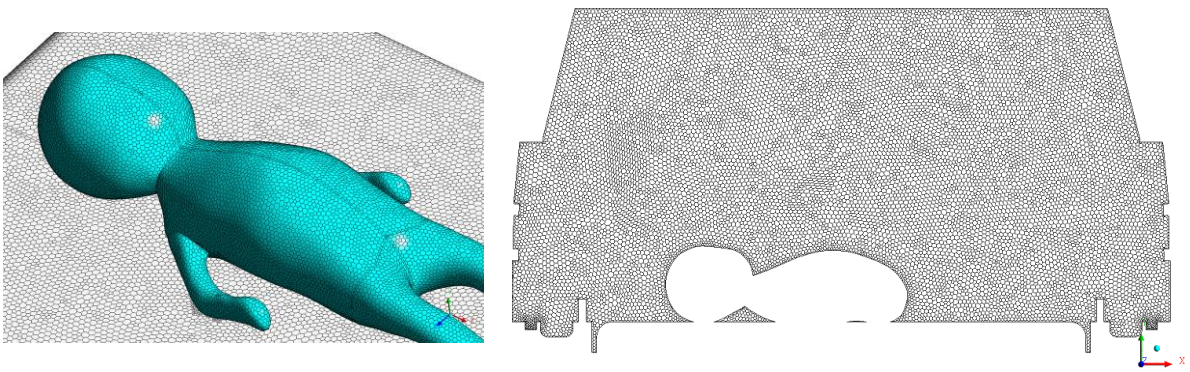

(a) (b)

Figure 4.2: (a) Polyhedral elements on the manikin skin surface and mattress and (b) cut on the symmetry plane showing the mesh.

Three different mesh densities were studied to evaluate the grid convergence index (GCI) based on the mesh sensitivity analysis suggested by Celik *et al.* [111]. The three mesh densities are given in Table 4.2. It is worthy to note that the intermediate and refined mesh densities given here are almost refined twice more than previous studies in the open literature dedicated for neonates inside incubators [15, 31].

The criterion for the mesh sensitivity analysis are the radiative and convective heat fluxes from the neonate skin inside the incubator for the highest flowrate (50 Liters/s) and an inlet air temperature of 33℃. Thus, according to the mesh sensitivity analysis, the GCI for the most refined mesh is 1.1% with an order of convergence equal 4. This refined mesh density with 2.5 million cells is adopted for the numerical simulations presented in this paper. The maximum y^+ value is lower than 2.2, ensuring that the near wall region, and especially the viscous sublayer region, is properly computed and thus the low Reynolds number correction approach could be safely adopted.

The mesh sensitivity analysis was also performed by comparing local distribution of the velocity and temperature inside the incubators at different critical areas, such as in the mid and symmetric plane, near the infant surface and near the air inlets. All this analysis proved that the fine mesh is enough to accurately compute the fluid flow and heat transfer in the present problem. However, for space limitation, we only present the mesh sensitivity analysis for the total rate of heat loss in Table 4.2, which is our quantity of interest.

Mesh	**Coarse**	**Intermediate**	**Fine**
Number of cells $(\times \mathbf{10^6})$	0.7	1.4	2.5
Total rate of heat loss (W)	5.813	5.843	5.914
Extrapolated relative error (%)		0.32	0.85
GCI (%)		0.4	1.1
Order of convergence			4

Table 4.2: Mesh sensitivity analysis.

Moreover, a sample result for the mesh sensitivity analysis for the convective and radiative heat fluxes from the neonate skin is shown in Figure 4.3. It is observed that beyond

the intermediate mesh, there is no significant change in the heat fluxes obtained from the CFD simulations.

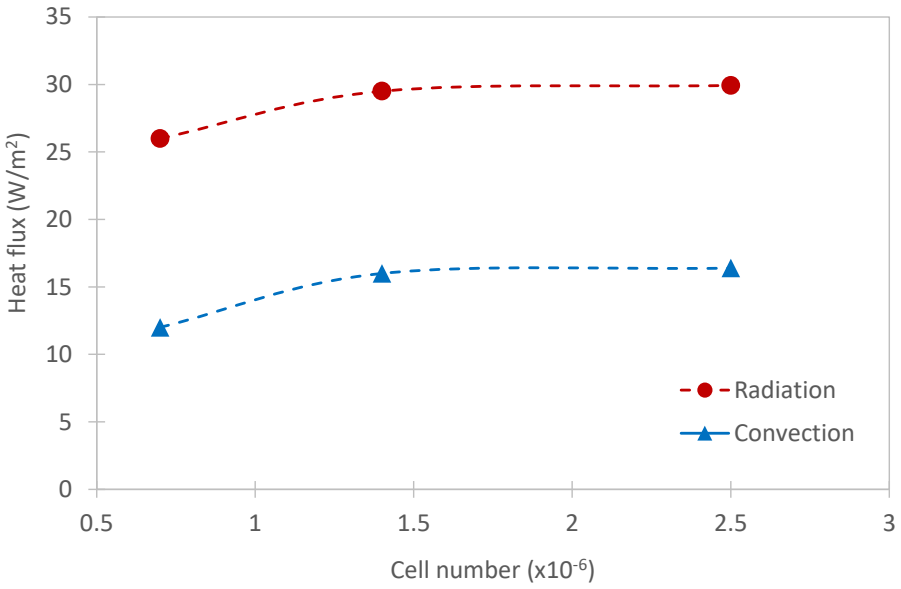

Figure 4.3: Mesh sensitivity for the body radiative and convection heat fluxes.

4.6 Heat Balance Model

Considering the preterm neonate as control volume, the energy balance in steady state reads the following:

$$q_m = q_{conv} + q_{rad} + q_{ev} + q_{res} \tag{4.5}$$

In this equation, the term on the left-hand side corresponds to the energy generated within the infant body due to metabolic heat, q_m. The terms on the right-hand side correspond to dry and latent heat losses from the neonate due to convection q_{conv}, thermal radiation q_{rad}, evaporation from skin q_{ev} and respiration q_{res}. While q_{conv} and q_{rad} are obtained from the present CFD simulations, the other terms in this equation are evaluated using empirical equations as discussed below.

The metabolic heat generation q_m is obtained from Brück's formula given as follows [67]:

$$q_m = m_{inf}(0.0522\tau_{PA} + 1.64) \tag{4.6}$$

In this equation, m_{inf} is the infant mass (expressed in kg) obtained from the revised Fenton growth chart [112] for a preterm neonate of 35 weeks of gestational age (τ_{GA}) in the 50th percentile and it is found equal to 2.5 kg. The term τ_{PA} represents the postnatal age (expressed in days) which is considered equal one. Thus, the rate of metabolic heat generation from the present thermal manikin is 4.23 W.

Preterm neonates do not sweat; however, they have very thin skin and thus they lose latent heat by evaporation due to transcutaneous water loss [113]. Thus, the rate of heat loss due to evaporation is obtained from the following expression [114]:

$$q_{ev} = h_{fg}\kappa\frac{A_{inf}}{m_{inf}}(p_s^* - \phi p_a^*) \tag{4.7}$$

where A_{inf} is the infant surface area introduced in section 3.3 and κ is the mass transfer coefficient of the infant skin due to diffusion which is related to the skin surface temperature and gestational age as described by Ultman [114]. h_{fg} is the enthalpy of vaporization equal to 2425 kJ/kg. ϕ is the relative humidity of the incubator air. Since we only want to analyze the effect of the studied air temperatures on the heat balance, a value of $\phi = 66\%$ is taken in the present study, which is in the range of typical value for 1st day nursing inside incubators [41].

The terms p_s^* and p_a^* are the equilibrium water vapor pressures evaluated at skin surface temperature and incubator air temperature using the following expression:

$$\log p^* = 7.092 - \frac{1668.21}{288 + T} \tag{4.8}$$

Hence the rate of evaporative heat loss from the skin could be readily obtained for each inlet air temperature by using equation (4.7) and its value varies between 0.323 and 0.388 W.

The rate of heat loss due to respiration is the total of dry and latent respiration heat transfer:

$$q_{res} = q_{res,dry} + q_{res,latent} \tag{4.9}$$

where the dry heat loss $q_{res,dry}$ accompanying respiration is written as follows:

$$q_{res,dry} = \dot{m}_{res} c_p (T_c - \bar{T}_a) \tag{4.10}$$

In this equation, $\bar{T}_a$ is the incubator air bulk temperature, c_p(J/kg. K) is the specific heat of air (1006 J/kg . K) and $\dot{m}_{res}$ is the infant respiration flowrate equal to 375.7 ml/min [60]. For the present preterm infant, the dry heat losses due to respiration range from 0.034 to 0.06 W.

The rate of evaporative heat loss $q_{res,latent}$ accompanying respiration is obtained from the following empirical equation obtained by Ultman [114]:

$$q_{res,latent} = h_{fg}\left(0.411 + 9.68 \times 10^{-4} T_a - 7.4 \frac{\phi p_a^*}{p_{atm} - \phi p_a^*}\right) \tag{4.11}$$

where p_{atm} is the standard atmospheric pressure. Hence the rate of evaporative heat loss accompanying respiration could be obtained for each inlet air temperature by using equation (4.11) and its value varies between 0.691 and 0.695 W. As denoted, the latent heat losses due to respiration are at least 10 times greater than the dry respiration heat loss.

The model developed here necessitates the evaluation of q_{conv} and q_{rad} using CFD simulations in parallel to computing the other rates of heat transfer using the empirical equations. The results will be used later in this paper to evaluate the energy balance of the neonate.

In the next section, we study the effect of incubator air temperature and flowrate on the rate of convective and radiative heat losses from the neonate. Then the correlations for convective and radiative heat transfer coefficients are obtained using power law functions. Finally, the thermal balance of the neonate is evaluated using the operative temperature and the heat balance model developed in the present section.

4.7 Results and Discussions

4.7.1 Effect of air temperature

In this section, we study the effect of varying the incubator entering air temperature on the heat transfer process for a fixed air flowrate corresponding to 5 ACH. Figure 4.4 shows the thermal plume ejected from neonate body colored by mean velocity. This thermal plume is detected by using temperature iso-surface. An ascending motion is clearly observed here where the air particles near the hot thermal manikin raise towards the incubator upper wall due to buoyancy. This raising flow hits the upper wall like an impinging jet showing thus stagnation regions. The flow cools down and slides against the incubator walls to leave through the outlets. Comparing the two cases presented in Figure 4.4 (a) and (b), it could be noticed that the up-wash velocity is slightly higher for the lower inlet temperature case due to higher temperature gradient causing thus faster motion of fluid particles.

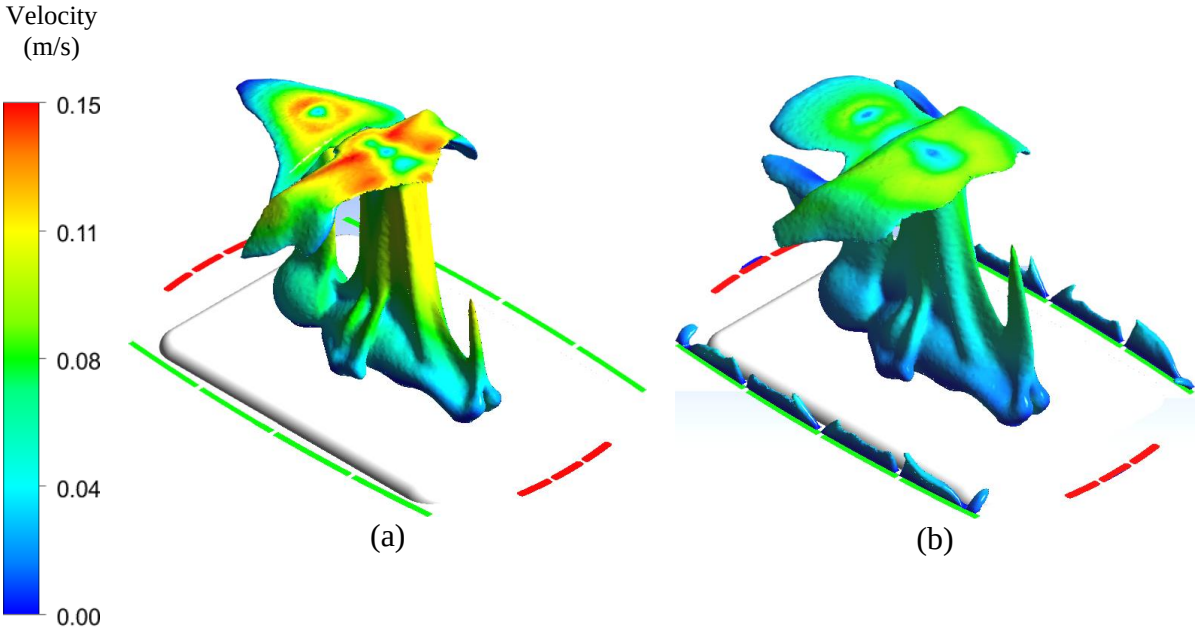

Figure 4.4: Thermal plume colored by velocity for same entering air flowrate corresponding to 5 ACH for two different air temperatures: (a) $T_{in} = 29℃$ with iso-surface at $T = 29.3℃$ and (b) $T_{in} = 35℃$ with iso-surface at $T = 32.1℃$.

To better visualize the flow structure, we plot the streamlines on the middle cross section, as shown in Figure 4.5, for two different inlet temperatures. In the streamlines shown in Figure 4.5 (a) corresponding to the lower inlet temperature we can see some eddies near the mattress from the inlet sides while for the higher temperature in Figure 4.5 (b) no eddies are observed. These eddies have negative impact and could interfere with the neonate comfort as reported earlier in the experimental and numerical analysis performed by Kim *et al.* [56] who observed similar flow structure. Moreover, these stagnant vortices form recirculation regions and the fluid particles in their core will not be efficiently renewed. It is worthy to note that the accuracy with which the CFD simulations predicts the onset of eddies has not been evaluated and future detailed experimental studies should be performed to assess the local flow structure.

In Figure 4.5, the temperature contours on the mid and symmetry planes are also shown for two different inlet temperatures. While the qualitative behavior is similar highlighted by the ascending motion due to buoyancy, however the temperature of the air inside the incubator for $T_{in} = 35℃$ is much greater than that for $T_{in} = 29℃$. This higher temperature, especially near the infant surface will lead to lower heat losses and thus better thermal balance as will be discussed later.

To highlight the effect of varying the inlet air temperature, the convective and radiative heat fluxes from the neonate skin surface are shown in Figure 4.6. In the case of lower temperature (Figure 4.6 (a)) the radiative and convective heat fluxes show a high value, around 70 and 50 W/m^2 respectively, especially on the head and extremities. Whereas, in the case of higher temperature (Figure 4.6 (b)) the radiative and convective heat flux are much lower and more homogenously distributed, whose maximum values are around 45 and 30 W/m^2 respectively. The highest radiative heat losses seem to be at the head and torso while the highest convective heat fluxes are present near the lower extremities which are farther from the airflow inlets, especially when the inlet air temperature is low. Moreover, higher convective heat fluxes are observed on the sides of the manikin where it was observed the presence of eddies earlier in this section.

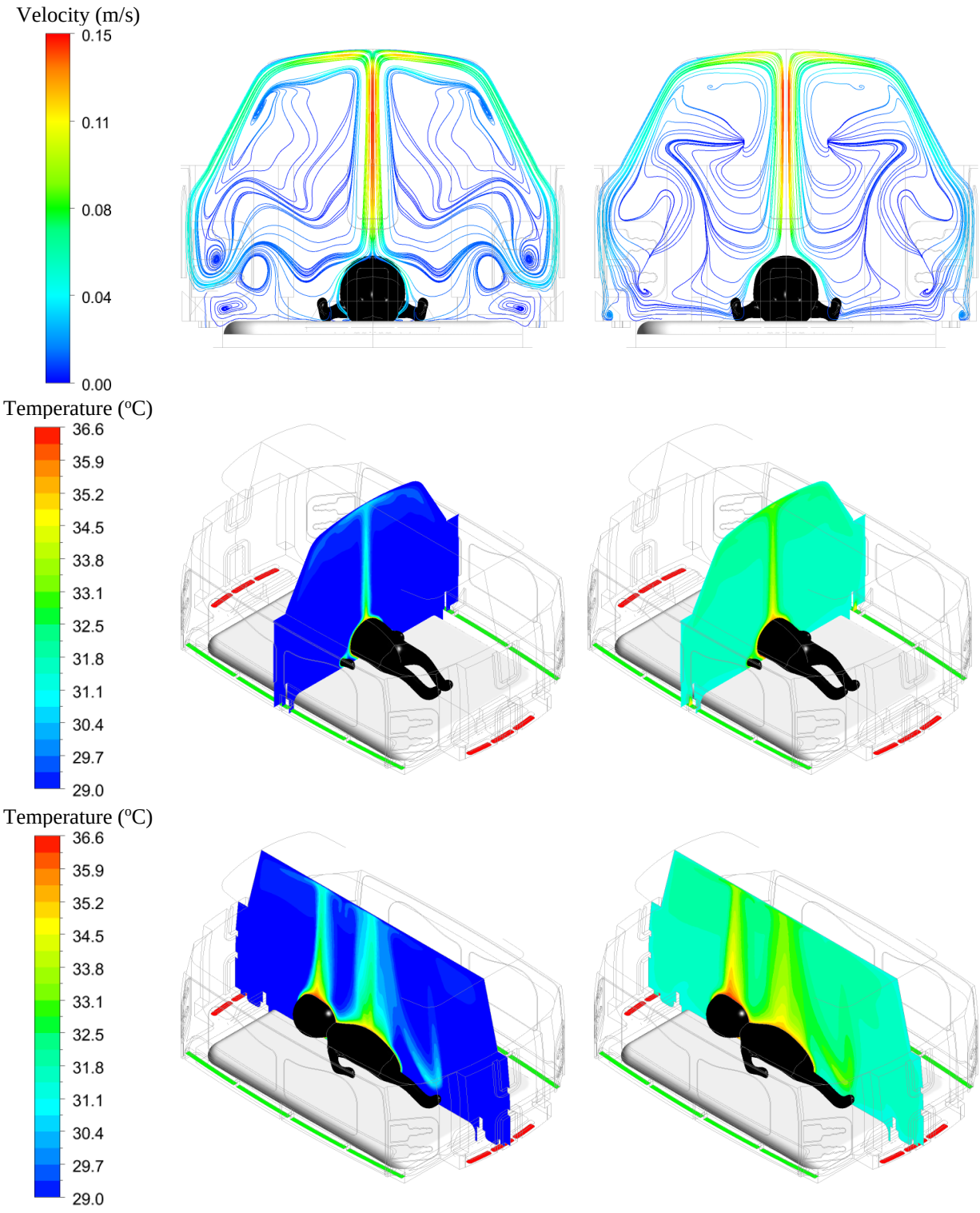

(a) (b)

Figure 4.5: Streamlines and temperature contours for same entering air flowrate corresponding to 5 ACH for two different air temperatures: (a) of $T_{in} = 29℃$ and (b) $T_{in} = 35℃$.

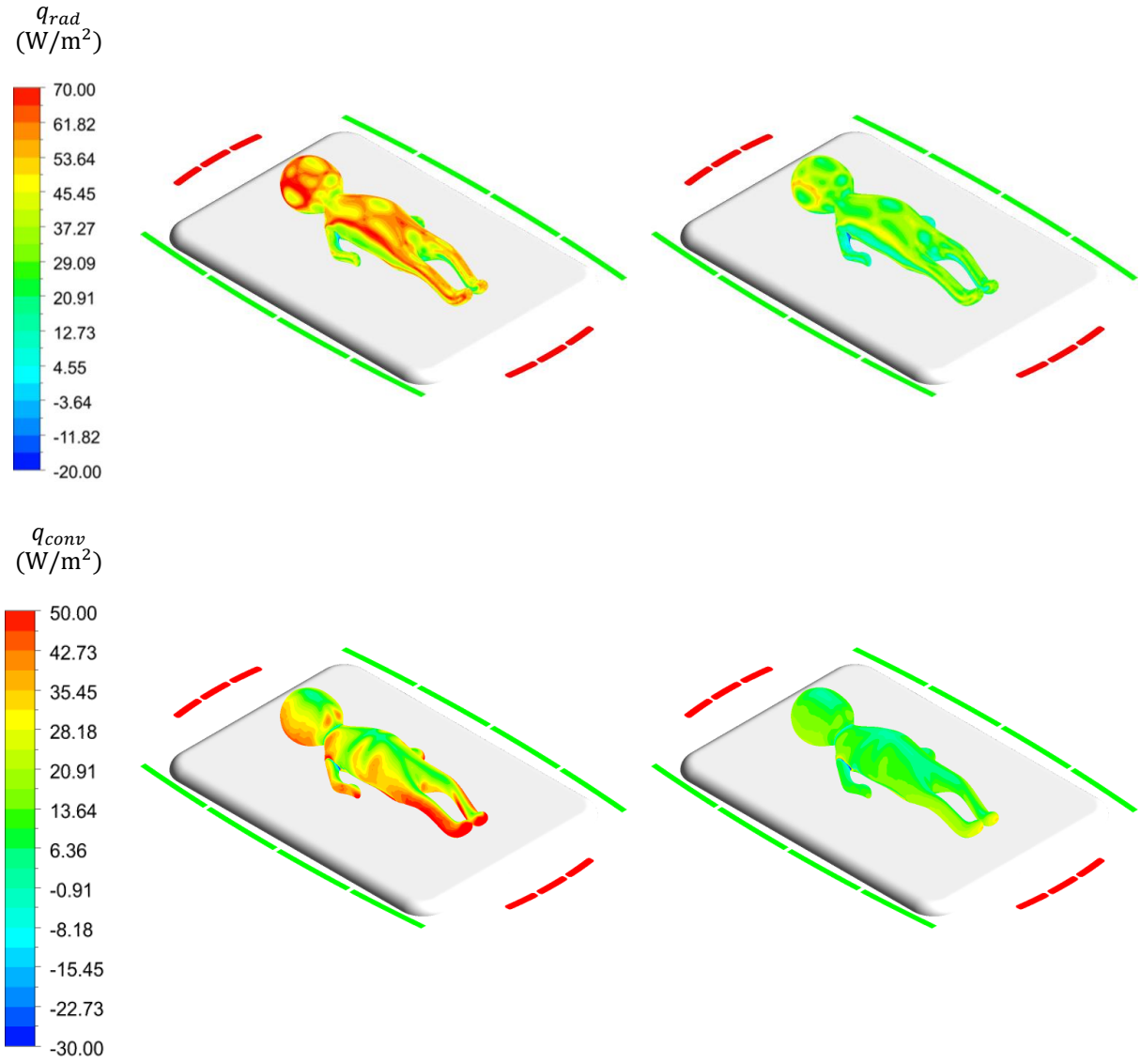

(a) (b)

Figure 4.6: Convection and radiation heat transfer rates for same entering air flowrate corresponding to 5 ACH for two different air temperatures: (a) of $T_{in} = 29℃$ and (b) $T_{in} = 35℃$.

The area weighted heat fluxes (expressed in W/m^2) over the different body segments are presented in Figure 4.7. This figure shows the variation of radiative, convective and total heat fluxes versus the inlet air temperature for fixed flow rate (5 ACH). It is well noticed that the heat fluxes decrease while increasing the air temperature due to the decrease in thermal gradients between the skin and surrounding environment such air and incubator wall

temperatures. From Figure 4.7 (a), two levels in the radiative heat flux q''_{rad} could be distinguished. The first level for the highest q''_{rad} occurs in the head, trunk and legs which are the most exposed to surrounding surfaces. Meanwhile, the second level with the lowest q''_{rad} occurs for the arms and back which are less exposed to the surroundings. In fact, the back is in direct contact with the mattress while the arms are relatively hidden by the preterm body and thus exchange less thermal radiation with the surrounding surfaces.

The small radiative heat loss from the back is also accompanied by the lowest convective heat losses due to the same reason (Figure 4.7 (b)). However, the highest convective heat fluxes are obtained from the legs followed by the head, which are on the extremities of the human body and thus almost fully surrounded by the air flow.

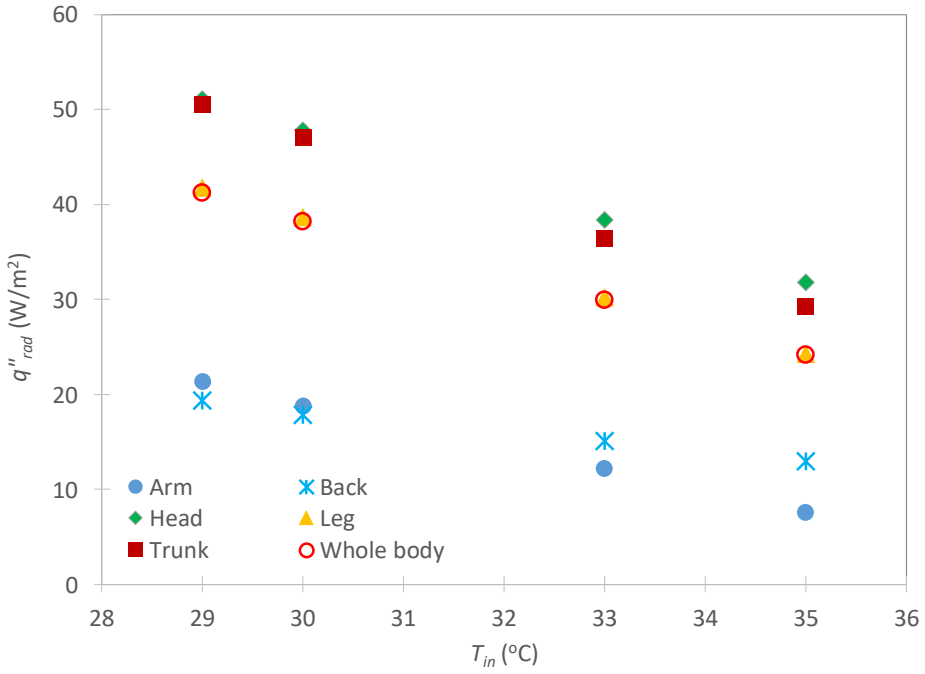

(a)

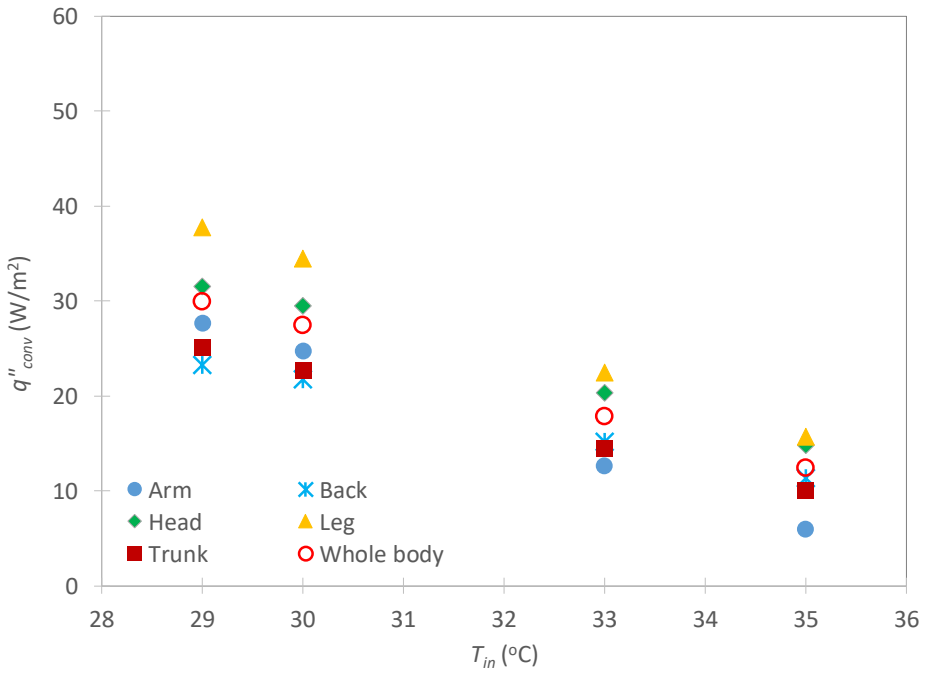

(b)

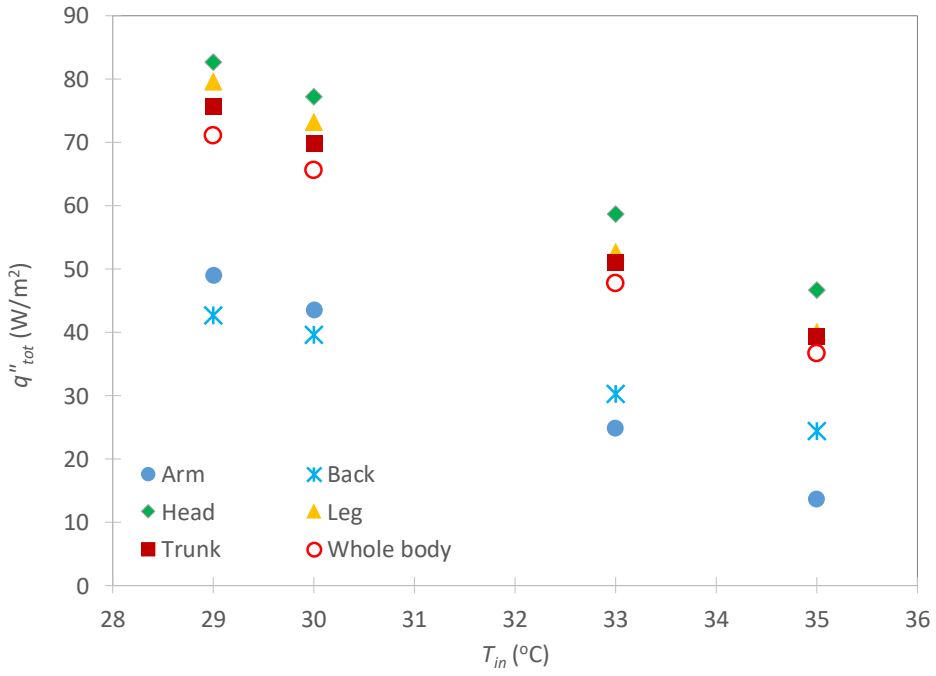

(c)

Figure 4.7: Variation of (a) radiative, (b) convective and (c) total heat fluxes (expressed in W/m^2) versus inlet air temperature for each body segment for the case where the air flowrate corresponds to 5 ACH.

Comparing the level of radiative heat fluxes to the convective ones, from Figure 4.7 (a) and (b), it is observed that the radiation heat losses are much more pronounced than convection heat loss for all body segments except the arms and back. For instance, the radiation heat fluxes from the whole body are around 25% higher than the convective heat losses. This is typical in infant incubators since the air flow is heated while the surrounding radiant surfaces are at much lower temperature. This problem could be solved for example by using radiant heating elements [7, 30]. Now calculating the total heat losses per unit surface area as the summation of convective and radiative heat fluxes, we observe in Figure 4.7 (c) that the head, legs and trunk are losing the most of heat. Hence, the intervention in case of hypothermia should be first by acting on these body segments at first. Moreover, the total heat flux on the whole body drops from around 70 to 37 W/m^2 which means a drop in the total rate of heat loss from 9 to around 5 W when the inlet temperature increases from 29 to 35℃.

4.7.2 Effect of air flow rate

In this section, we study the effect of varying the incubator entering air flowrate on the heat transfer process for a fixed inlet air temperature corresponding to 33℃. Figure 4.8 shows the streamlines and temperature contours for two different air flowrates corresponding to 5 and 20 ACH. By examining the streamlines, it could be noticed that there is almost no significant difference between the lowest and highest flowrate. The ascending motion due to buoyancy observed earlier in the previous section is also obtained in the present cases. However, the eddies are now shifted towards the upper corners of the incubator farther from the infant body. The effect of the flow structure is clearly highlighted by the temperature contours shown in this figure. The main difference between the lower and higher flowrates is by the level of temperatures. In fact, higher inlet flowrates lead to higher overall temperature inside the incubator enhancing thus the incubator thermal homogeneity.

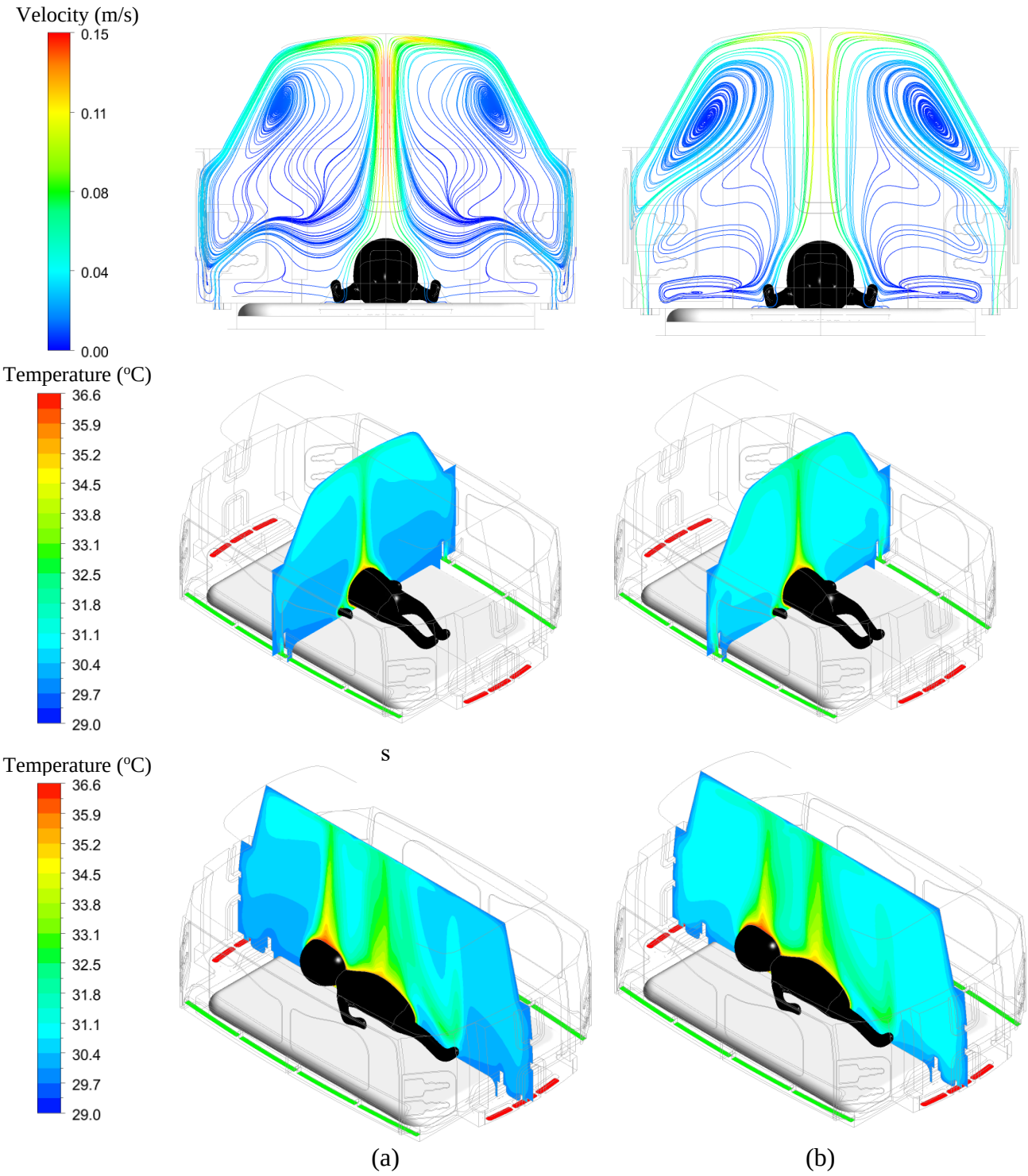

Figure 4.8: Streamlines and temperature contours for same airflow inlet temperature of $T_{in} =$ 33℃ for two different air changes: (a) 5 ACH and (b) 20 ACH.

To assess the effect of air flowrate on the heat losses from the different neonate segments, we present the contours of radiative and convective heat losses on the manikin skin for two different flowrates corresponding to 5 and 20 ACH as shown in Figure 4.9. It is noticed that the radiative and convective heat losses do not change with varying inlet flowrates. In fact, relating this to what has been observed above in the incubator air temperature at the different sections, it could be noticed that the air temperature near the manikin skin is not significantly affected by the inlet flow rate. And since the heat losses are directly related to the temperature gradient near the skin surface, thus there was no effect of increasing the air flowrate on the heat losses.

To better quantify the effect of varying the inlet flowrate on the heat losses, we analyze the area weighted average of the heat fluxes (expressed in W/m^2) over the different body segments and plot them against ACH in Figure 4.10. As shown in this figure, the radiative, convective and total heat fluxes are almost constant in terms of the air flowrate.

Hence it could be concluded that the only benefits of increasing the inlet air flowrate is the better homogeneity of the temperature inside the incubator. Moreover, the heated air inlets are located near the incubator windows and they play the role of air curtains when these windows are open during clinical intervention.

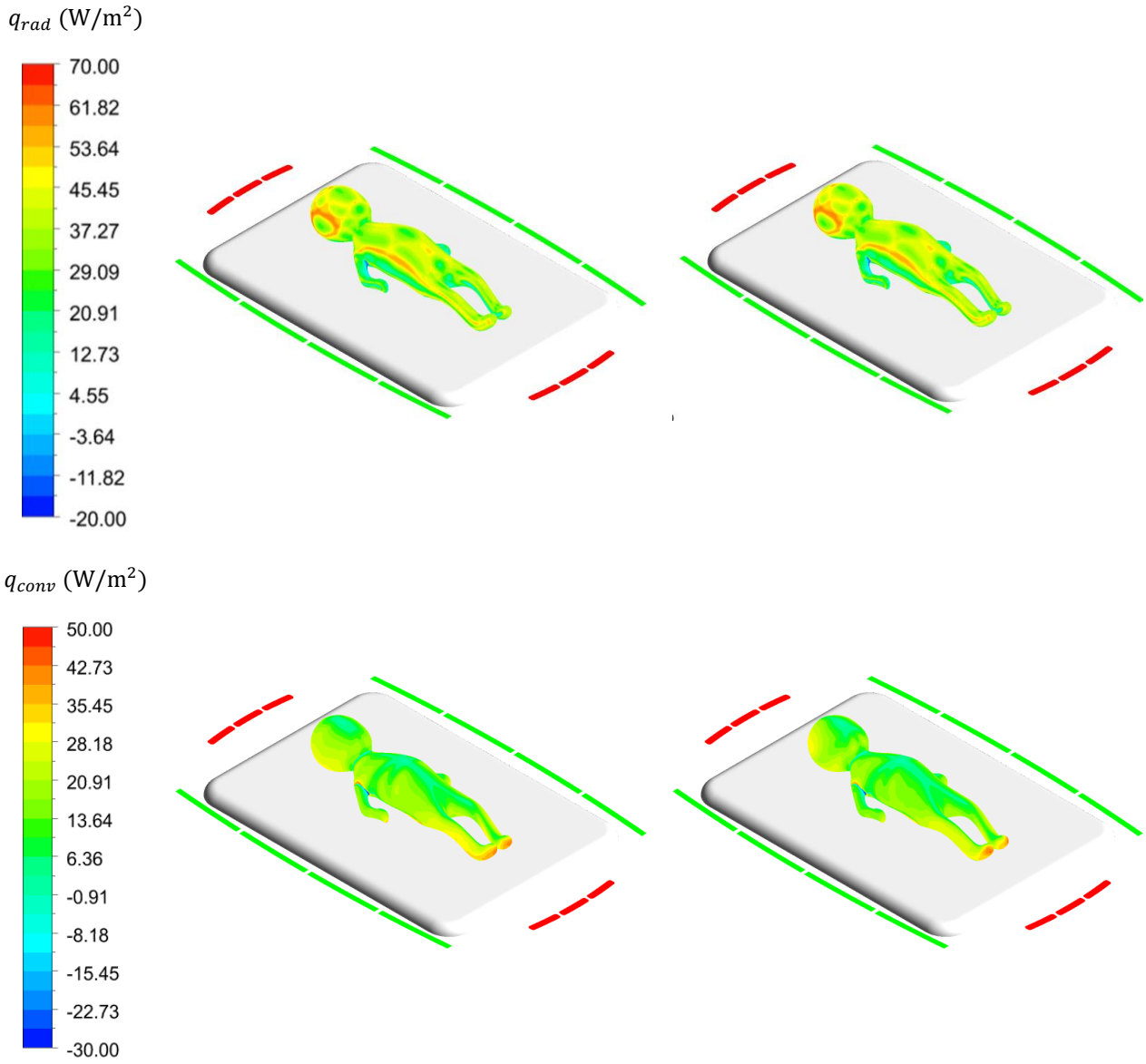

Figure 4.9: Convection and radiation heat transfer rates for same airflow inlet temperature of $T_{in} = 33℃$ for two different air changes: (a) 5 ACH and (b) 20 ACH.

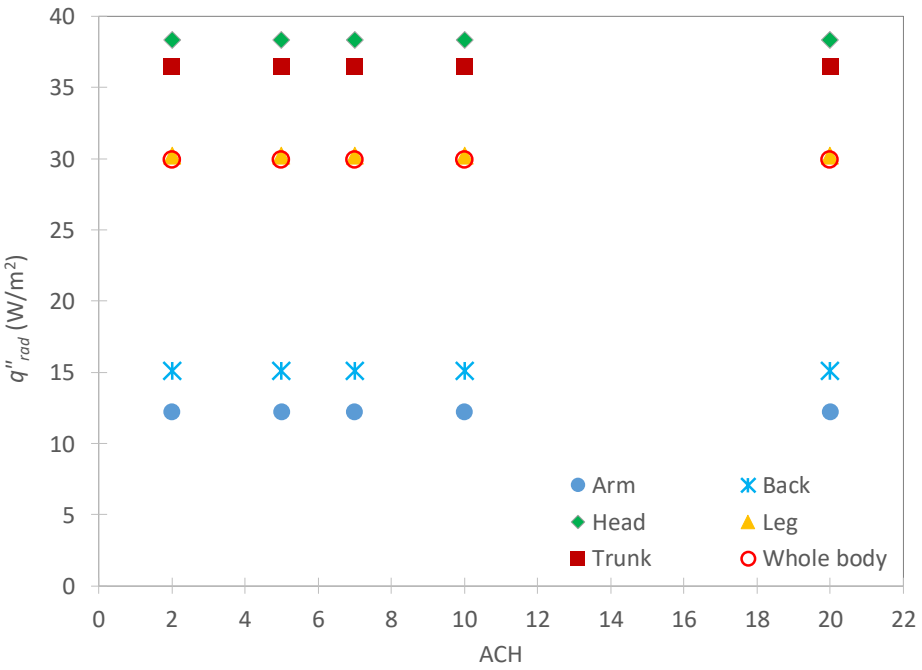
40
35
30
25
20
15
10
5
0
0
2
4
6
8
10
12
14
16
18
20
22
ACH
q'' rad (W/m2)
Arm
Back
Head
Leg
Trunk
Whole body

(a)

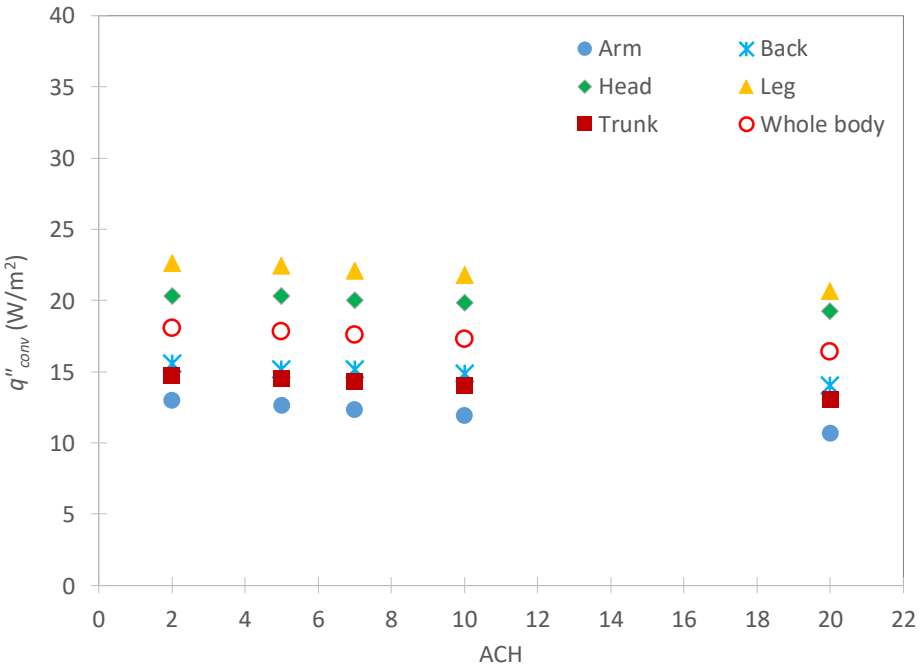
40
35
30
25
20
15
10
5
0
0
2
4
6
8
10
12
14
16
18
20
22
ACH
q'' conv (W/m2)
Arm
Back
Head
Leg
Trunk
Whole body

(b)

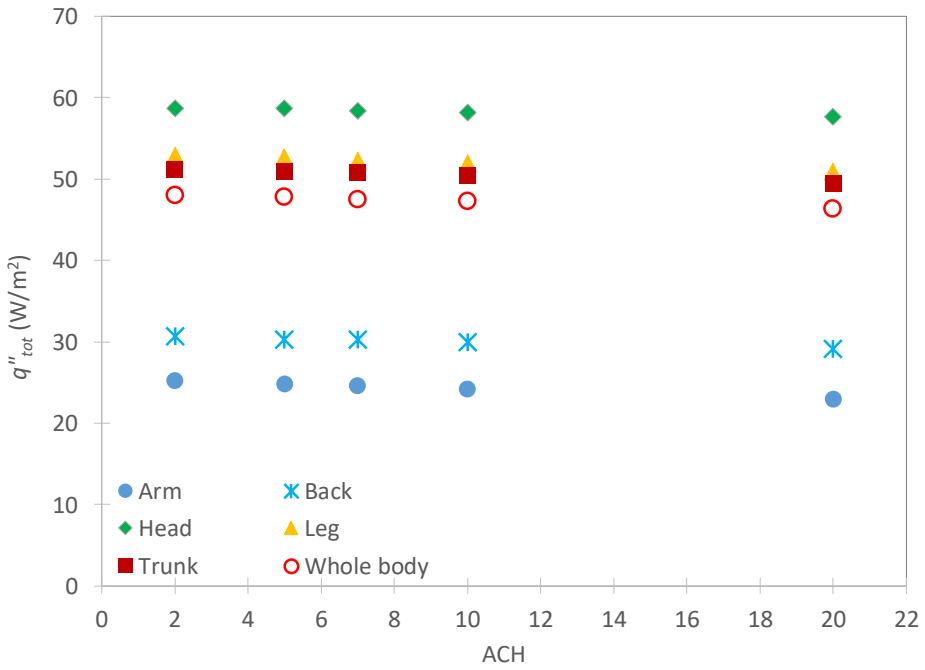

(c)

Figure 4.10: Variation of (a) radiative, (b) convective and (c) total heat fluxes (expressed in W/m^2) versus air change per hour for each body segment for the case where $T_{in} = 33$℃.

4.7.3 Correlations for heat transfer coefficients

After discussing the effect of inlet air temperature and flowrate on the convective and radiative heat losses, it is found that the entering flowrate has no significant effect on the rate of heat losses. However, the increase in the inlet air temperature leads to a decrease in the heat losses. Thus, it could be concluded that the convective heat transfer is due to buoyancy and it is natural convection.

In this section, we determine correlations for the radiative and convective heat transfer coefficients in terms of suitable temperature differences. Using Stephan-Boltzmann and Newton's cooling laws, the rates of convective and radiative heat losses read the following, respectively:

$$q_{rad} = h_{rad} A_i \left(T_{s,i} - T_r\right) \tag{4.12}$$

$$q_{conv} = h_{conv} A_i \left(T_{s,i} - \bar{T}_a\right) \tag{4.13}$$

where A_i and $T_{s,i}$ are respectively the surface area and temperature of the given body segment, T_r is the radiant temperature obtained from equation (4.1), and $\bar{T}_a$ is the incubator air bulk temperature. Thus, for each case, knowing q_{rad} and q_{conv}, the radiative and convective heat transfer coefficients could be readily obtained from equations (4.12) and (4.13).

Figure 4.11 shows the variation of the radiation heat transfer coefficient versus the temperature difference $\Delta T_{\mathrm{sr}} = T_s - T_r$ for different body segments as well as for the whole body. Hence, ΔT_{sr} is different for each body segment. From this figure, it is observed that h_{rad} decreases with the temperature difference and the highest values are reported for the head and trunk as already discussed in the previous sections. These data are fitted with power low curves using a linear regression to obtain correlations of the form:

$$h_{rad} = A\Delta T_{sr}^{B} \tag{4.14}$$

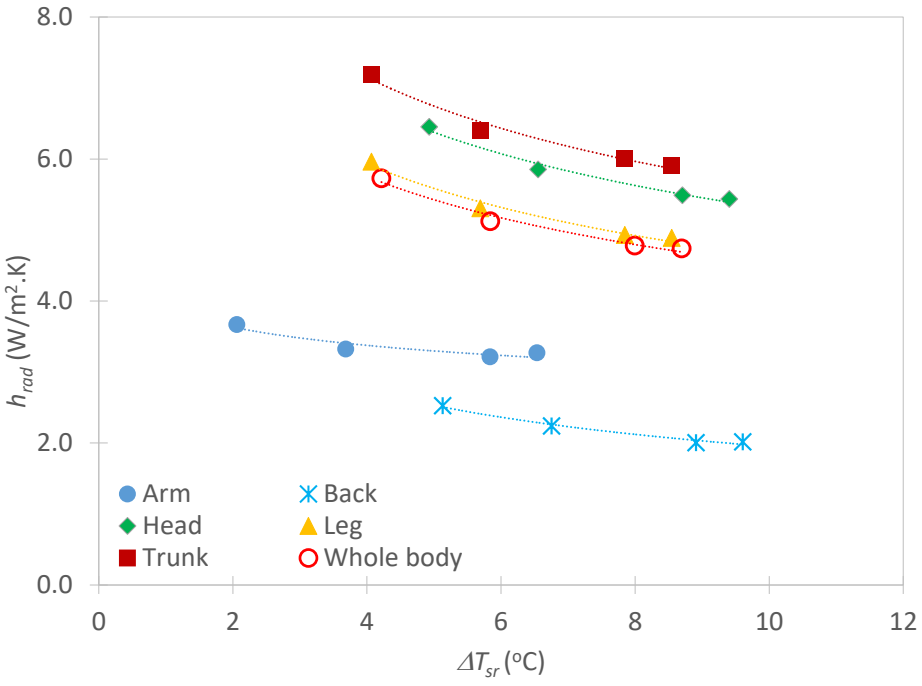

Figure 4.11: Variation of the radiation heat transfer coefficient versus ΔT_{sr} for different segments as well as for the whole body.

The correlations for h_{rad} for each body segment as well as for the whole body are reported in Table 4.3. The correlations are obtained using linear regression and the R^2 values are given next to the correlations as shown in Table 4.3.

The data for h_{rad} obtained in the present study are compared to results from the open literature using numerical and experimental methods. Figure 4.12 (a) compares the variation of h_{rad} versus ΔT_{sr} with that obtained by Museux *et al.* [79] for the whole body. In their study, Museux *et al.* [79] studied radiative heat transfer coefficient for higher range of temperature difference ΔT_{sr} between 9 and 14 while in our study ΔT_{sr} ranges from around 4 to 9. From Figure 4.12 (a) it is well observed that the current numerical results are in the continuity of the experimental data reported by Museux *et al.* [79] where the whole body radiative heat transfer coefficient decreases with the temperature difference ΔT_{sr}. Figure 4.12 (b) compares the averaged radiative heat transfer coefficient for the whole body with those obtained by Museux *et al.* [79] and Wheldon [40] since there is no data in the open literature available for each body segment. The present data are in fair agreement with those reported in earlier experimental studies with slight differences related to the difference in the manikin and incubator geometry. For instance our radiative heat transfer coefficient reached around 5 for the whole body while in Wheldon [40] it is 3.7 and 4.6 in Museux *et al.* [79].

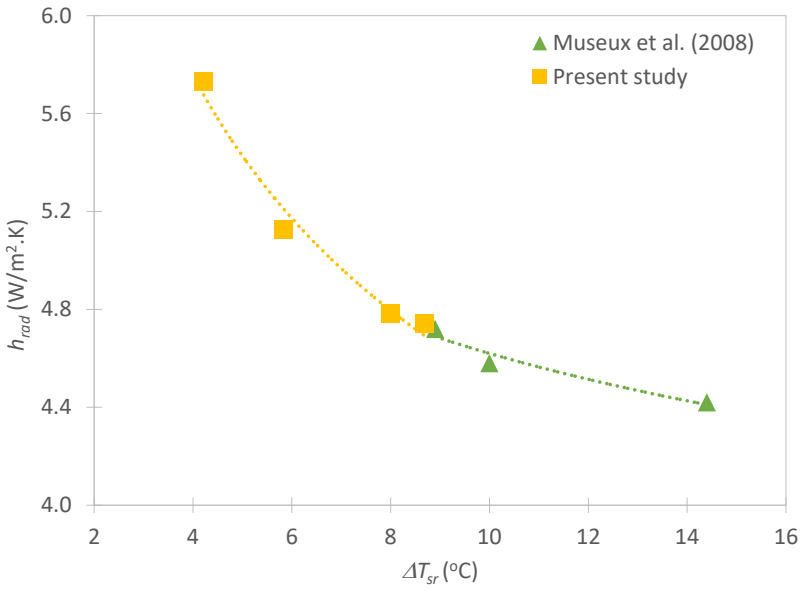

(a)

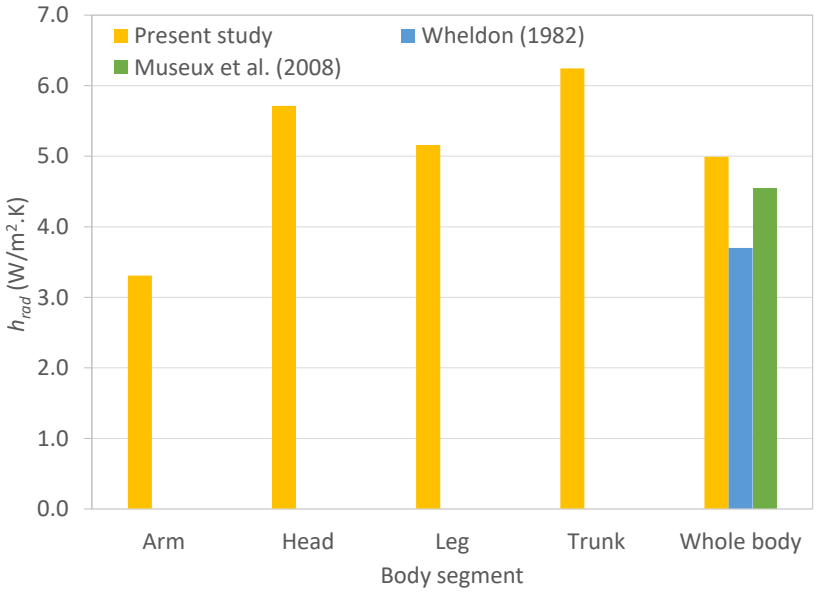

(b)

Figure 4.12: Comparison of radiation heat transfer coefficient with that obtained from open literature (a) for whole body versus temperature difference ΔT_{sr} and (b) its temperature weighted average value for each body segment and whole body for ΔT_{sr} ranging from 4 to 14.

Figure 4.13 shows the variation of the convection heat transfer coefficient versus the temperature difference $\Delta T_{sb} = T_s - \bar{T}_a$ for different body segments as well as for the whole body. It is worthy to note that ΔT_{sb} varies between the different body segments. From this figure, it is observed that h_{conv} increases with the temperature difference and the highest values are reported for the arms and legs. These data are fitted with power low curves to obtain correlations of the form:

$$h_{conv} = C\Delta T_{sb}^{D} \tag{4.15}$$

The correlations for h_{conv} for each body segment as well as for the whole body are reported in Table 4.3.

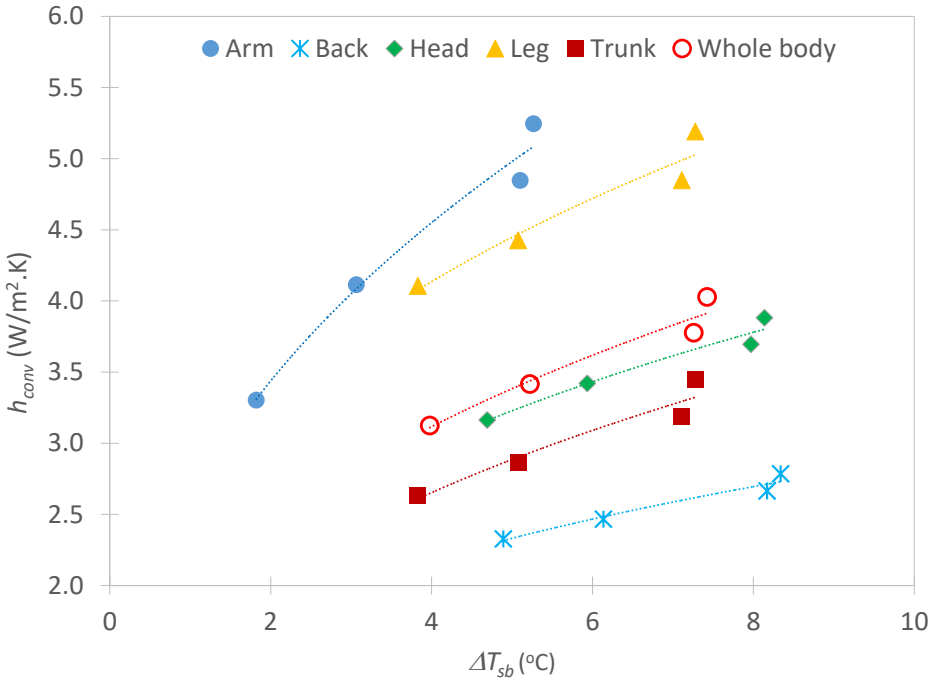

Figure 4.13: Variation of the convection heat transfer coefficient versus ΔT_{sb} for different segments as well as for the whole body

The data for h_{conv} obtained in the present study are compared to results from the open literature using numerical and experimental methods. Figure 4.14 (a) compares the variation of h_{conv} versus ΔT_{sb} with that obtained by Museux *et al.* [79] and Decima *et al.* [39] for the whole body. It is observed that the current numerical results are closer to the correlations obtained by Museux *et al.* [79] with a relative difference around 11% while this difference increases to around 30% relative to data reported by Decima *et al.* [39]. This difference could be related to the different type of incubator used in the other studies as well as the accuracy of measurement tools. Figure 4.14 (b) compares the averaged convective heat transfer coefficient for the whole body and different segments with those obtained in the open literature. It is worthy to note that the convective heat transfer coefficients for different body segments obtained by Belghazi *et al.* [41] are computed from the evaporative heat transfer coefficient measured experimentally by using Lewis equation [115]. From this figure, it is shown that the present data are in fair agreement with those reported in earlier experimental studies with slight differences related to the difference in the manikin, incubator geometry and the temperature difference ΔT_{sb}.

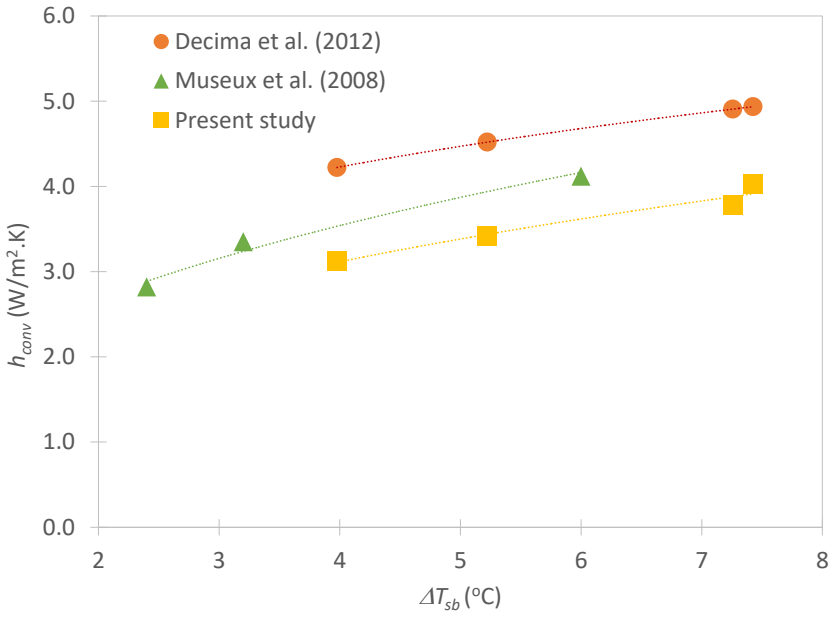

(a)

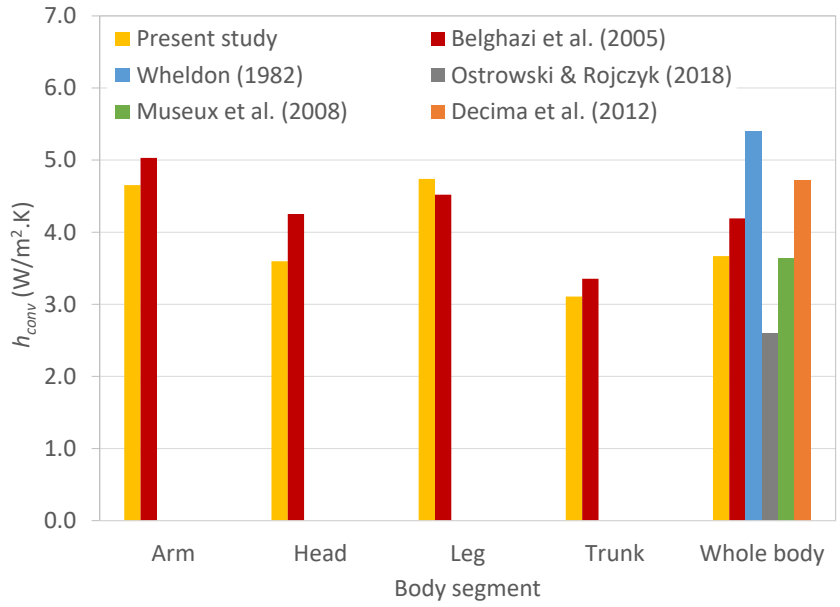

(b)

Figure 4.14: Comparison of convection heat transfer coefficient with that obtained from open literature (a) for whole body versus temperature difference ΔT_{sb} and (b) its temperature weighted average value for each body segment and whole body.

Body Segment	h_{rad} (W/m^2.K)	h_{conv} (W/m^2.K)
Arm	$3.91\Delta T_{sr}^{-0.11}$ $(R^2 = 0.8792)$	$2.60\Delta T_{sb}^{0.40}$ $(R^2 = 0.9821)$
Back	$4.63\Delta T_{sr}^{-0.38}$ $(R^2 = 0.9787)$	$1.42\Delta T_{sb}^{0.31}$ $(R^2 = 0.9578)$
Head	$9.78\Delta T_{sr}^{-0.27}$ $(R^2 = 0.9822)$	$1.88\Delta T_{sb}^{0.34}$ $(R^2 = 0.9633)$
Leg	$8.62\Delta T_{sr}^{-0.27}$ $(R^2 = 0.9798)$	$2.63\Delta T_{sb}^{0.33}$ $(R^2 = 0.9371)$
Trunk	$10.27\Delta T_{sr}^{-0.26}$ $(R^2 = 0.9796)$	$1.57\Delta T_{sb}^{0.38}$ $(R^2 = 0.9361)$
Whole body	$8.29\Delta T_{sr}^{-0.26}$ $(R^2 = 0.9797)$	$1.87\Delta T_{sb}^{0.37}$ $(R^2 = 0.9567)$

Table 4.3: Summary of the correlations for the heat transfer coefficients in terms of corresponding temperature differences showing the R^2 index

Empirical correlations for the Nusselt number Nu versus Rayleigh number Ra could be also obtained as follows:

$$Nu = cRa^d \tag{4.16}$$

The Nusselt number is defined as follows:

$$Nu = \frac{h_{conv} L_{s,i}}{k_{air}} \tag{4.17}$$

where $L_{s,i} = A_{s,i}^{1/2}$ is the characteristic length of a body segment i of surface area $A_{s,i}$ and k_{air} is the thermal conductivity of air equal to 0.0242 W/m.K.

The Rayleigh number is obtained as follows:

$$Ra = \frac{g\beta\left(T_{s_i} - T_a\right)L_{seg}^3}{\nu\alpha} \tag{4.18}$$

with $\beta = 2/(T_s + T_a)$ is the air thermal expansion coefficient, ν the kinematic viscosity of air and α the air thermal diffusivity.

The variation of the Nusselt number versus Rayleigh number for different segments as well as for the whole body is shown in Figure 4.15 along with the power law fitting curves. From this figure it is observed that the Nusselt number increases with the Rayleigh number due to the increase in the buoyancy forces, and thus higher convection heat losses. The differences in the Rayleigh numbers for the different body segments is caused by the different

characteristic lengths. The empirical correlations for the Nusselt numbers are summarized in Table 4.4 showing a range for the power law between 0.3 and 0.4.

	Arms	Back	Head	Legs	Trunk	Body
$\boldsymbol{Nu} =$	$0.099Ra^{0.40}$	$0.178Ra^{0.30}$	$0.167Ra^{0.33}$	$0.264Ra^{0.32}$	$0.081Ra^{0.37}$	$0.101Ra^{0.36}$
$\boldsymbol{R^2} =$	0.9821	0.9580	0.9633	0.9372	0.9362	0.9568

Table 4.4: Empirical correlations for the Nusselt numbers

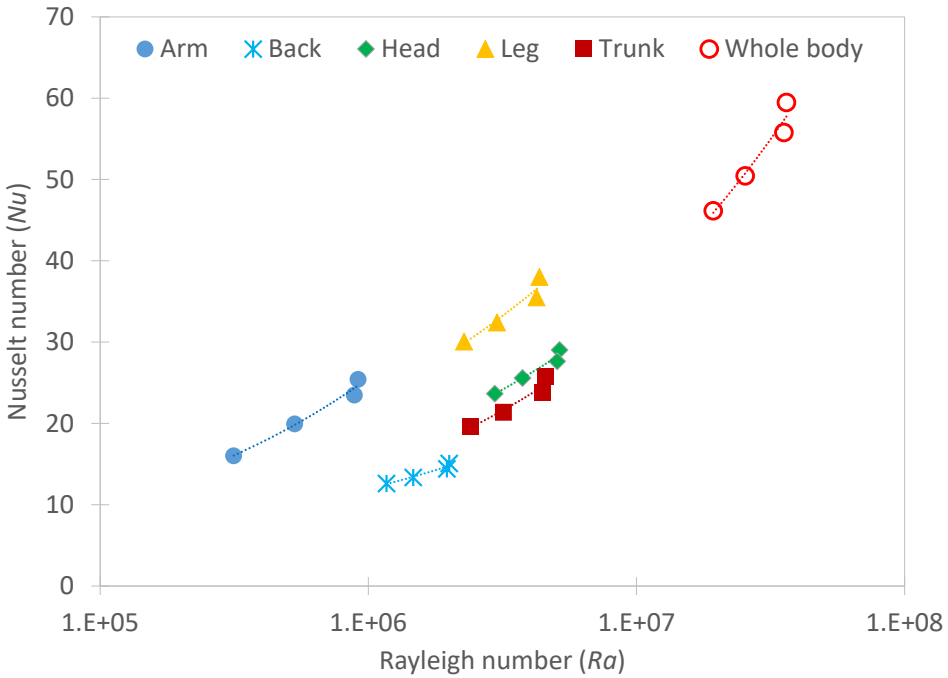

Figure 4.15: Variation of the Nusselt number versus Rayleigh number for different segments as well as for the whole body.

4.7.4 Operative temperature

The operative temperature T_o sensed by the neonate inside the incubator is obtained from the average of the mean radiant and incubator air temperature weighted by their respective heat transfer coefficients [81]:

$$T_o = \frac{h_{rad}T_r + h_{conv}\bar{T}_a}{h_{rad} + h_{conv}} \tag{22}$$

Thus, the operative temperature takes into account not only the air temperature inside the incubator but also the temperature of the surrounding incubator walls. Figure 4.16 shows the variation of the operative temperature for the different body segments as well as for the whole body versus the inlet air temperature T_{in}. From this figure, it is first noticed that all body segments have almost the same operative temperature, with a standard deviation of 1.6℃, which means that they sense the same temperature, especially for increasing inlet air temperature. The operative temperature increases linearly with increasing the inlet air temperature with a difference ranging between 1.5 and 3.5℃ less than T_{in}. The sensed temperature is lower than the incoming heated air temperature since the mean radiant temperature is smaller than the air temperature. Thus, to maintain similar levels of T_o, one could use radiant heating elements and decrease T_{in} without significant increase in energy. The benefit of using radiant heaters is to provide a better homogeneity of the heat fluxes.

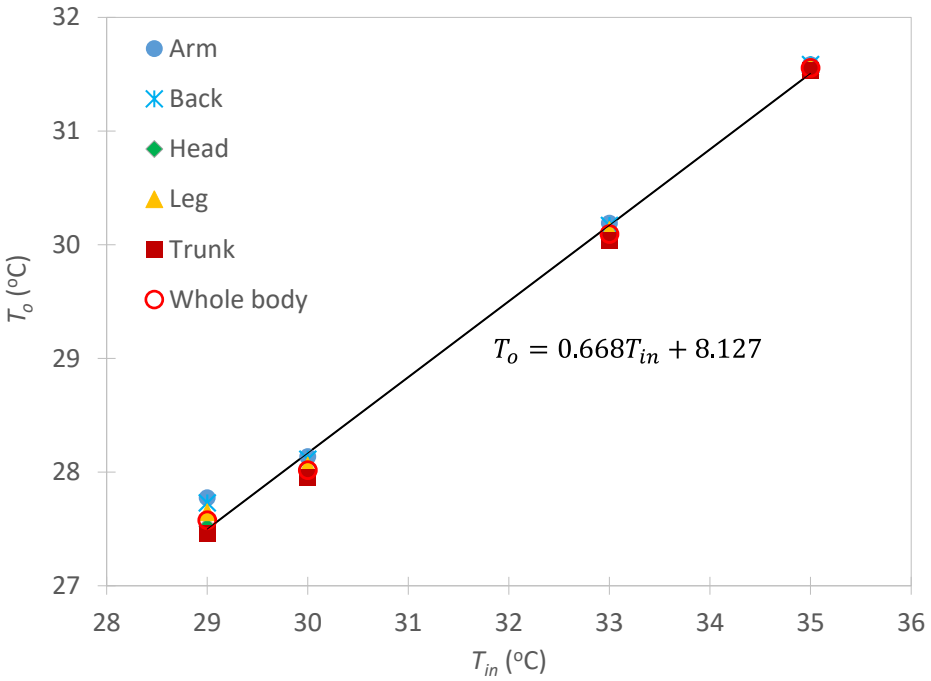

Figure 4.16: Variation of the operative temperature versus T_{in} for different segments as well as for the whole body.

4.7.5 Assessing neonate thermal comfort

Thermal comfort in adults is evaluated subjectively by assessing their satisfaction with the hygrothermal environment [116]. Meanwhile, since preterm neonates cannot explicitly express their feeling, there is no procedure or standard in the open literature that could be used to quantitatively assess their satisfaction to the environmental conditions.

Thus, we suggest two approaches to access the thermal comfort of the preterm neonate inside the incubator. The first is the homogeneity of the heat fluxes on the skin surface and the second is the energy balance. In fact, a heterogeneous distribution of the heat flux on the skin can lead to a sensation of cold in some regions and hot in others. This could also lead to an increase in evaporative heat losses. The second is the energy balance that can be used to verify if the total heat lost from the skin is greater than that generated by the preterm neonate.

Figure 4.17 shows the coefficient of variation (CoV) of convective and radiative heat fluxes for the whole body versus inlet air temperature. The CoV is a good measure of the homogeneity since it is the ratio of the heat flux standard deviation $\sigma_{q"}$ to the area weighted average value of the heat flux $q"$ ($CoV = \sigma_{q"}/q"$). From this figure, it is observed that both CoV increase with increasing inlet air temperature while the convective heat fluxes show higher CoV reflecting lower homogeneity on the skin surface. The decrease in the homogeneity of the heat fluxes is accompanied by an increase in the evaporative heat losses and lesser thermal comfort for the neonates [41]. This could be partially solved by adding for instance radiant heaters to better distribute the heat flux over the body skin surface.

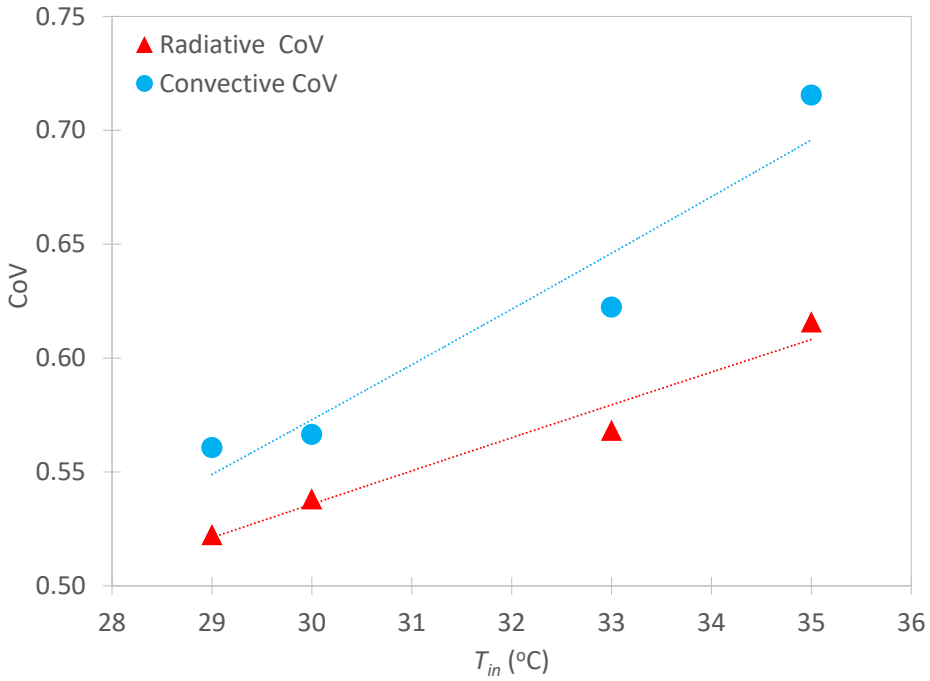

Figure 4.17: Coefficient of variation of convective and radiative heat fluxes for the whole body versus inlet air temperature.

According to equation (4.5) and to the heat balance model presented in section 4.6, in thermoneutrality, the heat losses due to convection, radiation, skin evaporation and respiration are balanced by metabolic heat generation within the infant body. However, if heat losses are greater than heat generation, the infant temperature will tend to decrease, and they might suffer from cold stress. Thus, let us define the heat difference as follows:

$$\Delta q = q_m - (q_{conv} + q_{rad} + q_{ev} + q_{res}) \tag{23}$$

When Δq is negative it means the infant is losing heat more than his body can produce. The objective is to minimize Δq; to, in turn, minimize heat or cold stress.

In Figure 4.18 we present the results obtained by combining the CFD data to the heat balance model and we compare them to the heat balance obtained from Drager heat balance program [117]. It could be observed that the heat difference is always negative, i.e., the air temperature is not enough to ensure a heat balance for the neonate. The best case is when $T_{in} = 35℃$ for which Δq is the smallest. The present results are different than those obtained in Drager calculator due to the difference in the empirical expressions and the radiation and

convection heat transfer coefficients and due to several simplifications in the Drager calculator. This difference ranges between 20 and 40%.

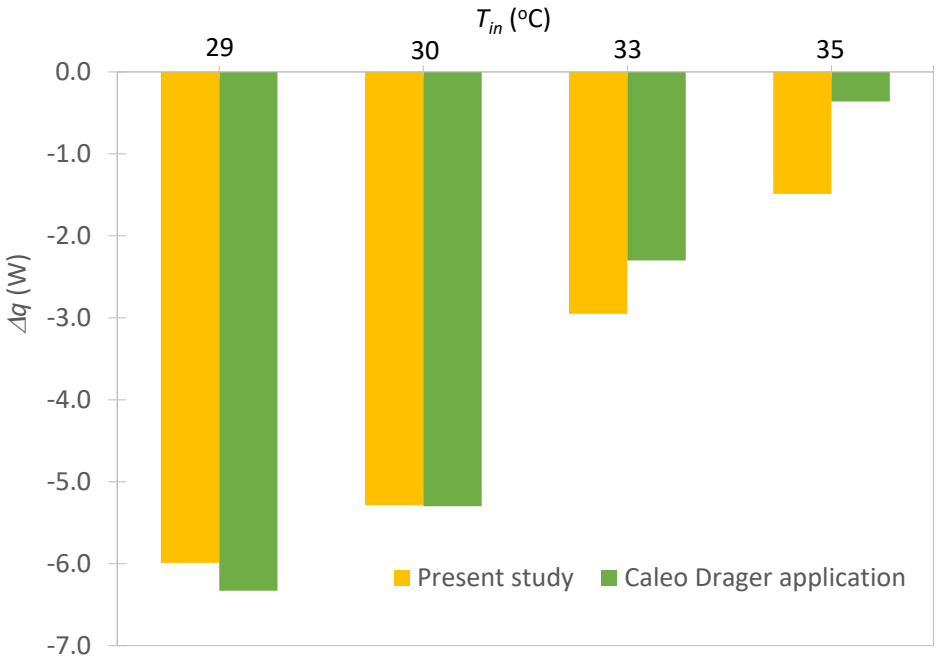

Figure 4.18: Heat balance on whole body obtained from present theoretical analysis and compared to that obtained by Drager heat balance model [117] for different inlet air temperatures and for a relative humidity of 66%.

4.8 Conclusions

Numerical simulations are carried out for a preterm neonate consisting of five segments (head, trunk, back, arms and legs) nursed inside an incubator. The air inlet temperature varies between 29 and 35℃ and the air flowrate varies between 5 and 50 Liters/min. The $k-\omega$ SST turbulence model is used with pseudo-transient and second order schemes.

It is found that, for the current operating conditions, the flow is dominated by natural convection. The heat losses vary with varying incubator air temperature while they are not significantly affected by the air flowrate which was increased by a factor of 10.

Correlations for the radiative and convective heat transfer coefficients are obtained for each body segment. These correlations are of great interest for thermoregulation and bioheat models aiming to study heat transfer in preterm infants. The radiative heat transfer coefficient varies between 2.2 and 6.2 W/m^2K while the convective heat transfer coefficient varies between 2.6 and 4.7 W/m^2K. The results were validated against available experimental data from the open literature.

Since thermal comfort could not be assessed in neonates, two methods are proposed in the present study to evaluate the heat balance and thermal comfort in neonates. The first consists on analyzing the homogeneity of heat flux distribution on the skin surface. In the second, a heat balance model is developed by taking into consideration the evaporative heat losses and respiration from neonates.

In future study, numerical simulations will be conducted to evaluate the evaporative heat transfer coefficients. This will be accomplished by directly computing the transport equation with suitable evaporation modeling.

Chapter 5 Experimental Analysis

Ce chapitre est consacré à l'étude expérimentale menée sur le mannequin thermique placé à l'intérieur de l'incubateur. Nous discutons dans ce chapitre l'instrumentation du mannequin avec des fils chauffants fixés sur la surface intérieure et avec des thermocouples fixés sur la surface extérieure. Un régulateur PID (proportionnel, intégral, dérivé) est utilisé pour contrôler les températures des différents segments du mannequin. Nous adoptons la méthode de Ziegler-Nichols qui est une méthode heuristique pour le réglage du régulateur PID. Le logiciel LabVIEW est utilisé ensuite pour créer l'instrument virtuel avec une interface graphique. Trois campagnes de mesures sont menées. La première consiste à fixer une température d'incubateur à 30°C et dans la deuxième la température est augmentée à 35°C tout en gardant les portes de l'incubateur fermées. Dans la troisième campagne de mesure, la température de l'incubateur est fixée à 35°C avec les portes de l'incubateur ouvertes. Les résultats issus des trois études expérimentales sont discutés en termes de variation temporelle des températures des différents segments du mannequin ainsi en analysant les pertes de chaleur par convection et rayonnement thermique qui sont obtenus en couplant les données expérimentales aux coefficients d'échange de convection et de rayonnement obtenues dans le Chapitre 4. Ces résultats sont aussi comparés avec des données numériques et expérimentales de la littérature. Nous constatons de cette comparaison que le mannequin conçu dans cette thèse ainsi que les méthodes expérimentales adoptées sont valides et donnent des résultats avec une bonne correspondance avec la littérature.

5.1 Introduction

While numerous thermal manikins representing adult human body were developed and studied in the open literature [91, 118, 119, 120], much less were devoted to the analysis of heat and mass transfer from preterm infants. Thermal manikins representing preterm infants were used in the literature to study the heat transfer inside infant incubators and radiant warmers as discussed in section 2.4.2. These thermal manikins were mostly manufactured by cast copper like in Elabbassi *et al.* [37] and Ostrowski *et al.* [85]. For instance, Elabbassi *et al.* [37] used heating wires from the inner side to heat the manikin and adopted the proportional integral and derivative (PID) regulator to control the manikin surface temperature. Meanwhile, Ostrowski *et al.* [85] used water heating system where hot water is circulating inside the thermal manikin and an advanced digital controller embedded in a heat pump system. In the present chapter, we show a new way of manufacturing a thermal manikin representing a preterm infant using the 3D printing technique. The manikin is heated from the inner surface using electric wires while the temperature on the outer surface is controlled via a PID regulator built using LabVIEW. The manikin is tested inside an infant incubator under three different scenarios. The convection and radiation heat fluxes from the different body segments are then obtained by coupling the experimental data to the heat transfer coefficients obtained numerically in Chapter 1.

5.2 Instrumentation

In this section, the instrumentation of the 3D printed thermal manikin with heating wires fixed on the inner surface and thermocouples fixed on the outer surface are discussed.

5.2.1 Heating wires

The heating of the thermal manikin is done by using a constant power supply connected to Nichrome heating wires. The heating is done separately for the seven body parts. In order to place the heating wires on the inner surface of the manikin, the different parts were cut carefully to have better access. Thus, the head was cut into four parts, namely

the back, left and right part. The chest is also cut into left and right part. Thus, the total number of parts with separate heating wires is ten.

Different methods were tested to fix the wires on the inner surface such as using silicone hot glue gun and epoxy resin superglue. However, these methods fail to maintain sustainable attachment of the heating wires to the inner surface of the preterm manikin.

Hence, soldering iron was finally adopted for fixing the heating wires. First, the Nichrome wire is laid on the inner surface of the manikin and the soldering iron is then passed over it. Due to the heating, a thin plastic layer of the manikin inner surface would melt around the wire which than become incased into the part. This process was deemed a success and all the parts were wired that way. In fact, this method tallows the wires to become embedded within the manikin surface increasing thus the contact area which led to decrease in the contact thermal resistance.

The heating wires are placed on the inner surface of the manikin with a maximum spacing of 5 mm between them to maintain as much as possible a uniform temperature distribution as shown in Figure 5.1 for the chest and head of the thermal manikin. This figure shows how the wires are carefully placed on the inner surface forming parallel lines with quasi-uniform distance and covering the entire surface area.

(a)

(b)

Figure 5.1: Heating wires fixed on the inner surface of the thermal manikin for (a) the left chest part and (b) left head part.

Once done with fixing the heating wires, the different body parts should be assembled. To do so, 3D printing PLA wires are melted on the joints which are fixed together while maintaining homogenous outer surface composition. After welding all the manikin parts together and closing all the gaps that were present in it, the manikin went into a grinding process to remove all the excess PLA from its surface.

Figure 5.2 shows the assembled thermal manikin where all the nichrome wires are connected to an insulated cable. Each part has two cables connecting it to the SSR and the power supply. All the cables from the different body parts are leaving the manikin from the head sides (on the ear location), so not to cause problems in the testing process in the incubator.

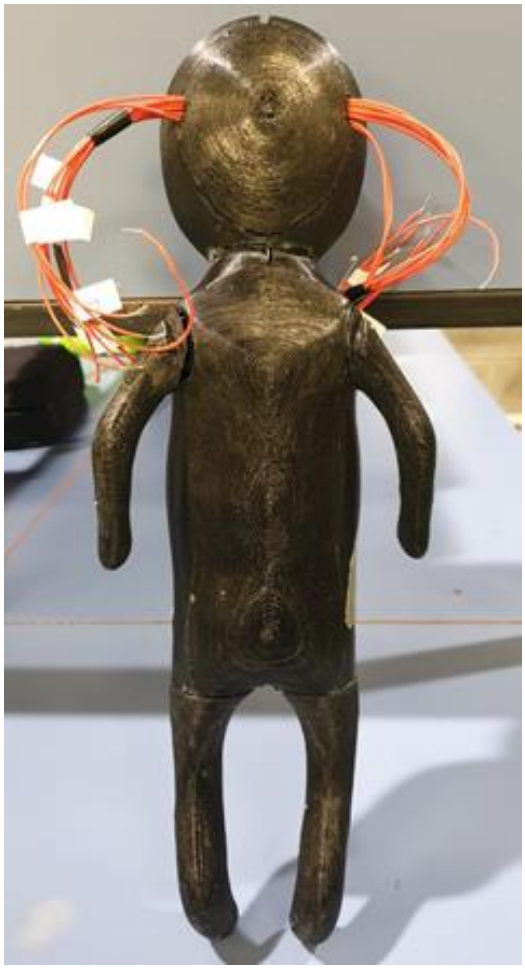

Figure 5.2: Preterm thermal manikin assembled after instrumenting with the heating wires. The cables connecting the heating wires to the power supply (in orange) are leaving through the head at the ear sides.

5.2.2 Thermocouples

The outer surface temperatures of the different body parts are measured with type J thermocouples. These thermocouples have a positive lead made of iron (white wire in Figure 5.3) and a negative lead made of constantan (orange wire in Figure 5.3), a copper-nickel alloy. The thermocouple leads are welded at the tip to form a spherical junction as shown in Figure 5.3.

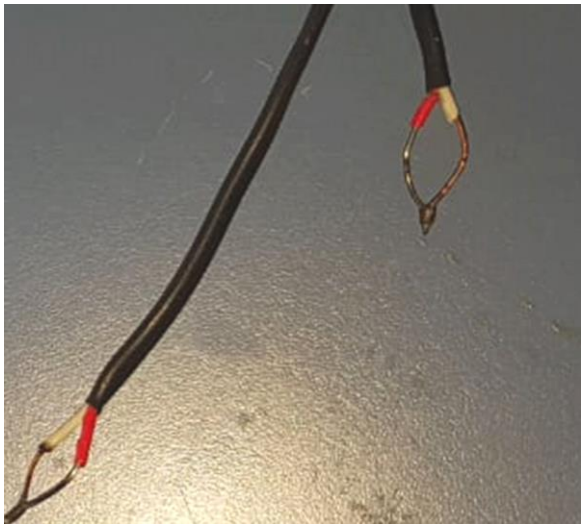

Figure 5.3: Image showing the type J thermocouples used to measure the manikin's external surface temperature showing the welded junction at the tip.

5.2.3 Uncertainty Analysis

The uncertainty analysis of the instrumented thermal manikin is undertaken by evaluating the experimental errors on the power supply, thermocouples and repeatability. The relative error on the power supply system is $e_{m,p} = \pm 0.7\%$. A repeatability test was performed to measure power for same conditions, and this led to a maximum relative error of $e_{r,p} = \pm 2.7\%$. Thus, according to the equation below, the accuracy of the temperature measurements in the present study is $e_p = \pm 2.8\%$.

$$e_p = \sqrt{e_{m,p}^2 + e_{r,p}^2} \tag{5.1}$$

The manufacturer accuracy of the thermocouples is $e_{m,th} = \pm 0.75\%$. The thermocouples were tested by measuring the air temperature inside the incubator and the manikin surface temperature at different locations and compared the reading to those obtained using the thermal sensors of the incubator explained in section 3.2. Then a repeatability test was performed to measure the outer surface temperature for same conditions, and this led to a maximum relative error of $e_{r,th} = \pm 1.7\%$. Another error is pertaining to the calculation of the average temperature of each body segment from the

different measuring thermocouples. This error is around $e_{u,th} = \pm 1.8\%$.. Thus, according to the equation below, the accuracy of the temperature measurements in the present study is $e_{th} = \pm 2.6\%$

$$e_{th} = \sqrt{e_{m,th}^2 + e_{r,th}^2 + e_{u,th}^2} \tag{5.2}$$

5.2.4 Solid-state relays

A solid-state relay (SSR) provides the same function as an electromechanical relay, but it has no moving parts. SSR will turn on and off when a small external voltage is applied across its control terminals. They consist of a sensor which can respond to a control signal where a solid-state electronic device switches the power to the load circuit and a coupling mechanism which enables the control signal to activate this switch.

For the bioheat modeling, normal relays cannot be used because of their slow response time and their ability to wear out fast because of the physical contact. Solid State relays have on the other hand fast switching speeds and no physical contact leading to longer lifespan. In the present study, a standard type SSR DC to DC, like the one shown in Figure 5.4, is used to control the heating process. The heating wires fixed on the inner surface of the manikin is connected to the SSRs which is their turn are connected to the data acquisition system (DAQ). The DAQ consists of a collection of software and hardware which enable the measurement of physical characteristics such as voltage, current and temperature.

Figure 5.4: Solid state relay SSR-25 DD. Standard type DC to DC. The input voltage ranges between 4 and 32 Volts. The response time is estimated to 1 ms [121].

5.3 PID Control

5.3.1 Fundamentals

The implementation of a controller for the thermal manikin is crucial for maintaining a constant temperature on the outer surface of the thermal manikin at the different body parts. Several types of controllers could be found in the open literature [119, 91, 120, 118]. The most widely used controllers for thermal analysis are the proportional, integral and derivative (PID) controllers [122]. They can also be used separately, P (proportional controller), I (integral controller), PI (Proportional-integral controller), PD (Proportional-Derivative controller), PID (Proportional-integral-derivative controller).

A PID controller is a feedback control loop where it continuously computes an error $e(t)$ as the difference between the setpoint temperature $r(t)$ and the measured valued $y(t)$. Then, it automatically applies the correction to the control function $u(t)$ based on the PID terms as shown in the block diagram represented in Figure 5.5. The control function is expressed as follows:

$$u(t) = K_p e(t) + K_i \int_0^t e(\tau)d\tau + K_d \frac{de(t)}{dt} \tag{5.3}$$

where K_p, K_i and K_d are the PID coefficients.

These parameters can be found by different methods when the exact mathematical model of the plant (thermal mannikin) is known. In our case, the model is not exactly known, these parameters will be found based on experimental tuning methods (i.e. Ziegler Nichols).

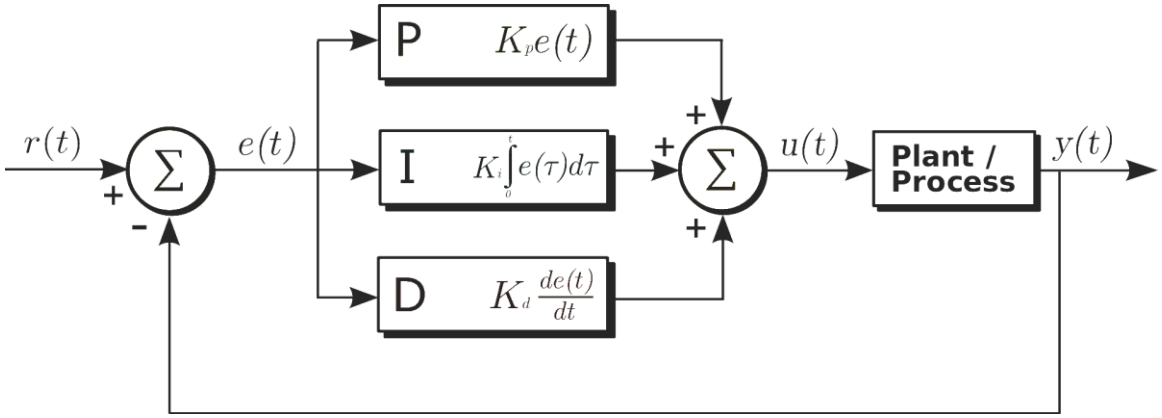

Figure 5.5: A block diagram of a PID controller where $r(t)$ is the setpoint temperature in our case, and $y(t)$ is the temperature value measured by the thermocouples.

In the present case, the PID controller is implemented as a virtual instrument using LabVIEW. The sensor plays an essential role in getting the desired output, so the accuracy of the sensor plays an essential role in the behavior of the control. Thus, to summarize, the controller represents the LabVIEW virtual instrument, while the plant consists of the thermocouples, the SSR and the thermal manikin. The system is a closed loop representation since the output is measured qualitatively using thermocouples, and a feedback element is present.

5.3.2 Ziegler-Nichols tuning method

Since the plant parameters are unknown, some PID tuning should be done to obtain the parameters. Various tuning methods exist in order to achieve better, and more acceptable control system response based on the desired control objective.

In order to tune the PID controller and get the initial estimation for the parameters that are to be used in the LabVIEW, the Ziegler-Nichols method was adopted. This method of tuning consists of trial-and-error testing; it is based on sustained oscillations. The method was applied on the system in order to get its desired behavior such as a small steady-state error, small overshoot, a fast-settling time and decrease the rise time.

The following steps are followed during the Ziegler-Nichols tuning method applied for the ten parts for which separate control was required [122]:

a) Start with small value for K_p while $K_i = K_d = 0$
b) Increase K_p gradually until it reaches the ultimate gain K_u at which neutral stability is reached where the temperature show periodic oscillations as shown in Figure 5.6.
c) Determine the critical period of oscillations T_u represented in Figure 5.6. This value was obtained used the search method to accurately capture the maxima.
d) Find K_p, T_i and T_d using the following equations:

$$K_p = 0.6K_u \tag{5.4}$$

$$T_i = 0.5T_u \tag{5.5}$$

$$T_d = 0.125T_u \tag{5.6}$$

e) Calculate K_i and K_d as follows:

$$K_i = \frac{K_p}{T_i} \tag{5.7}$$

$$K_d = K_p T_d \tag{5.8}$$

Using these parameters, the correction function $u(t)$ in equation (4.3) is now established which has the following transfer function:

$$u(s) = K_p\left(1 + \frac{1}{T_i s} + T_d s\right)e(s) \tag{5.9}$$

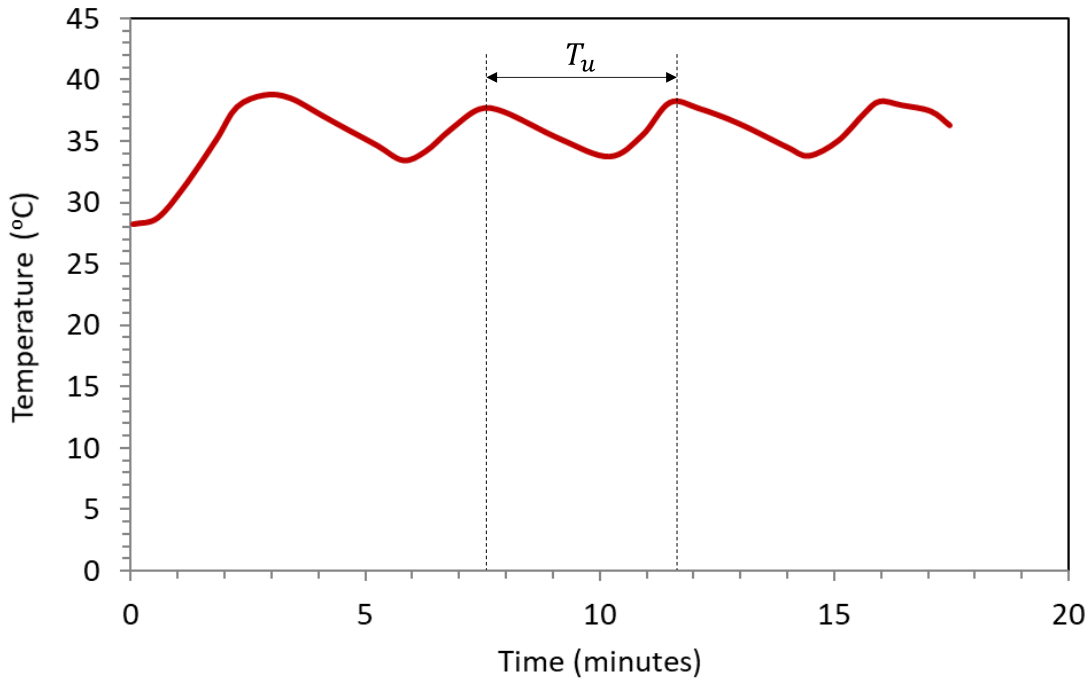

Figure 5.6: Temporal variation of the back head surface temperature with proportional control alone.

Each part has to be tested for a specific voltage depending on the length of the heating wire. This voltage (V) coupled with the electric resistance of each wire (R_{el}), which was obtained by measurement using an ohmmeter, provides the power (P) needed for each part following Ohm's law:

$$P = \frac{V^2}{R_{el}} \tag{5.10}$$

The length of the nichrome wires used can also be determined using the resistance value. Since the nichrome wire used is a 0.5 mm diameter wire, we can get from the datasheet of the wire its resistance per length which is found equal to $5.55\ \Omega/\mathrm{m}$ [123].

	Voltage (V)	Resistance (Ω)	Length (m)	Power (W)
Back head	4.5	8.0	1.44	2.53
Left head	20.0	28.0	5.05	14.29
Right head	20.0	28.0	5.05	14.29
Back	5.5	16.4	2.95	1.84
Left chest	18.5	22.5	4.05	15.21
Right chest	18.5	22.5	4.05	15.21
Left arm	8.2	18.5	3.33	3.63
Right arm	8.2	18.5	3.33	3.63
Left leg	15.0	21.6	3.89	10.42
Right leg	15.0	21.6	3.89	10.42

Table 5.1: Characteristics of the heating methods applied on the different body parts during the Ziegler-Nichols tuning method

After computing the gains as summarized in Table 5.2, the values are implemented into the LabVIEW virtual instrument which can now be used to maintain a constant surface temperature for the manikin during steady-state operation. The difference between two symmetric body parts is caused by the impurities and non-idealized cuts.

	K_u	T_u	K_p	T_i	T_d	K_i	K_d
Back head	105	4.07	63.00	2.03	0.51	30.98	32.03
Left head	130	3.66	78.00	1.83	0.46	42.58	35.72
Right head	130	3.32	78.00	1.66	0.41	47.04	32.34
Back	130	4.15	78.00	2.07	0.52	37.61	40.45
Left chest	170	3.03	102.00	1.52	0.38	67.25	38.68
Right chest	170	3.58	102.00	1.79	0.45	57.01	45.62
Left arm	70	2.95	42.00	1.48	0.37	28.47	15.49
Right arm	70	3.65	42.00	1.83	0.46	23.01	19.16
Left leg	100	2.95	60.00	1.48	0.37	40.65	22.14
Right leg	100	3.75	60.00	1.88	0.47	31.97	28.15

Table 5.2: PID gains computed using the Ziegler-Nichols method

5.3.3 LabVIEW Virtual Instrument

LabVIEW was used to implement the controller into the system by creating a virtual instrument. The input is taken from the DAQ that measures the real-world physical conditions of the system. The temperature is measured using thermocouples and the resulting data is converted into digital numerical values that work as an input for the controller. The controller then analyzes these values in order to get the desired results on the system.

Figure 5.7 shows the LabVIEW flowchart where the user picks a desired temperature setpoint for the manikin body part denoted by $r(t)$ in the PID control as explained in the previous paragraph. The interval for which the user can specify the temperature ranges from 36℃ to 42℃. The thermocouples measure the surface temperatures which are input to the DAQ to convert it to a digital input for the VI. Based on the gains of the PID, the pulse width modulation (PWM) is generated and sent to the SSR which will allow the electric power to flow into the heating elements. The PWM method is used to discretize the average power delivered by an electrical signal where the average current fed to the load is controlled by turning the switch between on and off and fast rate. This loop is repeated until the setpoint temperature is reached. At this stage, the controller will work on maintaining the measure temperature $y(t)$ close to the set point temperature $r(t)$ by continuously reducing the error $e(t)$. This is done by implementing the gains of the PID control. For the case when the measured temperature exceeds 43℃, the controller will turn off the PWM signal automatically avoiding the SSR from relaying any signal that enables wires to heat up to avoid damage to the 3D printed thermal manikin.

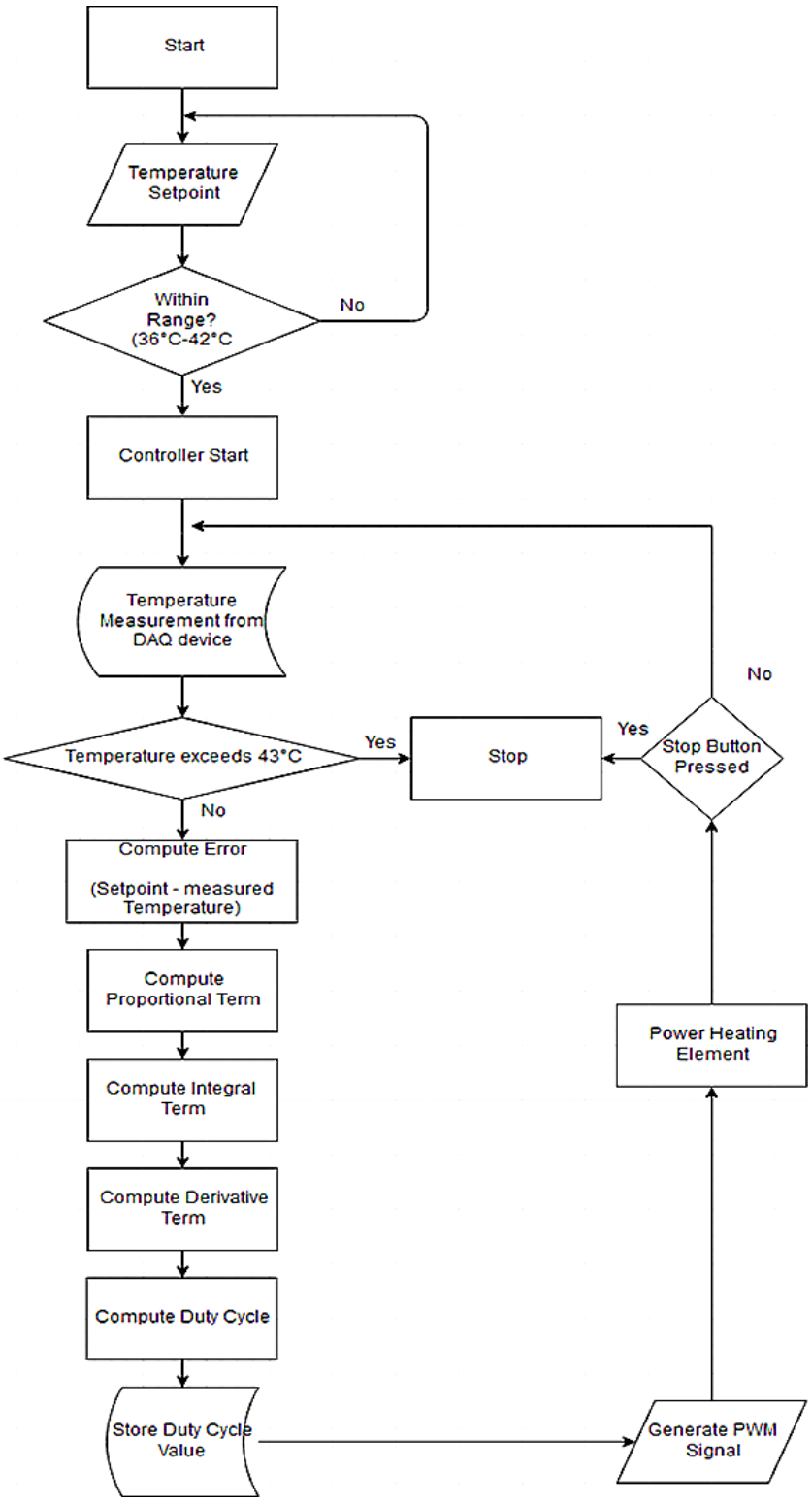

Figure 5.7: Flowchart of the LabVIEW program used to build the virtual instrument.

Figure 5.8 shows the LabVIEW graphical user interface (GUI) where the user can set the desired surface temperature for the different body parts. The real-time variation of the temperature measured on the different parts is shown in this GUI. There is a possibility to select a control method based on the surface temperature, as explained in the previous sections, or based on the heat flux and thermal comfort which will be studied in the future.

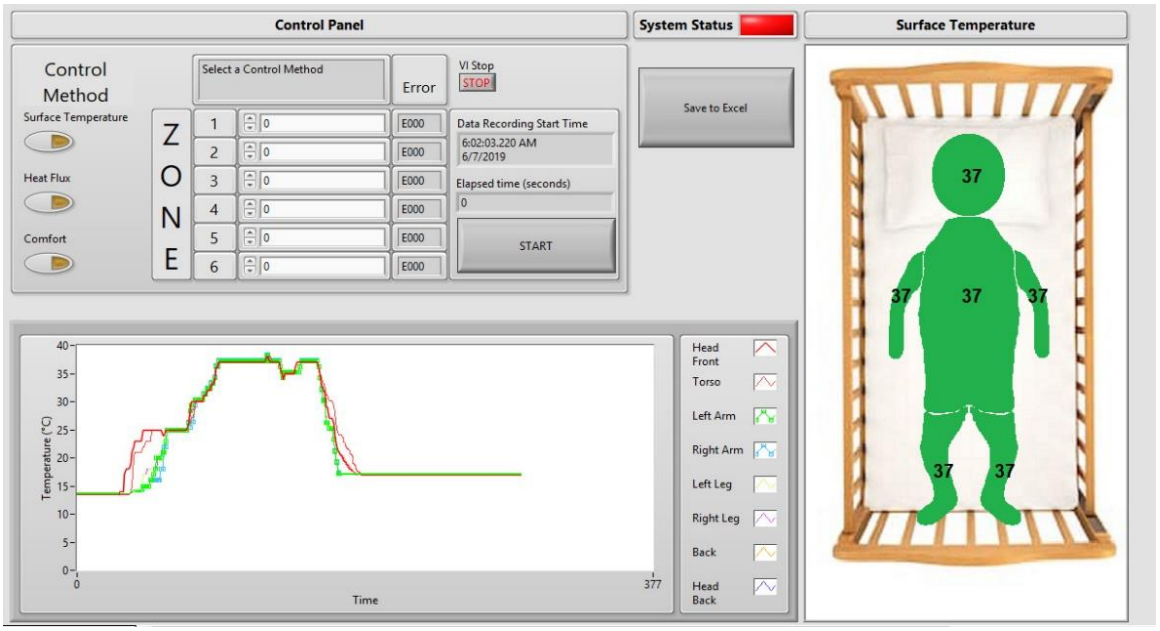

Figure 5.8: LabVIEW graphical user interface showing the set temperatures for the different body parts, the heating method used and the real-time graph of the temperature variation.

5.4 Experimental Setup

After performing the Ziegler-Nichols method on the different body parts and obtaining the different values for the gain and time periods, as well as the values for the voltage of each part, the next phase of testing could begin.

To conduct the experiments, the manikin is welded together before being placed in the incubator as explained in section 5.2. The heating wires of the manikin are connected to the SSR panel and then to the power supplies. Four power supply were used and seven SSR's. The thermocouples were attached to the different body parts of the manikin. All the

thermocouples are connected to the DAQ which in turn is connected to both a power supply and the laptop that contains the controller.

The experimental setup is shown in Figure 5.9 with the different components used for the thermal control.

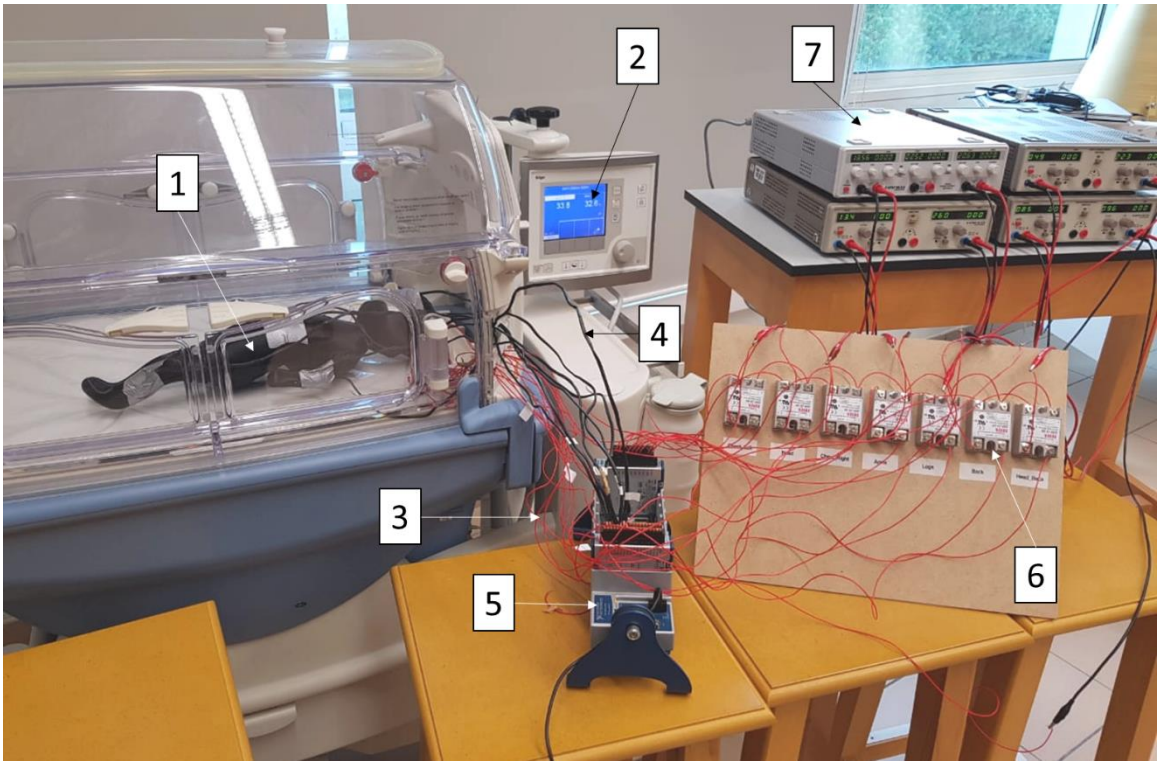

Figure 5.9: Experimental setup showing the thermal manikin inside the infant incubator (1), the incubator temperature and humidity control panel (2), the heating wires (3), the thermocouples (4) connected to the DAQ (5), the SSR panel (6) and the power supplies (7).

Three experiments are performed in the present study as explained below. For all the experiments, the incubator humidity was kept constant at 50% and the thermal manikin surface temperature is 36.7℃.

a) Experiment 1: the incubator set temperature is 30℃ with all ports closed.
b) Experiment 2: the incubator set temperature is 35℃ with all ports closed.
c) Experiment 3: the incubator set temperature is 35℃ with all ports open.

The results obtained for the three experiments are discussed in the next section.

5.5 Experimental Analysis

5.5.1 Temperature variation

In this section we analyze the results obtained for the three different experiments introduced in the previous section. Since for these experiments the initial temperature was not the same, and for better comparison and data analysis we introduce the following normalized temperature:

$$\theta = \frac{T - T_0}{T_{set} - T_0} \tag{5.11}$$

where in this equation, T is the body part measured temperature, T_0 is the body part initial temperature and $T_{set} = 36.7℃$.

The temporal variation of the normalized temperature for the different body segments is shown in Figure 5.10 for the three experiments. For the case of experiment 1 represented in Figure 5.10 (a), for which the incubator temperature is 30℃ and the ports are closed, the thermal manikin parts temperatures increase from their initial value to reach steady-state close to the set temperature used in the PID controller. From this graph it is observed that the parts in direct contact with the mattress, such as the back and head back, take longer time to reach steady state. This is caused to the conduction heat transfer with the mattress which is initially at around 25℃. Meanwhile, the trunk and face of the manikin reach steady-state temperature after about 7 minutes. All the manikin body parts show relatively good stable temperature during steady-state regime except for the arms which show small fluctuations around the set temperature. This could be caused to the fact that the arms are close to the incubator air inlet ports.

Now let us move to the second experiment represented in Figure 5.10 (b), during which the incubator temperature is increased to 35℃ and the ports are still closed. It is observed here that the normalized temperature variation shows similar qualitative behavior as in experiment 1. The temperature at the back of the manikin was the hardest to control since it was in direct contact with the mattress and thus it has very small heat loss when compared to that in the other parts.

Finally, in experiment 3, the incubator air set temperature was kept 35℃, however the ports of the incubator were opened to simulate the intervention of medical staff. From Figure 5.10 (c), it could be observed that an overshoot in the temperature of the thermal manikin was obtained due to the sudden change in the environment inside the incubator during the opening of the ports. However, the PID controller was able to quickly manage the temperature as observed from the variation of the normalized temperature in this figure. Moreover, the normalized temperature shows slight oscillations around the set value for most of the body parts. This could be caused by the fact that opening the ports will perturbate the flow inside the incubator which lead to oscillations in the measured temperature.

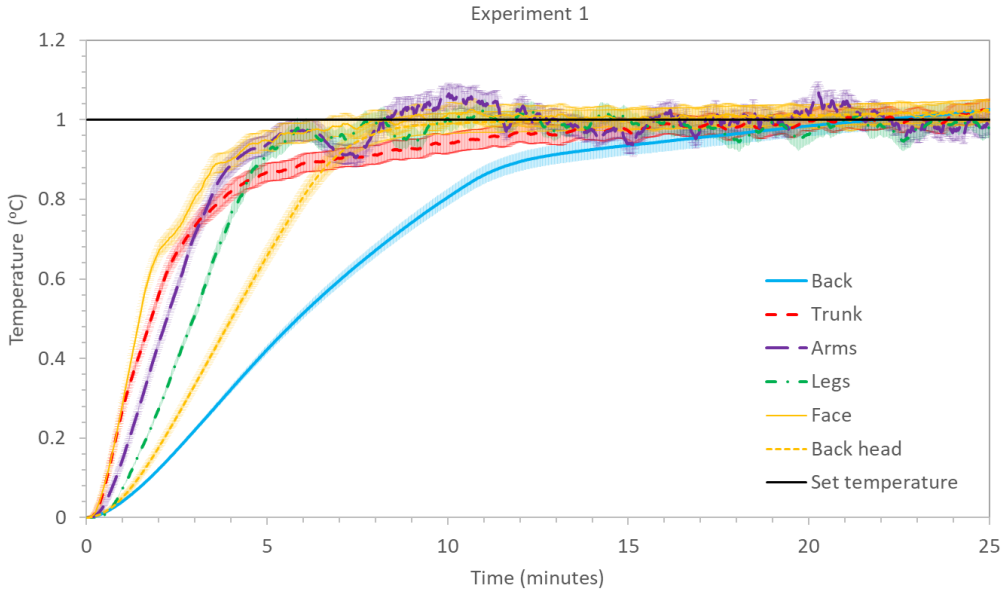

(a)

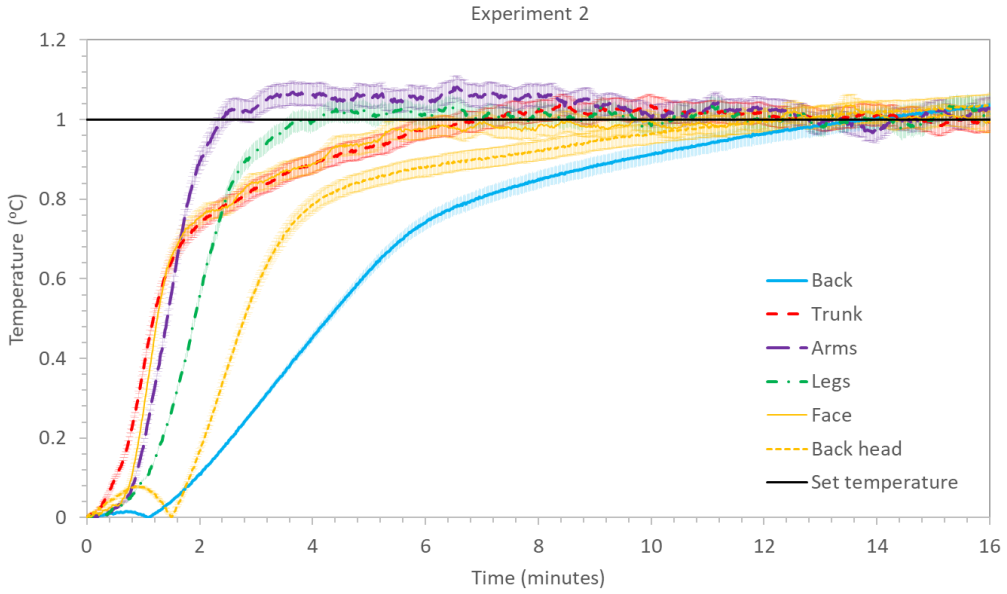

(b)

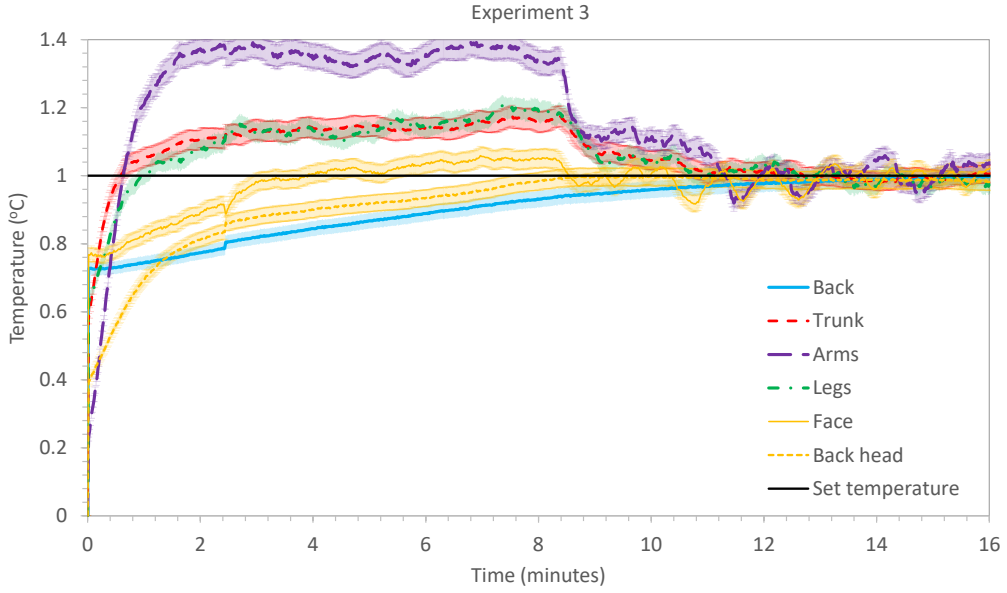

(c)

Figure 5.10: Temporal variation of the temperature for (a) experiment 1, (b) experiment 2 and (c) experiment 3.

5.5.2 Electric power

The power required for each body part to be maintained at the set temperature using the PID controller is determined during steady-state operation as discussed hereafter. During the heating process, the PID control send a signal to the SRR to turn on or off the electric power of the heating wires. Thus, as represented in Figure 5.11, the duty cycle will have values between zero, when the power is off, and one, when the power is on. To get the power from the duty cycle, the time the SSR is on needs to be determined. Hence, the electric power P_{el} required by each body segment is obtained as:

$$P_{el} = \frac{V^2}{R_{el}}\tau \tag{5.12}$$

where in this equation V is the voltage supplied to the body part, R_{el} the electric resistance for the heating wire and τ is the time during which the SSR was open.

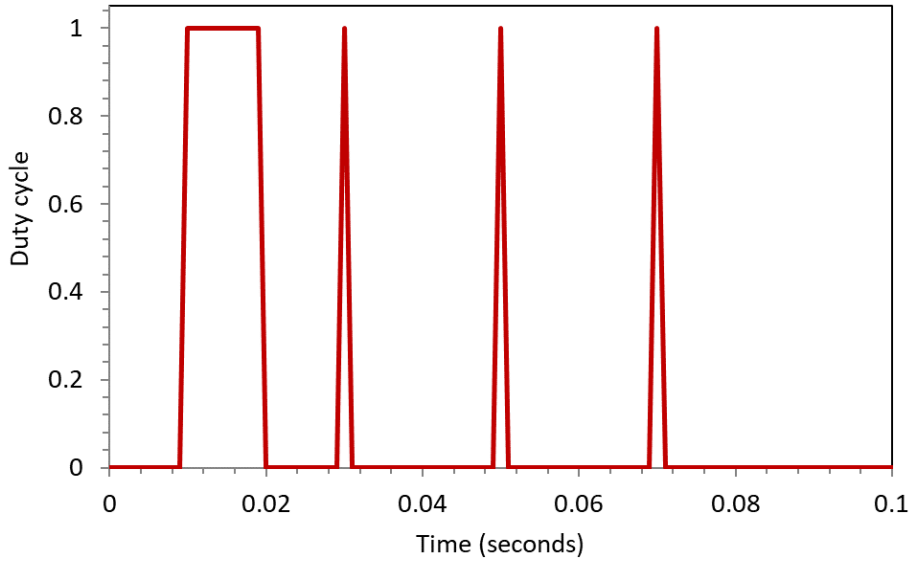

Figure 5.11: Small part of the duty cycle for the face during experiment 2

Figure 5.12 shows the electric power obtained for each body segment as well as for the whole body during the three different experiments. In this figure it can be observed that for experiment 1 during which the incubator air temperature was the lowest, the power required to maintain the manikin surface at set temperature was the highest almost for all the

body segments. Meanwhile, experiment 2 with higher incubator air temperature and closed ports show the lowest electric power consumption due to the lowest heat losses. For instance, for the whole body in experiment 1, the electric power reaches 73 W and it drops to 60 W for experiment 3 and then to 56 W during the 2nd experiment. Meanwhile, for the comparison of the heat losses between the different body segments to be meaningful, one should scale out the size of the body part and thus using the heat fluxes as discussed in the next section.

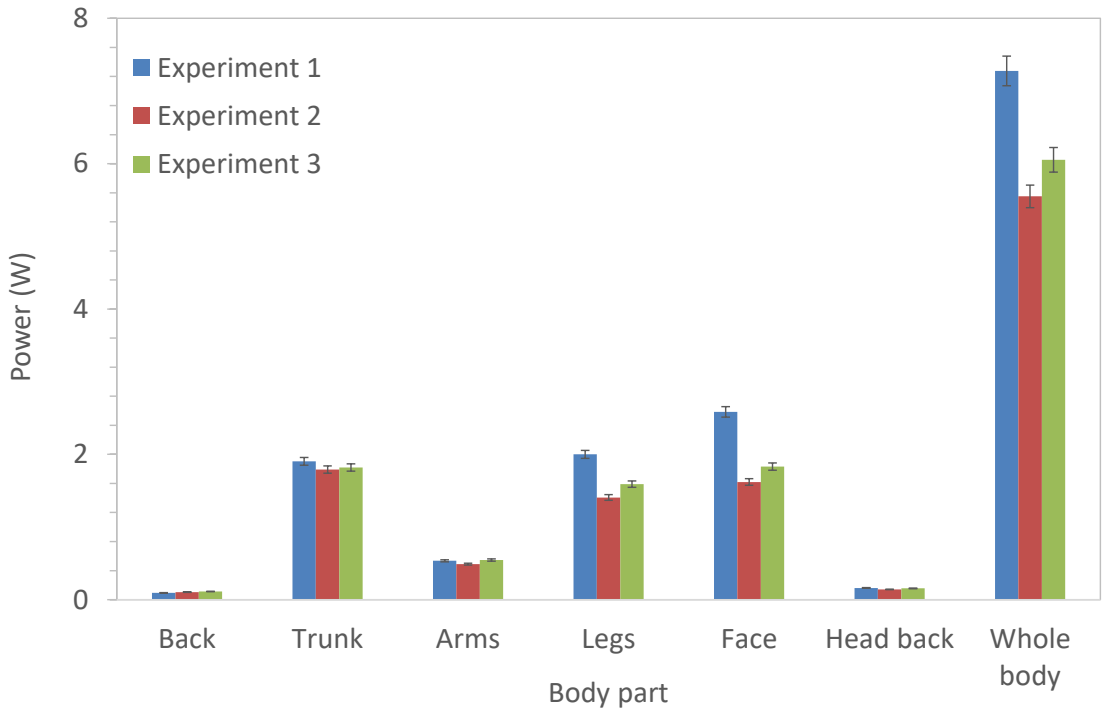

Figure 5.12: The total electric power representing the heat loss from each body segment for the three different experiments

5.5.3 Thermal analysis

To better analyze the heat transfer from the thermal manikin, we first need to scale out the effect of the body segments size. Thus, we use the heat flux, which is the ratio of electric power, determined in the previous section representing the rate of heat loss, and the surface area of the corresponding body part already given in section 3.3.

Figure 5.13 shows the heat fluxes of the different body segments during the three experimental cases studied here. As shown in this figure, the highest heat losses are exhibited

in the face of the manikin. The face here represents the head without the small part touching the mattress which is called the head back and has much lower heat losses since it is in direct contact with the mattress. The face is then followed by the trunk and legs and then by the arms and head back which show moderate heat losses. The back which almost completely lays on the mattress show very small heat losses. As discussed in the previous section, the heat loss during the first experiment with lower incubator air temperature is the highest while the second case with higher incubator air temperature and closed ports exhibit the lowest heat loss.

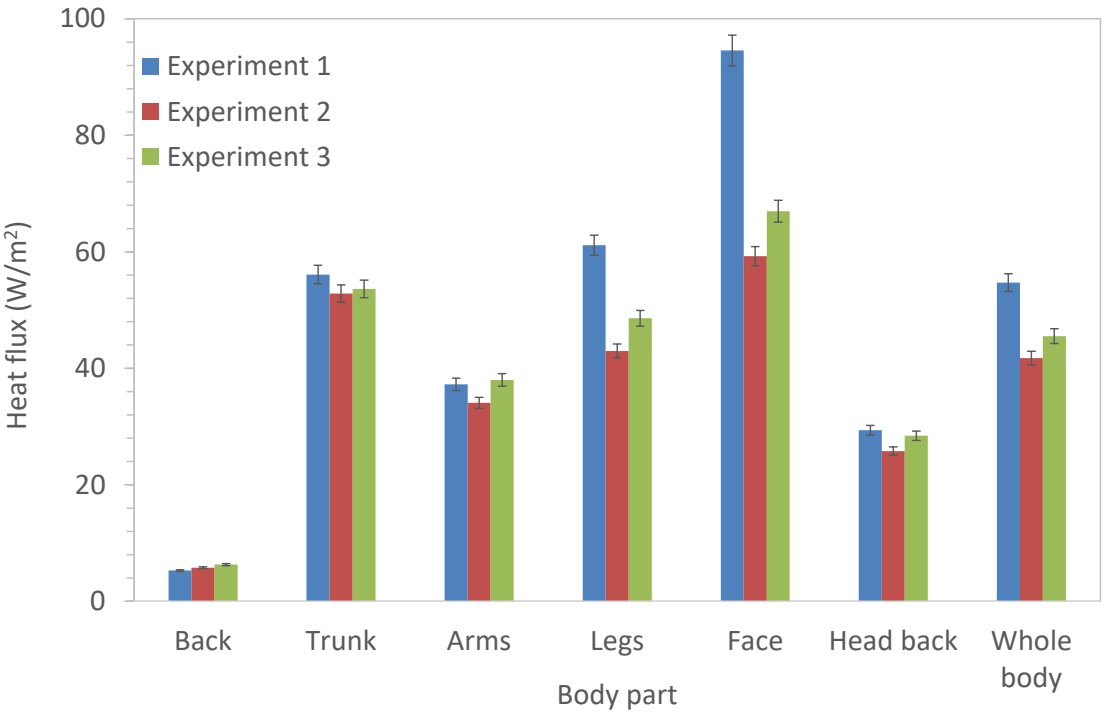

Figure 5.13: Heat flux for the different body segments during the three experimental cases

Figure 5.14 compares the heat losses obtained from the present experimental study to those obtained from CFD numerical simulations in Chapter 1 and to those obtained in the open literature. Here we compare the data for a cool incubator for which the temperature is set to 30℃, i.e., experiment 1, (Figure 5.14 (a)) and for a warm incubator with set temperature of 35℃, i.e., experiment 2, (Figure 5.14 (b)) where the ports are always closed.

From these figures, a fair agreement is obtained between present experimental data and CFD results except for the back where the modeling in CFD analysis it was assumed in

contact with an adiabatic mattress. The relative difference between experimental data and CFD results ranges between 5 and 26%. Moreover, for the whole-body heat flux, our experimental results correspond well to those obtained by most of the studies in the open literature. The relatively elevated difference between the various results presented in this figure are also caused to the difference in the thermal manikin shape, the geometry of the incubator and to other factors pertaining to the experimental conditions.

However, a fair satisfactory agreement is attained from the present experimental study especially for the warm incubator case presented in Figure 5.14 (b). For instance, evaluating the relative error between the present experimental results for the whole-body and the average value for the data obtained from the open literature, it yields 0.34%. This reflects the high fidelity of the present numerical methodology.

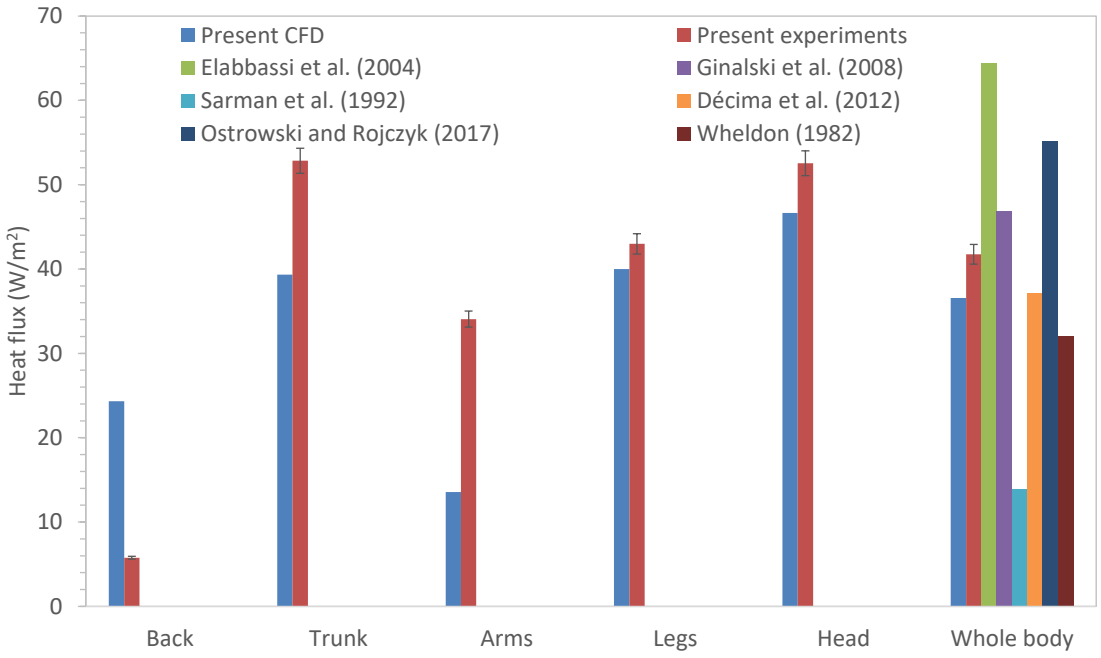

(a)

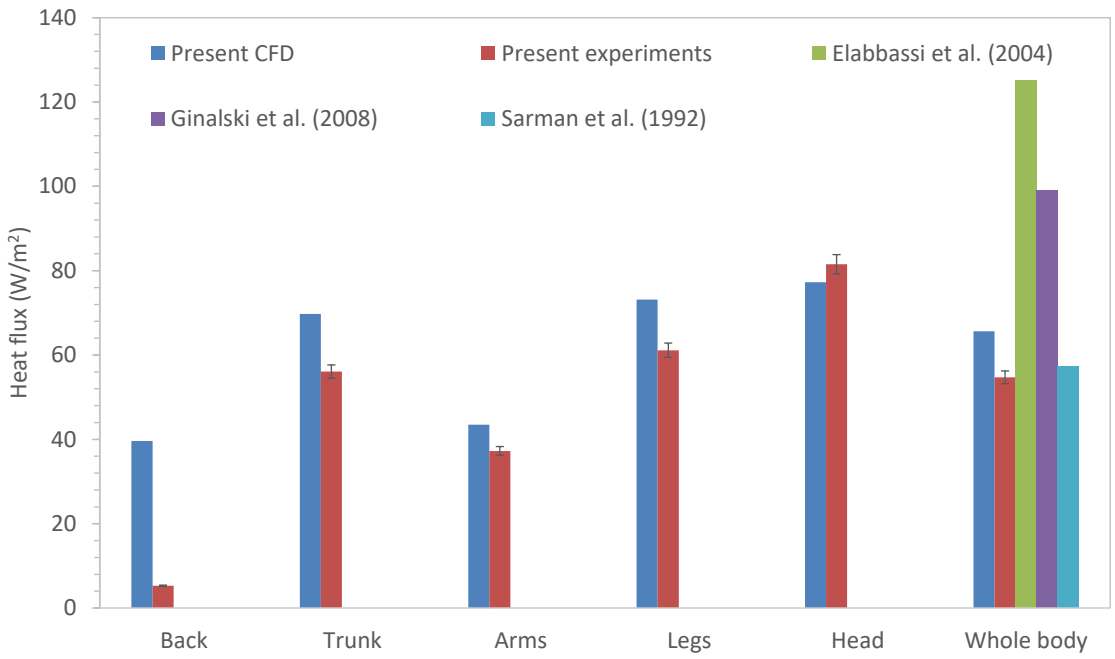

(b)

Figure 5.14: Total heat flux for the different body segments compared to CFD data and to values from the open literature: (a) cool incubator at 30℃ and (b) warm incubator at 35℃. Both cases the ports are closed.

Neglecting the conduction heat transfer between the manikin and the incubator mattress, the total heat lost from the manikin is divided into two parts. The first is the convective heat loss to the incubator air flow, and the second is the radiation heat transfer with surrounding surfaces. To determine these two modes of heat transfer, according to equations (3.12) and (3.13), we can use the correlation of the convective and radiative heat transfer coefficients, h_c and h_r respectively, derived in section 4.7.3. These coefficients are correlated to the temperature difference between the manikin segment surface temperature $T_{s,i}$ and the incubator bulk temperature $\overline{T_a}$, for convection, and between the manikin segment surface temperature and the radiative temperature T_r, obtained from equation (3.1). Hence, for easier referencing, we recall these equations below:

$$T_r = 0.724(\overline{T}_a - 31.93) + 29 \tag{5.13}$$

$$q_r^{"} = h_r\left(T_{s,i} - T_r\right) \tag{5.14}$$

$$q_c^{"} = h_c\left(T_{s,i} - \bar{T}_a\right) \tag{5.15}$$

where h_r is a function of T_r and h_c is a function in terms of $\bar{T}_a$ according to the correlations.

Thus, in these three equations we have four unknowns, which are $T_r, \bar{T}_a, q_r$ and q_c. The fourth equation from the energy rate balance equation on the manikin segments leads to the total heat flux obtained experimentally:

$$q_{tot}^{"} = q_r^{"} + q_c^{"} \tag{5.16}$$

Thus, we have now four nonlinear equations with four unknowns. To obtain the solution we use MATLAB unconstrained nonlinear optimization with the objective function being the difference between the actual measured total heat flux and the one obtained from equation (4.16). The optimization parameter is the bulk incubator air temperature.

The data obtained for the convective and radiative heat fluxes for the three different experiments are plotted in Figure 5.15 (a) and (b), respectively. In Figure 5.15 (a), it is observed that the convective heat losses are the highest for experiment 1 corresponding to a cool incubator and the lowest for experiment 2 corresponding to the warm incubator with closed ports. In experiment 3, the ports opening leads to an increase in convective heat loss from the thermal manikin by about 25%, relative to the case where the ports were kept open. Moreover, the thermal manikin head exhibits the highest convective heat losses, which explains why neonates always wear a hat when nursed inside incubators.

From Figure 5.15 (b), it is noticed that the radiation heat losses are much larger than convective heat loss, which is well known in infant incubators, on the opposite of radiant warmers. The highest radiation heat loss is in the manikin head, like for the convection case. The lowest radiation heat transfer occurs for the warm closed incubator, experiment 2, while the highest occurs for the cool incubator, experiment 1, similarly to what was observed for the convection heat transfer.

Finally, in average, we can estimate that the radiation heat losses from preterm thermal manikin are responsible of about 70% of the total heat loss while the remaining is caused by convection heat transfer. This could be reduced for instance by using radiant elements especially for very preterm infants with very low metabolic heat generation.

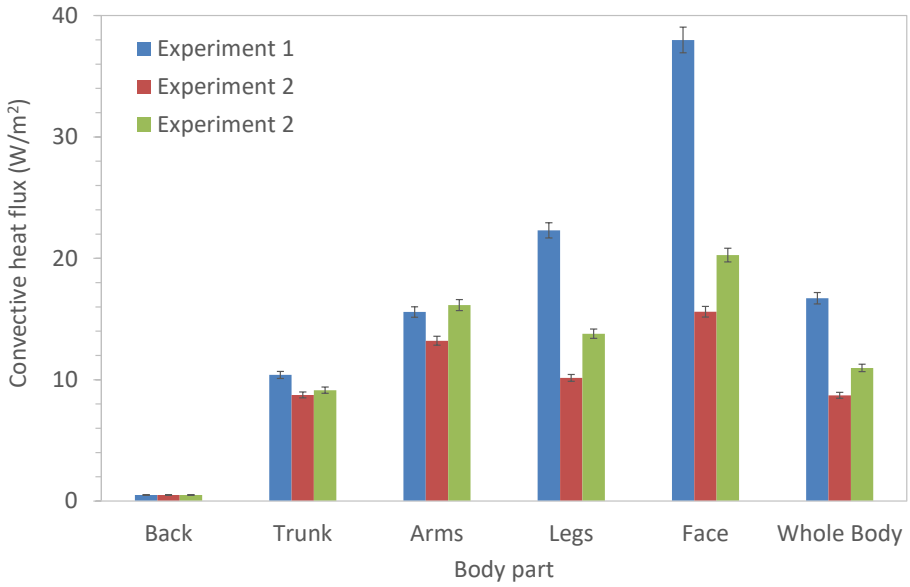

(a)

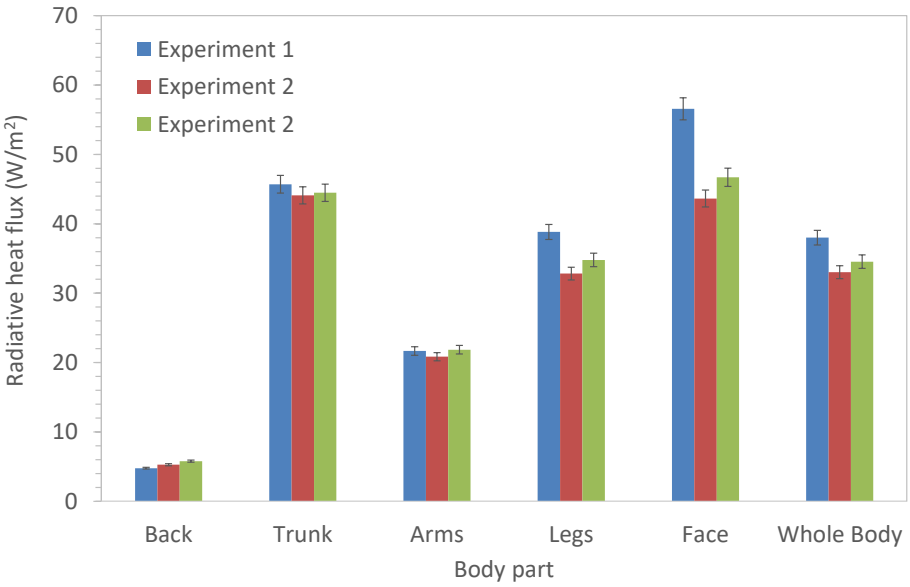

(b)

Figure 5.15: (a) Convective and (b) radiative heat losses from the manikin body segments

5.6 Conclusions

Experimental study on the 3D printed thermal manikin representing a preterm infant nursed inside an incubator are carried out. The manikin is instrumented with electrical heating wires from the inner surface, and it consists of six segments: back, trunk, legs, arms, face and head back. Thermocouples are fixed on the outer surface of each segment and used to measure the manikin skin temperature. This temperature is set as feedback to the PID regulator which controls the power input to the heating wires with the aim to maintain a constant surface temperature of the manikin. The PID regulator was first tuned using the Ziegler-Nichols method. LabVIEW is adopted to create a virtual instrument with graphical user interface. Three experimental studies were performed. In the first the incubator air temperature is set at 30℃ while in the second the incubator is heated to 35℃, where for both cases the incubator ports were kept closed. Meanwhile, in the third case, the incubator temperature was kept 35℃ and the ports were open.

The thermal manikin with the PID control were able to well behave under the different thermal conditions in the three experiments. The convection and radiation heat losses are the highest for the case with the cold incubator while they were the lowest in the case of warm incubator with closed ports. Opening the incubator ports showed an increase in heat loss by about 9% relative the closed ports case which proves the importance of having the air curtains in the incubator. In all the three cases, the radiation heat losses are almost the double of convection heat losses. Thus, adding for instance radiant elements to the incubator would be beneficial in case additional and faster heating is required.

The experimental results obtained in the present study are compared to those obtained from numerical and experimental studies in the open literature. It is found that the present results are in fair agreement with those obtained in the open literature. For instance, the difference between the total heat loss from the current thermal manikin is 0.34% different than the average of the heat loss values obtained in the open literature for the case of warm incubator with closed ports.

Chapter 6 Conclusions and Perspectives

Worldwide, in 2015, 45.7% of the 5.9 million deaths of children under 5 years of age occurred during the neonatal period. The **leading cause of death** of children under 5 years of age was **preterm birth complications** with a percentage of 17.9% [1, 2].

Newborns, especially preterm and sick ones, have d**ifficulties in controlling their body temperature**. Thus, they are placed inside incubators with control hygrothermal conditions and where we monitor their temperature and other vital signs. The complex processes of heat and mass transfer between neonates and the surrounding air and surfaces are **key factors in their growth and survival**.

Several methods are used to better understand the physical phenomena of neonatal heat loss and body-environment interaction. These methods can be classified into three main categories: **analytical** analysis of human thermoregulation, **computational fluid dynamics** (CFD) and **experimental** studies. The objective of these methods is to analyze the effect of different environmental conditions, such as air temperature and humidity, on heat transfer by convection, conduction and radiation as well as on latent heat loss due to skin evaporation and respiration. A **comprehensive state of the art** is presented in **Chapter 2** discussing the different methods used to analyze heat transfer in neonatal incubators. Furthermore, based on these methods, we discuss different techniques developed to improve hygrothermal conditions in incubators.

In this thesis, an **anthropomorphic mannequin** representing a preterm infant aged 35 gestational weeks is fabricated by **3D printing method**, and it consists of **5 body segments**: head, arms, torso, back and legs. A virtual geometry of this mannequin is also used in numerical simulations by the **finite volume method**. The mannequin is placed inside a **Caleo Drager incubator**. The operation of this incubator is presented in detail in **Chapter 3**. A virtual model of the incubator is prepared by CAD software to be used in the numerical simulations.

Several thermoregulation and heat transfer models for preterm neonates are used to study the heat transfer inside the incubators. These models require the individual radiation

and convection heat transfer coefficients for **different body segments**. In **Chapter 4**, numerical simulations are performed for the preterm neonate consisting of 5 segments placed inside an incubator. The studies are conducted by varying the incubator inlet temperature between 29 and 35°C and different air flow rates between 5 and 50 liters/min. It is found that the heat transfer processes depend mainly on the air temperature in the incubator. It is shown that the air flow rate in the incubator does not significantly affect the convective heat transfer. Thus, it is concluded that heat transfer between the incubator air and the infant is caused by **natural convection**. The effect of flow structure on temperature distribution is investigated and **correlations for radiative and convective heat transfer coefficients** are obtained for each body segment. The radiative heat transfer coefficient varies between 2.2 and 6.2 W/m^2K while the convective heat transfer coefficient varies between 2.6 and 4.7 W/m^2K. The results are **validated by experimental data from the literature**. Finally, a **thermoregulation model is developed** considering heat and mass losses due to skin evaporation and respiration. This model is used to quantify the heat balance in preterm neonates in incubators.

Chapter 5 is devoted to the **experimental study** conducted on the **thermal manikin** placed inside the incubator. We discuss in this chapter the instrumentation of the manikin with heating wires fixed on the inner surface and with thermocouples fixed on the outer surface. The **PID (proportional-integral-derivative) controller** is used to control the temperatures of the different segments of the dummy. We adopt the **Ziegler-Nichols method** which is a heuristic method for tuning the PID controller. LabVIEW software is then used to create the virtual instrument with a graphical interface. Three measurement campaigns are made. The first one consists in setting the incubator temperature at 30°C and in the second one the temperature is increased to 35°C while keeping the incubator doors closed. In the third measurement campaign, the incubator temperature is set at 35°C with the incubator doors open. The results from the three experimental studies are discussed in terms of the **temporal variation of the temperatures of the different segments** of the manikin as well as analyzing the **convective and radiative heat losses** that are obtained by **coupling** the experimental data to the convective and radiative exchange coefficients obtained in Chapter 4. These results are also compared with numerical and experimental data from the literature. From this comparison we find that the thermal manikin designed in this thesis as well as the

experimental methods adopted are **valid and give results with good correspondence** with the literature.

Hence, to summarize, the main original outputs of this thesis are the following:

- **Comprehensive state of the art** on the heat and mass transfer from preterm neonates using theoretical modeling, numerical simulations and experimental techniques.
- Evaluation of the **convective and radiative heat transfer coefficients for individual body segments** using numerical simulations.
- **Development and instrumentation of a 3D printed thermal manikin** representing a preterm neonate.
- **Experimental study** performed on the manikin under different scenarios and combining experimental data to numerical results to obtain the convective and radiative heat losses.

As for the **perspectives for future work**, we will couple i**nfrared thermography to PID control**. The input will be the temperature obtained from the infrared camera and an image processing algorithm should be capable of reading the temperature distribution for the different body segments. This method allows noninvasive measurement of the neonate skin temperature in real time. Another future plan concerns the **PIV (particle image velocimetry)** measurement of the velocity and turbulence field around the neonate inside the incubator to better understand the effect of the flow field on the heat transfer.

From numerical simulations, we will include in the future the **latent heat losses** by computing the **mass balance equation** coupled to the heat transfer equation. This will permit the analysis of both **temperature and humidity effects** on the heat losses from neonates. An **active thermoregulation model** will be also used to better model the physiological responses of the neonate to the different environmental conditions.

Bibliography

[1] H. Blencowe, S. Cousens, M. Z. Oestergaard, D. Chou, A. B. Moller, R. Narwal, A. Adler, C. Vera Garcia, S. Rohde, L. Say and J. E. Lawn, "National, regional, and worldwide estimates of preterm birth rates in the year 2010 with time trends since 1990 for selected countries: A systematic analysis and implications," *The Lancet*, vol. 379, no. 9832, pp. 2162-2172, 6 2012.

[2] L. Liu, S. Oza, D. Hogan, Y. Chu, J. Perin, J. Zhu, J. E. Lawn, S. Cousens, C. Mathers and R. E. Black, "Global, regional, and national causes of under-5 mortality in 2000–15: an updated systematic analysis with implications for the Sustainable Development Goals," *The Lancet*, vol. 388, no. 10063, pp. 3027-3035, 12 2016.

[3] C. Howson, M. Kinney and J. Lawn, "March of Dimes, PMNCH, Save the Children, WHO. Born Too Soon: The Global Action Report on Preterm Birth," World Health Organization, Geneva, Switzerland, 2012.

[4] D. You, L. Hug, S. Ejdemyr, P. Idele, D. Hogan, C. Mathers, P. Gerland, J. R. New and L. Alkema, "Global, regional, and national levels and trends in under-5 mortality between 1990 and 2015, with scenario-based projections to 2030: A systematic analysis by the un Inter-Agency Group for Child Mortality Estimation," *The Lancet*, vol. 386, no. 10010, pp. 2275-2286, 12 2015.

[5] U. N. G. Assembly, "Resolution adopted by the General Assembly: United Nations

Millennium Declaration," United Nations, Geneva, Switzerland, 2000.

[6] W. H. Organization, "WHO recommendations on interventions to improve preterm birth outcomes," World Health Organization, Geneva, Switzerland, 2015.

[7] M. Al-Othmani, N. Ghaddar and K. Ghali, "A multi-segmented human bioheat model for transient and asymmetric radiative environments," *International Journal of Heat and Mass Transfer,* vol. 51, no. 23-24, pp. 5522-5533, 11 2008.

[8] W. Weng, X. Han and M. Fu, "An extended multi-segmented human bioheat model for high temperature environments," *International Journal of Heat and Mass Transfer,* vol. 75, pp. 504-513, 8 2014.

[9] Y. Tang, Y. He, H. Shao and C. Ji, "Assessment of comfortable clothing thermal resistance using a multi-scale human thermoregulatory model," *International Journal of Heat and Mass Transfer,* vol. 98, pp. 568-583, 7 2016.

[10] F. Mneimneh, N. Ghaddar, K. Ghali, I. Omeis and C. Moussalem, "An altered Bioheat model for persons with cervical spinal cord injury," *Journal of Thermal Biology,* vol. 77, pp. 96-110, 10 2018.

[11] C. Porth and L. Kaylor, "Temperature Regulation in the Newborn," *The American Journal of Nursing,* vol. 78, no. 10, pp. 1691-1693, 1978.

[12] R. B. Knobel, D. Holditch-Davis, T. A. Schwartz and J. E. Wimmer Jr, "Extremely low birth weight preterm infants lack vasomotor response in relationship to cold body temperatures at birth," *Journal of Perinatology,* vol. 29, p. 814–821, 12 2009.

[13] A. K. Adams, R. A. Nelson, E. F. Bell and C. A. Egoavil, "Use of infrared thermographic calorimetry to determine energy expenditure in preterm infants,"

American Journal of Clinical Nutrition, vol. 71, p. 969–977, 2000.

[14] A. Lyon, "Temperature control in the neonate," *Paediatrics and Child Health,* vol. 18, no. 4, pp. 155-160, 4 2008.

[15] M. K. Ginalski, A. J. Nowak and L. C. Wrobel, "A combined study of heat and mass transfer in an infant incubator with an overhead screen," *Medical Engineering and Physics,* vol. 29, p. 531–541, 2007.

[16] A. Hannouch, V. Mitilian, M. Hajj-Hassan, H. Khachfe and C. Habchi, "Computational Fluid Dynamics Model for a Closed Infant Incubator," 2016.

[17] S. Delanaud, P. Decima, A. Pelletier, J. P. Libert, E. Durand, E. Stephan-Blanchard, V. Bach and P. Tourneux, "Thermal management in closed incubators: New software for assessing the impact of humidity on the optimal incubator air temperature," *Medical Engineering and Physics,* vol. 46, p. 89–95, 2017.

[18] A. Coccarelli, E. Boileau, D. Parthimos and P. Nithiarasu, "An advanced computational bioheat transfer model for a human body with an embedded systemic circulation," *Biomechanics and Modeling in Mechanobiology,* vol. 15, p. 1173–1190, 2016.

[19] M. Salloum, N. Ghaddar and K. Ghali, "A new transient bioheat model of the human body and its integration to clothing models," *International Journal of Thermal Sciences,* vol. 46, no. 4, pp. 371-384, 2007.

[20] D. Fiala, K. J. Lomas and M. Stohrer, "Computer prediction of human themoregulatory and temperature responses to a wide range of environmental conditions," *Int J Biometeorol,* vol. 45, p. 143–159, 2001.

[21] C. B. Pereira, K. Heimann, M. Czaplik, V. Blazek, B. Venema and S. Leonhardt,

"Thermoregulation in premature infants: A mathematical model," *Journal of Thermal Biology*, vol. 62, p. 159–169, 2016.

[22] H. M. Patil and R. Maniyeri, "Finite difference method based analysis of bio-heat transfer in human breast cyst," *Thermal Science and Engineering Progress*, vol. 10, p. 42–47, 2019.

[23] J. Marn, M. Chung and J. Iljaž, "Relationship between metabolic rate and blood perfusion under Fanger thermal comfort conditions," *Journal of Thermal Biology*, vol. 80, p. 94–105, 2019.

[24] S. Delanaud, P. Decima, A. Pelletier, J. P. Libert, E. Stephan-Blanchard, V. Bach and P. Tourneux, "Additional double-wall roof in single-wall, closed, convective incubators: Impact on body heat loss from premature infants and optimal adjustment of the incubator air temperature," *Medical Engineering and Physics*, vol. 38, p. 922–928, 2016.

[25] D. M. C. Goffau, K. A. Bergman, D. H. J. Vries, N. E. L. L. Meessen, J. E. Degener, V. J. M. Dijl and H. J. M. M. Harmsen, "Cold Spots in Neonatal Incubators Are Hot Spots for Microbial Contamination," *Applied and Environmental Microbiology*, vol. 77, p. 8568–8572, 2011.

[26] A. Hannouch, T. Lemenand, K. Khoury and C. Habchi, "Coupled Radiative and Convective Heat Losses from Preterm Infant Inside an Incubator with Radiant Heaters," Sitges, 2019.

[27] H. Pennes, "Analysis of Tissue and Arterial Blood Temperatures in the Resting Human Forearm," *Applied Physiology*, vol. 1, p. 93–122, 1948.

[28] R. Holopainen, "A human thermal model for improved thermal comfort," Aalto University, 2012.

[29] A. Fraguela, F. D. Matlalcuatzi and Á. M. Ramos, "Mathematical modelling of thermoregulation processes for premature infants in closed convectively heated incubators," *Computers in Biology and Medicine*, vol. 57, p. 159–172, 2015.

[30] H. J. Dane and P. J. J. Sauer, "Dynamics of thermoregulation," *Periodica Polytechnica Electrical Engineering (Archives)*, vol. 28, p. 215–226, 1984.

[31] L. C. Wrobel, M. K. Ginalski, A. J. Nowak, D. B. Ingham and A. M. Fic, "An overview of recent applications of computational modelling in neonatology," *Philosophical Transactions of the Royal Society A: Mathematical, Physical and Engineering Sciences*, vol. 368, p. 2817–2834, 2010.

[32] J. S. Greenspan, A. B. Cullen, S. M. Touch, M. R. Wolfson and T. H. Shaffer, "Thermal Stability and Transition Studies With a Hybrid Warming Device for Neonates," *Journal Of Perinatology*, vol. 21, p. 167, 19 7 2001.

[33] A. K. Abbas and S. Leonhardt, "Intelligent neonatal monitoring based on a virtual thermal sensor," *BMC Medical Imaging*, vol. 14, 2014.

[34] P. J. J. J. J. Sauer, H. J. Dane and H. K. A. A. A. Visser, "Influence of Variations in the Ambient Humidity on Insensible Water Loss and Thermoneutral Environment of Low Birth Weight Infants," *Acta Pædiatrica*, vol. 73, p. 615–619, 1984.

[35] A. E. Wheldon and N. Rutter, "The heat balance of small babies nursed in incubators and under radiant warmers," *Early Human Development*, vol. 6, p. 131–143, 1982.

[36] S. Xu, L. Sun, G. K. Rohde, A. K. Abbas, K. Heimann, K. Jergus, T. Orlikowsky and

S. Leonhardt, "Neonatal non-contact respiratory monitoring based on real-time infrared thermography," *BioMedical Engineering OnLine,* vol. 5, p. 1124–1135, 2014.

[37] E. B. Elabbassi, K. Chardon, V. Bach, F. Telliez, S. Delanaud and J. P. Libert, "Head insulation and heat loss in naked and clothed newborns using a thermal mannequin," *Medical Physics,* vol. 29, p. 1090–1096, 2002.

[38] I. Sarman, D. Bolin, I. Holmér and R. Tunell, "Assessment of Thermal Conditions in Neonatal Care: Use of a Manikin of Premature Baby Size," *American Journal of Perinatology,* vol. 9, p. 239–246, 1992.

[39] P. Décima, E. Stephan-Blanchard, A. Pelletier, L. Ghyselen, S. Delanaud, L. Degrugilliers, F. Telliez, V. Bach and J. P. Libert, "Assessment of radiant temperature in a closed incubator," *European Journal of Applied Physiology,* vol. 112, p. 2957–2968, 2012.

[40] A. E. Wheldon, "Energy balance in the newborn baby: Use of a manikin to estimate radiant and convective heat loss," *Physics in Medicine and Biology,* vol. 27, p. 285–296, 2 1982.

[41] K. Belghazi, E. B. Elabbassi, P. Tourneux and J. P. Libert, "Assessment of whole body and regional evaporative heat loss coefficients in very premature infants using a thermal mannequin: Influence of air velocity," *Medical Physics,* vol. 32, p. 752–758, 2005.

[42] G. Sedin, K. Hammarlund and B. Stromberg, "Transepidermal water loss in full-term and pre-term infants," *Acta Paediatrica Scandinavica,* vol. 31, p. 305–327, 1983.

[43] K. Hammarlund, G. Nilsson, P. Oberg and G. Sedin, "Transepidermal water loss in

newborn infants I. Relation to ambient humidity and site of measurement and estimation of total transepidermal water loss," *Acta Paediatrica,* vol. 66, p. 553–562, 1977.

[44] E. H. Wissler, "Pennes ' 1948 paper revisited," *Applied Physiology,* p. 35–41, 1998.

[45] T. C. Shih, P. Yuan, W. L. Lin and S. H. Kou, "Analytical analysis of the Pennes bioheat transfer equation with sinusoidal heat flux condition on skin surface," *Medical Engineering and Physics,* vol. 29, p. 946–953, 2007.

[46] A. Lakhssassi, E. Kengne and H. Semmaoui, "Modifed pennes' equation modelling bio-heat transfer in living tissues: analytical and numerical analysis," *Natural Science,* vol. 02, p. 1375–1385, 2010.

[47] P. K. Gupta, J. Singh and K. N. N. Rai, "A numerical study on heat transfer in tissues during hyperthermia," *Mathematical and Computer Modelling,* vol. 57, p. 1018–1037, 1 3 2013.

[48] D. Fiala, "Dynamic simulation of human heat transfer and thermal comfort," De Montfort University, 1998.

[49] H. J. Dane, "Climate control of incubators related to growth and thermoregulation of newborn infants," *IFAC Proceedings Volumes,* vol. 18, p. 1603–1606, 1987.

[50] A. B. C. G. G. Silva, J. Laszczyk, L. C. Wrobel, F. L. B. B. Ribeiro and A. J. Nowak, "A thermoregulation model for hypothermic treatment of neonates," *Medical Engineering and Physics,* vol. 38, p. 988–998, 2016.

[51] A. B. d. C. G. e. Silva, "A Finite Element Thermoregulation Model of the Human Body for Hypothermia Treatment in Adults and Neonates," COPPE, 2016.

[52] D. Fiala, G. Havenith, P. Bröde, B. Kampmann and G. Jendritzky, "UTCI-Fiala multi-node model of human heat transfer and temperature regulation," *International Journal of Biometeorology,* vol. 56, p. 429–441, 2012.

[53] A. Peliowski-Davidovich, "Hypothermia fo newborns with hypoxic ischemic encephalopathy," *Paediatr Child Health,* vol. 17, p. 41–43, 2012.

[54] D. Bandoła, A. J. Nowak, Z. Ostrowski, M. Rojczyk and W. Walas, "Measurement and computational experiments within newborn's brain cooling process," 2018.

[55] J. Laszczyk, "The Analysis of a Newborn ' s Brain Cooling Process," Silesian University of Technology, 2014.

[56] J. E. Laszczyk and A. J. Nowak, "Computational modelling of neonate's brain cooling," *International Journal of Numerical Methods for Heat and Fluid Flow,* vol. 26, p. 571–590, 2016.

[57] Y. H. Kim, C. H. Kwon and S. C. Yoo, "Experimental and numerical studies on convective heat transfer in a neonatal incubator.," *Medical & biological engineering & computing,* vol. 40, p. 114–121, 2002.

[58] I. Amezzane, A. Awada, M. Sawan and F. Bellemare, "Modelling and simulation of an infant's whole body plethysmograph," *Medical and Biological Engineering and Computing,* vol. 44, p. 823–828, 2006.

[59] ASHRAE, "ASHRAE 62.1 - Ventilation for Acceptable Indoor Air Quality," Atlanta, 2016.

[60] M. K. Ginalski, A. J. Nowak and L. C. Wrobel, "Modelling of heat and mass transfer processes in neonatology," *Biomedical Materials,* vol. 3, 2008.

[61] Dräger, "The Caleo Effect: Caleo provides superior care for very low birth weight infants," Lübeck, Germany, 2015.

[62] E. B. Elabbassi, K. Belghazi, S. Delanaud and J. P. Libert, "Dry heat loss in incubator: Comparison of two premature newborn sized manikins," *European Journal of Applied Physiology,* vol. 92, p. 679–682, 2004.

[63] Y. A. Cengel, Heat Transfer: A Practical Approach, New york, 2003.

[64] S. Murakami, S. Kato and J. Zeng, "Combined simulation of airflow, radiation and moisture transport for heat release from a human body," *Building and Environment,* vol. 35, p. 489–500, 2000.

[65] M. Kilic and G. Sevilgen, "Modelling airflow, heat transfer and moisture transport around a standing human body by computational fluid dynamics," *International Communications in Heat and Mass Transfer,* vol. 35, p. 1159–1164, 1 11 2008.

[66] G. Pichurov and P. Stankov, "Integration of thermophysiological body model in CFD," *Central European Journal of Engineering,* vol. 3, p. 513–521, 2013.

[67] K. Brück, "Temperature regulation of the newborn infant," *Biology of the Neonate,* vol. 3, p. 65–119, 1961.

[68] J. Hall, Guyton and Hall Textbook of Medical Physiology, Philadelphia: Saunders, 2016.

[69] J. Rennie and G. Kendall, A Manual of Neonatal Intensive Care, Boca, Raton: CRC Press, 2013.

[70] E. Sulyok, E. Jéquier and L. S. Prod'hom, "Respiratory contribution to the thermal balance of the newborn infant under various ambient conditions," *American Academy*

of Pediatrics, vol. 51, p. 641–650, 1973.

[71] A. M. Fic, D. B. Ingham, M. K. Ginalski, A. J. Nowak and L. Wrobel, "Heat and mass transfer under an infant radiant warmer - development of a numerical model," *Medical Engineering and Physics,* vol. 32, no. 5, pp. 497-504, 2010.

[72] A. M. Fic, D. B. Ingham, M. K. Ginalski, A. J. Nowak and L. C. Wrobel, "Modelling and optimisation of the operation of a radiant warmer," *Medical Engineering and Physics,* vol. 36, no. 1, pp. 81-87, 2014.

[73] M. Rojczyk and I. Szczygieł, "Numerical analysis of radiant warmer," *Computer Assisted Mechanics and Engineering Sciences,* vol. 20, no. 3, pp. 237-265, 2013.

[74] R. A. Wahyuono, R. Hantoro and G. Nugroho, "Study on Dry Heat Loss of a Very Low Birth Weight (VLBW) Newborn Nursed in an Infant Incubator with Overhead Screen," in *13th Seminar on Intelligent Technology and Its Application (SITIA)*, Surabaya, Indonesia, 2012.

[75] R. A. Wahyuono, N. Dahliyah, I. Putri, T. Setiawan and R. Hantoro, "Partial Double Wall Incubator for Proposed Optimal Thermoregulator Supporting Media of Newborn Care," in *International Conference on Physics*, Yogyakarta, Indonesia, 2012.

[76] P. J. J. J. J. Sauer, H. J. Dane and H. K. A. A. A. Visser, "New standards for neutral thermal environment of healthy very low birthweight infants in week one of life," *Archives of Disease in Childhood,* vol. 59, p. 18–22, 1984.

[77] J. A. J. Stolwijk and J. D. Hardy, "Temperature regulation in man, a theoretical study," *Pfliigers Archives,* vol. 291, p. 129–162, 1966.

[78] P. Chessex, B. L. Reichman, G. J. E. E. Verellen, G. Putet, J. M. Smith, T. Heim and P.

R. Swyer, "Influence of postnatal age, energy intake, and weight gain on energy metabolism in the very low-birth-weight infant," *The Journal of Pediatrics,* vol. 99, p. 761–766, 11 1981.

[79] N. Museux, V. Cardot, V. Bach, S. Delanaud, L. Degrugilliers, B. Agourram, E. B. Elabbassi and J. P. Libert, "A reproducible means of assessing the metabolic heat status of preterm neonates," *Medical Physics,* vol. 35, p. 89–100, 2008.

[80] G. Lusk, The Element of Science and Nutrition, 4th ed., Philadelphia: WB Saunders, 1928.

[81] W. Oh and S. Kato, "The effect of airspeed and wind direction on human's thermal conditions and air distribution around the body," *Building and Environment,* vol. 141, p. 103–116, 2018.

[82] R. J. De Dear, E. Arens, Z. Hui and M. Oguro, "Convective and radiative heat transfer coefficients for individual human body segments," *International Journal of Biometeorology,* vol. 40, p. 141–156, 1997.

[83] A. V. M. Oliveira, A. R. Gaspar, S. C. Francisco and D. A. Quintela, "Analysis of natural and forced convection heat losses from a thermal manikin: Comparative assessment of the static and dynamic postures," *Journal of Wind Engineering and Industrial Aerodynamics,* vol. 132, p. 66–76, 2014.

[84] K. Adamsons and M. E. Towell, "Thermal homeostasis in the fetus and newborn," *Anesthesiology,* vol. 26, 1965.

[85] Z. Ostrowski, M. Rojczyk, I. Szczygieł, J. Łaszczyk and A. J. Nowak, "Dry heat loses of newborn baby in infant care bed: Use of a thermal manikin," *Journal of Physics:*

Conference Series, vol. 745, p. 1–8, 2016.

[86] Z. Ostrowski and M. Rojczyk, "Natural convection heat transfer coefficient for newborn baby: Thermal manikin assessed convective heat loses," *Heat and Mass Transfer/Waerme- und Stoffuebertragung,* p. 1–9, 2017.

[87] K. Belghazi, P. Tourneux, E. B. Elabbassi, L. Ghyselen, S. Delanaud and J. P. Libert, "Effect of posture on the thermal efficiency of a plastic bag wrapping in neonate: Assessment using a thermal "sweating" mannequin," *Medical Physics,* vol. 33, p. 637–644, 2006.

[88] I.-h. Kang and T. Tamura, "A Study on the Development of an Infant-sized Movable Sweating Thermal Manikin," *Journal of the Human-Environmental System,* vol. 5, no. 1, pp. 49-56, 2001.

[89] C. Ferré, W. Callaghan, C. Olson, A. Sharma and W. Barfield, "Effects of Maternal Age and Age-Specific Preterm Birth Rates on Overall Preterm Birth Rates - United States, 2007 and 2014," *Morbidity and Mortality Weekly Report CDC,* vol. 65, p. 1181–1184, 2016.

[90] Autodesk, "3DS Max - 3D modeling and rendering software for design visualization, games, and animation," Autodesk Inc., 2018. [Online]. Available: https://www.autodesk.com/products/3ds-max/overview?term=1-YEAR&support=null. [Accessed 12 2021].

[91] Z. Lei, "Review of application of thermal manikin in evaluation on thermal and moisture comfort of clothing," *Journal of Engineered Fibers and Fabrics,* vol. 14, pp. 1-10, 2019.

[92] D. Wyon, "Use of thermal manikins in environmental ergonomics," *Scandinavian Journal of Work, Environment & Health,* vol. 1, pp. 84-94, 1989.

[93] S. Delanaud, F. Chahin Yassin, E. Durand, P. Tourneux and J.-P. Libert, "Can Mathematical Models of Body Heat Exchanges Accurately Predict Thermal Stress in Premature Neonates?," *Applied Sciences,* vol. 9, 2019.

[94] S. C. Daminabo, S. Goel, S. A. Grammatikos, H. Y. Nezhad and V. K. Thakur, "Fused deposition modeling-based additive manufacturing (3D printing): techniques for polymer material systems," *Materials Today Chemistry,* vol. 16, p. 100248, 2020.

[95] Flashforge, "Flashforge Guider II," Flashforge , [Online]. Available: https://www.flashforge.com/product-detail/10. [Accessed 25 February 2021].

[96] A. Varotsis, "Introduction to FDM 3D printing," 3D HUBS, [Online]. Available: https://www.3dhubs.com/knowledge-base/introduction-fdm-3d-printing/#what. [Accessed 25 02 2021].

[97] N. Mao, M. Song, D. Pan and S. Deng, "Computational fluid dynamics analysis of convective heat transfer coefficients for a sleeping human body," *Applied Thermal Engineering,* vol. 117, pp. 385-396, 2017.

[98] N. Ismail, N. Ghaddar and K. Ghali, "Electric circuit analogy of heat losses of clothed walking human body in windy environment," *International Journal of Thermal Sciences,* vol. 127, pp. 105-116, 2018.

[99] H. Ishigaki, T. Horikoshi, T. Uematsu, M. Sahashi, T. Tsuchikawa, T. Mochida, T. Hieda, N. Isoda and H. Kubo, "Experimental study on convective heat transfer coefficient of the human body," *Journal of Thermal Biology,* vol. 18, no. 5-6, pp. 455-

458, 12 1993.

[100] Y. Kurazumi, T. Tsuchikawa, J. Ishii, K. Fukagawa, Y. Yamato and N. Matsubara, "Radiative and convective heat transfer coefficients of the human body in natural convection," *Building and Environment,* vol. 43, no. 12, pp. 2142-2153, 2008.

[101] S. Gao, R. Ooka and W. Oh, "Formulation of human body heat transfer coefficient under various ambient temperature, air speed and direction based on experiments and CFD," *Building and Environment,* vol. 160, p. 106168, 2019.

[102] C. Li and K. Ito, "Numerical and experimental estimation of convective heat transfer coefficient of human body under strong forced convective flow," *Journal of Wind Engineering and Industrial Aerodynamics,* vol. 126, pp. 107-117, 2014.

[103] X. Li and J. Tu, "Evaluation of the eddy viscosity turbulence models for the simulation of convection–radiation coupled heat transfer in indoor environment," *Energy and Buildings,* vol. 184, pp. 8-18, 2019.

[104] Caleo, *Draeger Medical UK Ltd,* 0.

[105] F. R. Menter, "Two-equation eddy-viscosity turbulence models for engineering applications," *AIAA Journal,* vol. 32, no. 8, pp. 1598-1605, 8 1994.

[106] J. Y. Murthy and S. R. Mathur, "Finite volume method for radiative heat transfer using unstructured meshes," *Journal of Thermophysics and Heat Transfer,* vol. 12, no. 3, pp. 313-321, 1998.

[107] E. H. Chui and G. D. Raithby, "Computation of radiant heat transfer on a nonorthogonal mesh using the finite–volume method," *Numerical Heat Transfer, Part B: Fundamentals,* vol. 23, no. 3, pp. 269-288, 1993.

[108] ANSYS, *ANSYS Fluent Academic Research*, 2019.

[109] R. F. Warming and R. M. Beam, "Upwind Second-Order Difference Schemes and Applications in Aerodynamic Flows," *AIAA Journal*, vol. 14, no. 9, pp. 1241-1249, 1976.

[110] J. Tu, G.-H. Yeoh, C. Liu, J. Tu, G.-H. Yeoh and C. Liu, "CFD Mesh Generation: A Practical Guideline," *Computational Fluid Dynamics*, pp. 125-154, 1 2018.

[111] I. B. Celik, U. Ghia, P. J. Roache, C. J. Freitas, H. Coleman and P. E. Raad, "Procedure for Estimation and Reporting of Uncertainty Due to Discretization in CFD Applications," *Journal of Fluids Engineering*, vol. 130, no. 7, 7 2008.

[112] T. R. Fenton and J. H. Kim, "A systematic review and meta-analysis to revise the Fenton growth chart for preterm infants," *BMC pediatrics*, vol. 13, p. 59, 4 2013.

[113] R. D. Rojas, E. F. Bell and E. L. Dove, "Mathematical model of premature baby thermoregulation and infant incubator dynamics," *International Conference on Simulation Modelling in Bioengineering, BIOSIM*, vol. 3, pp. 23-38, 1996.

[114] J. S. Ultman, "Computational Model for Insensible Water Loss From the Newborn," *Pediatrics*, vol. 79, no. 5, pp. 760 LP - 765, 5 1987.

[115] W. Lewis, "The evaporation of a liquid into a gas," *ASME Transaction*, vol. 44, pp. 325-340, 1922.

[116] ANSI/ASHRAE, "ANSI/ASHRAE 55 - Thermal Environmental Conditions for Human Occupancy," ANSI/ASHRAE, Atlanta, GA, , 2017.

[117] Drager, "Drager heat balance program," 2019. [Online]. Available: https://legacy.draeger.com/US/heat-balance/index.jsp.

[118] E. T. Özkan, "Using Thermal Manikin Systems for Thermophysiological Comfort Evaluations- A Review," *Journal of Textile Science & Fashion Technology,* vol. 7, no. 5, pp. 1-7, 2021.

[119] J. Fan, "Thermal Manikins and Modelling," in *6th International Thermal Manikin and Modeling Meeting*, Kowloon, Hong Kong, 2006.

[120] A. Psikuta, J. Allegrini, B. Koelblen, A. Bogdan, S. Annaheim, N. Martínez, D. Derome, J. Carmeliet and R. M. Rossi, "Thermal manikins controlled by human thermoregulation models for energy efficiency and thermal comfort research – A review," *Renewable and Sustainable Energy Reviews,* vol. 78, pp. 1315-1330, 10 2017.

[121] Fotek, "SSR-DD series single phase solid state module (SSR)," [Online]. Available: www.fotek.com.tw/en-gb/product-category/144. [Accessed 23 May 2021].

[122] J. G. Ziegler and N. B. Nichols, "Optimum Settings for Automatic Controllers," *ASME J. Dyn. Sys., Meas., Control.,* vol. 115, no. 2B, pp. 220-222, 1993.

[123] WireTonic, "Current / Temperature Table – Ni Cr A (80) & Ni Cr C (60)," WireTonic Inc., 2017. [Online]. Available: www.easycalculation.com/engineering/electrical/nichrome-wire-chart.php. [Accessed 23 05 2021].

DOCTORAT BRETAGNE SCIENCES LOIRE POUR L'INGENIEUR

université angers

Titre : Analyses Numérique et Expérimentale du Transfer Thermique dans un Incubateur Nouveaux Nés utilisant un Mannequin Imprimé 3D

Mots clés : Thermorégulation ; Transfer de chaleur ; Simulation CFD ; Contrôle PID ; Incubateur nouveau-né ; Mannequin thermique prématuré

Résumé : Les nouveau-nés prématurés sont fréquemment nourris dans des incubateurs bébés en raison de la thermorégulation non mûre qui pourra éventuellement conduire à des difficultés à contrôler leur température. Ces incubateurs jouent un rôle crucial dans la survie des nouveau-nés prématurés en fournissant des conditions hygrothermiques contrôlées. Une meilleure compréhension du transfert de chaleur complexe et du champ de l'écoulement à l'intérieur de ces systèmes est fondamentale pour améliorer leurs performances. Dans la présente thèse, des simulation numérique CFD et des techniques expérimentales sont utilisées pour étudier le transfert de chaleur et les champs de l'écoulement à l'intérieur d'un incubateur équipé d'un mannequin thermique prématuré imprimé en 3D.

Dans une première partie, un état de l'art détaillé est réalisé d'un point de vue de l'ingénierie pour discuter sur les progrès et les points manquants dans ce domaine.
Dans la deuxième partie, des simulations CFD sont effectuées pour évaluer les coefficients de transfert de chaleur radiatif et convectif pour chaque segment du corps des nouveau-nés prématurés. Ces coefficients sont importants pour développer des modèles de thermorégulation robustes et précis.
Dans la troisième partie, un mannequin thermique imprimé en 3D est construit avec un contrôle PID et testé pour différents scénarios à l'intérieur d'un incubateur. Le nouveau design du mannequin thermique est promettant.

Title: Numerical and Experimental Analyses of the Heat Transfer inside Infant Incubators using 3D Printed Thermal Manikin

Keywords: Thermoregulation; Heat transfer; CFD simulations; PID control; Neonatal incubator; Preterm thermal manikin

Abstract: Preterm neonates are frequently nursed inside infant incubators due to unmature thermoregulation leading to difficulty in controlling their body temperature. These incubators play a crucial role in the survival and growth of preterm neonates by providing controlled hygrothermal conditions and by monitoring the infant temperature and vital signs. The better understanding of the complex heat transfer and flow pattern inside these systems is fundamental for enhancing their performances.
In the present thesis, advanced computational fluid dynamics (CFD) and experimental techniques are performed to study the heat transfer processes and analyze the flow patterns inside an infant incubator equipped with a 3D printed preterm thermal manikin.

In the first part, a detailed state of the art is performed from an engineering point of view to shed light on the progress and lacking points in this domain.
In the second part, CFD simulations are carried to evaluate the radiative and convective heat transfer coefficients for each body segment of the preterm neonates. These coefficients are important to developing robust and accurate thermoregulation models.
In the third part, a 3D printed thermal manikin is built with PID control and tested for different scenarios inside an incubator. The new design of thermal manikin shows excellent promises.